3He-4He II mixtures : thermodynamic and hydrodynamic properties

Document Version:

Publisher's PDF, also known as Version of Record (includes final page, issue and volume numbers)

Please check the document version of this publication:

• A submitted manuscript is the version of the article upon submission and before peer-review. There can be important differences between the submitted version and the official published version of record. People interested in the research are advised to contact the author for the final version of the publication, or visit the DOI to the publisher's website.
• The final author version and the galley proof are versions of the publication after peer review.
• The final published version features the final layout of the paper including the volume, issue and page numbers.

[Link to publication](#)

³He-⁴He II MIXTURES: THERMODYNAMIC AND HYDRODYNAMIC PROPERTIES

J.G.M. KUERTEN

^{3}He-^{4}He II MIXTURES:

THERMODYNAMIC AND HYDRODYNAMIC PROPERTIES

PROEFSCHRIFT

ter verkrijging van de graad van doctor aan de Technische Universiteit Eindhoven, op gezag van de rector magnificus, prof. dr. F.N. Hooge, voor een commissie aangewezen door het college van dekanen in het openbaar te verdedigen op vrijdag 18 september 1987 te 16.00 uur

door

JOHANNES GERARDUS MARIA KUERTEN

geboren te Bergen op Zoom

Dit proefschrift is goedgekeurd door de promotoren
prof. dr. H.M. Gijsman en prof. dr. J.T.L. Devreese;
co-promotor: dr. A.T.A.M. de Waele

Aan mijn ouders

TABLE OF CONTENTS

I GENERAL INTRODUCTION

Mixtures of ^{3}He and ^{4}He have a number of special properties. In the first place, like pure ^{3}He and pure ^{4}He, they remain liquid at absolute zero for pressures below 2.0 MPa. In Fig. 1 the phase diagram of ^{3}He-^{4}He mixtures at saturated vapour pressure is represented in a T-x diagram, where x is the molar ^{3}He concentration and T the temperature. The left vertical axis describes pure ^{4}He. Below the λ-point, at 2.17 K, pure ^{4}He is superfluid. This means, among other things, that the fluid can flow through very narrow pores without friction. The second special property is that in region II, on the left side of the λ-curve, the ^{4}He component in the mixture is superfluid. On the right side of this curve, in region I, the ^{4}He in the solution is a normal fluid.
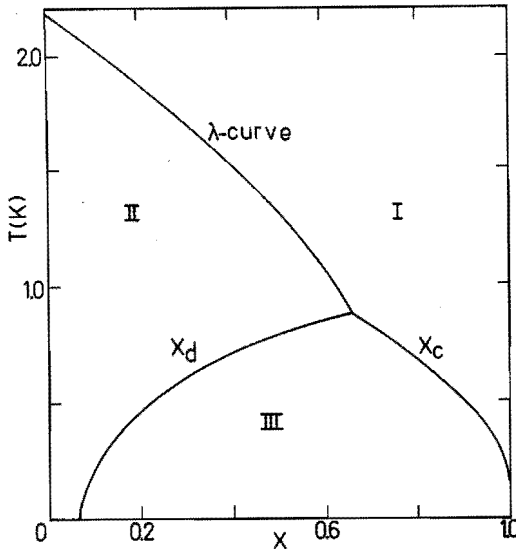

Fig. 1 *The phase diagram of ^{3}He-^{4}He mixtures at saturated vapour pressure. Below 0.87 K phase separation occurs in region III. The λ-curve separates the normal region (I) from the region in which the ^{4}He component is superfluid (II).*

A third special property can be seen in the same figure. Below 0.87 K the phenomenon of phase separation occurs. If a solution is cooled to a temperature that would correspond with a point inside region III, it will separate into two phases: the concentrated phase on curve x_c with a relatively high ^{3}He concentration, and the dilute phase on curve x_d with a lower concentration. At temperatures below 100 mK the ^{4}He concentration of the concentrated phase is negligible. On the other hand, even at absolute zero, the concentration of the dilute phase is nonzero, as is shown in the experiments of Edwards and Daunt [1].

A fourth special property is provided by the Fermi character of the ^{3}He component. At low temperatures the ^{3}He component behaves as a degenerate Fermi gas. This leads to a specific heat which is high compared to pure ^{3}He and pure ^{4}He. This property, together with the solubility of ^{3}He in ^{4}He at zero temperature, also leads to a relatively high osmotic pressure.

Finally, the vapour pressure of ^{3}He is much higher than of ^{4}He. This property implies that it is possible to extract almost pure ^{3}He from the mixture by continually removing the vapour.

Due to all these properties ^{3}He-^{4}He mixtures can be used for a cooling process to ultra low temperatures. The best known example of a cooling machine using these mixtures is the ^{3}He circulating dilution refrigerator, which can maintain temperatures of the order of a few millikelvin. Moreover, dilution refrigerators are used as a first cooling stage for single-cycle refrigeration to even lower temperatures, like adiabatic nuclear demagnetization.

In a dilution refrigerator the cooling is produced, using the property that at a given temperature the specific heat, and hence the enthalpy, of the concentrated phase (pure ^{3}He) is lower than of the dilute phase. Hence, when ^{3}He in the concentrated phase crosses the phase boundary into the dilute phase, heat has to be supplied from the surroundings, or the temperature of the liquid decreases. The property that approximately 6.6% ^{3}He can be dissolved in ^{4}He at absolute zero, makes this method useful at very low temperatures. The ^{3}He can be diluted continuously, if it is extracted from the dilute phase. This is possible, since the partial vapour pressure of ^{3}He is much higher than of ^{4}He. The property that the osmotic pressure is high, permits

the transport of ^{3}He through the dilute phase. The superfluidity of the ^{4}He brings about that this transport does not involve a high dissipation.

From the fundamental point of view, ^{3}He-^{4}He mixtures and pure ^{4}He are of interest, because they exhibit macroscopic quantum effects. In pure ^{4}He these effects have been studied extensively during the last decades. The most pronounced manifestation is the quantization of the circulation of the superfluid, suggested by Onsager [2]. This suggestion has led to the notion of quantized vortex lines with a core of atomic size, the existence of which has been shown in a large variety of experiments.

In many flow situations the evolution of these vortex lines leads to the development of a tangle of quantized vortex lines. This situation is called superfluid turbulence and has been studied both experimentally [3,4] and by numerical simulations [5]. It is interesting to note in this respect, that in the numerical study of vorticity in classical fluids the approximation is often made that the vorticity is restricted to singular curves [6,7]. This approximation is valid, if the core radius of the vortex line is small compared to its radius of curvature. In classical fluids the vorticity is not quantized and the region of vorticity may extend over a large volume. Thus, the condition that the core radius of a vortex line is small compared to its radius of curvature is only satisfied in special situations. On the other hand, the core radius of a quantized vortex line in helium is of the order of 1 Å, so that this condition is always satisfied. Hence, some theories of classical turbulence are even more applicable to the quantumfluids.

Presently, there is a wide interest in chaos and the route to turbulence in many branches of physics and other sciences [8]. Two well-known examples from the field of hydrodynamics are the Couette-Taylor flow of a fluid between two rotating cylinders, and the Rayleigh-Bénard instability in a fluid with an inhomogeneous temperature. These examples have also been studied with quantumfluids [9,10]. The transition to turbulence in open flow systems has been studied recently with a classical fluid [11] and with superfluid ^{4}He [12]. In the two fluid model of pure ^{4}He II the density of the normal component is completely determined by the temperature. In ^{3}He-^{4}He mixtures, on the other hand, the temperature and density of the normal

3

component (which comprises the ^{3}He) are independently variable. Therefore, ^{3}He-^{4}He mixtures have a big advantage over pure ^{4}He in the study of quantized vortices: the effects of temperature and normal density on the turbulence can be studied independently. In this way, a contribution can be made to the understanding of the general problem concerning the route to turbulence and chaos.

Around 1981 a study of ^{3}He-^{4}He II mixtures at temperatures below 250 mK, both experimental and theoretical, was initiated at the Eindhoven University of Technology. At that time the understanding of these mixtures was unsatisfactory in several ways. First of all, the thermodynamic quantities of ^{3}He-^{4}He mixtures as calculated and tabulated by Radebaugh in 1967 [13] and commonly used by the low temperature community, showed significant discrepancies with measured values of important quantities, like the osmotic pressure and the osmotic enthalpy. Furthermore, there was no generally accepted model for the hydrodynamics of ^{3}He-^{4}He mixtures. On the one hand, there was a model by Wheatley [14], in which it is assumed that there is no dissipative interaction between ^{3}He and ^{4}He. Measurements at low ^{3}He velocities confirmed this model [15]. On the other hand, measurements at higher ^{3}He velocities, performed at the Eindhoven University of Technology, indicated that this model certainly is not generally valid [16]. These measurements led to the proposal of the existence of mutual friction between ^{3}He and ^{4}He, comparable with mutual friction between the normal and superfluid components in pure ^{4}He II [3].

In the work described in this thesis a study of the thermo-dynamics and hydrodynamics of ^{3}He-^{4}He II is made in order to clarify these problems. This study will be restricted to temperatures below 250 mK, where the ^{4}He component is superfluid (region II in Fig. 1). Occasionally, pure ^{3}He will be considered.

Chapter II deals with the thermodynamic properties of ^{3}He-^{4}He mixtures. It is shown that all thermodynamic properties of ^{3}He-^{4}He mixtures at zero pressure can be calculated, if the specific heat is known as a function of ^{3}He concentration and temperature, the osmotic pressure at zero temperature and the specific heats and molar volumes of the pure substances. All these quantities are known with sufficient accuracy from experiments to calculate the other quantities to a high precision. In this way, all quantities are calculated at zero pressure

4

as functions of x and T, and the first order terms in the pressure are given. The results are in agreement with all experimentally determined quantities to a precision of 1%.

In chapter III first a review of some important theoretical properties of superfluid ^{4}He and ^{3}He-^{4}He mixtures, such as the quantization of circulation and the interaction between ^{3}He and ^{4}He, is given. Next, the hydrodynamics of ^{3}He-^{4}He mixtures is extended to include mutual friction. In a ^{3}He circulating dilution refrigerator ^{3}He flows through the superfluid background. Hence, mutual friction between the two components plays an important role in these refrigera- tors and in order to design a dilution refrigerator satisfying specified requirements for the minimum temperature and cooling power, it is necessary to know the thermodynamic and hydrodynamic properties of ^{3}He-^{4}He mixtures. In chapter IV, after a more detailed description of the ^{3}He circulating dilution refrigerator, the results of chapters II and III are applied to this refrigerator. In this way, the influence of mutual friction on the operation of the ^{3}He circulating dilution refrigerator is calculated.

Chapter V describes the experiments in which the link between the models *with* and *without* mutual friction is established. By varying the dimensions of the flow channel, it is shown that there is a continuous transition from the Mechanical Vacuum Model to the Mutual Friction Model. In the intermediate regime, the combined-dissipation regime, the mutual frictional force and the viscous force are both important, whereas in both limiting cases one force dominates the other. There is another –discontinuous– transition from the Mechanical Vacuum Model to the Mutual Friction Model. Recent measurements showed, that also for ^{3}He-^{4}He mixtures below a certain critical ^{3}He velocity no mutual friction occurs [17]. At the value of the critical velocity, which depends on the diameter of the flow channel, the sudden dissipation gives rise to jumps in the temperature, the ^{3}He concentration and the pressure. In the experiments described in chapter V this transition cannot be detected, since it occurs at ^{3}He velocities too low to be realized in the flow channels in consideration.

Finally, chapter VI deals with the mesoscopic explanation of mutual friction. In analogy with ^{4}He II it is assumed that mutual friction arises from the interaction between the ^{3}He particles and quantized vortices in ^{4}He, which are formed if the ^{3}He velocity

5

exceeds a certain critical value. An investigation is started in order to obtain insight in the influence of walls on the critical velocity and the influence of the ^{3}He velocity profile on the mutual friction, by making a numerical simulation of the motion of quantized vortices. In this way, it will also be possible to calculate the fluctuations in measurable quantities, like the temperature and ^{3}He concentration. The first results of these simulations, concerning the interaction of a vortex ring with a rigid smooth surface are reported in this chapter.

Throughout this thesis SI-units will be used, unless stated otherwise.

References

[1]   D.O. Edwards, and J.G. Daunt, Phys. Rev. **124**, 640 (1961).

[2]   L. Onsager, Nuov. Cim. **6**, Supp. **2**, 249 (1949).

[3]   J.T. Tough, in Progress in Low Temperature Physics, Vol VIII, D.F. Brewer, ed, (North-Holland, Amsterdam, 1982), Ch. 3.

[4]   G. Marees, and H. van Beelen, Physica **133B**, 21 (1985).

[5]   K.W. Schwarz, Phys. Rev. Lett. **49**, 283 (1982).

[6]   P.G. Saffman, and G.R. Baker, Ann. Rev. Fluid Mech. **11**, 95 (1979).

[7]   A. Leonard, Ann. Rev. Fluid Mech. **17**, 323 (1985).

[8]   See for example the articles in Chaos, A.V. Holden, ed. (Manchester University Press, Manchester, 1986).

[9]   H. Haucke, and R. Ecke, Physica **25D**, 307 (1987).

[10]   C.E. Swanson, and R.J. Donnelly, J. Low Temp. Phys. **67**, 185 (1987).

[11]   K.R. Sreenivasan, and R. Ramshankar, Physica **23D**, 246 (1986).

[12]   G. Marees, R.F. Mudde, and H. van Beelen, Physica **144B**, 292 (1987).

[13]   R. Radebaugh, NBS Technical Note 362 (1967).

[14]   J.C. Wheatley, Am. J. Phys. **36**, 181 (1968).

[15]   J.C. Wheatley, R.E. Rapp, and R.T. Johnson, J. Low Temp. Phys.
       4, 1 (1971).

[16]   G.M. Coops, A.T.A.M. de Waele, and H.M. Gijsman, Phys. Rev.
       B25, 4879 (1982);
       C.A.M. Castelijns, J.G.M. Kuerten, A.T.A.M. de Waele,
       and H.M. Gijsman, Phys. Rev. **B32**, 2870 (1985).

[17]   J. Zeegers, J.G.M. Kuerten, A.T.A.M. de Waele,
       and H.M. Gijsman, to be published.

II THERMODYNAMICS OF ^{3}He-^{4}He MIXTURES[1]

2.1 *Introduction*

The thermodynamic properties of liquid ^{3}He-^{4}He mixtures are of great practical importance for low temperature physics. In 1967 Radebaugh performed calculations of these properties with applications to the ^{3}He-^{4}He dilution refrigerator [1]. Since that time, however, measurements on the osmotic pressure [2,3] and the osmotic enthalpy [4] have been performed that do not agree with Radebaugh's results. Therefore, it was necessary to recalculate the thermodynamic quantities. A new calculation scheme is used, starting from experimentally determined values of the osmotic pressure of the mixture and the molar volume and specific heat of the mixture and the pure substances. The calculations are restricted to temperatures below 250 mK, where the deviations from the Landau-Pomeranchuk quasiparticle spectrum as observed by Greywall [5] can be neglected. In the main part of this chapter the pressure is chosen to be equal to zero.

In section 2 the thermodynamic relations at zero pressure are given. The calculation scheme for the numerical results is presented in section 3. In section 4 applications of the calculations to ^{3}He-^{4}He dilution refrigeration are given in the low-temperature approximation. The results of the calculations are presented in section 5. In section 6 the calculation is extended to include first order terms in the pressure. A comparison with the measurements and with Radebaugh's calculations is made in section 7.

2.2 *Thermodynamics of ^{3}He-^{4}He mixtures at zero pressure*

In this section the thermodynamic relations for ^{3}He-^{4}He mixtures at zero pressure will be derived. The thermodynamics of a general two-component mixture is treated extensively by Guggenheim [6]. His results can also be used for ^{3}He-^{4}He mixtures. They will be extended to incorporate a phenomenological relation for the specific heat. A basic thermodynamic relation for a two-component mixture is the Gibbs-Duhem equation, which shows that the temperature T, the pressure p, and the molar chemical potentials of both components cannot be independently variable, but are related. The Gibbs-Duhem equation for a ^{3}He-^{4}He mixture reads:

$$x d\mu_3 + (1-x) d\mu_4 = -S_m dT + V_m dp \quad , \tag{1}$$

where x is the molar ^{3}He concentration, S_m the molar entropy and V_m the molar volume of the mixture; μ_3 and μ_4 are the molar chemical potentials of the ^{3}He and ^{4}He components respectively.

In general, the entropy of the mixture can be written in terms of the partial entropies S_3 and S_4 of the two components:

$$S_m = x S_3 + (1-x) S_4 \quad . \tag{2}$$

The partial entropies are defined as:

$$S_3 = (\partial S/\partial N_3)_{p,T,N_4} \tag{3a}$$

and

$$S_4 = (\partial S/\partial N_4)_{p,T,N_3} \quad , \tag{3b}$$

where N_3 and N_4 are the numbers of moles of ^{3}He and ^{4}He respectively and S is the total entropy. It follows that

$$S_3 = S_m + (1-x)(\partial S_m/\partial x)_{T,p} \tag{4}$$

and

$$S_4 = S_m - x(\partial S_m/\partial x)_{T,p} \quad . \tag{5}$$

10

In order to calculate the entropy of the mixture the experimental observation [5,7] that the molar specific heat of the mixture, C_m, can be written as:

$$C_m = xC_{vF} + (1-x)C_{v4}^0 \quad , \tag{6}$$

will be the starting point. In this equation C_{v4}^0 is the molar specific heat of pure ^{4}He at constant volume and C_{vF} is the specific heat at constant volume of an ideal Fermi gas at the same quasiparticle density as the ^{3}He particle density in the mixture and with effective quasiparticle mass m^x. Equation (6) is only valid for temperatures below 0.25 K [5] and ^{3}He concentrations below 0.3 [1]. In general, the superscript ^{0} refers to a pure substance, and the subscripts 3 and 4 refer to ^{3}He and ^{4}He respectively.

The specific heat of an ideal Fermi gas is a function of the reduced temperature $t = T/T_F$ only, where T_F is the Fermi temperature of the quasiparticle gas, given by:

$$T_F = \frac{\hbar^2}{2m^x k} \left[3\pi^2 \frac{xN_A}{V_m} \right]^{2/3} \quad . \tag{7}$$

where k is Boltzmann's constant and N_A Avogadro's number [8].

From the specific heat, other thermodynamic quantities can be derived. For example, the entropy of the quasiparticle gas, S_F, is related to its specific heat according to:

$$S_F = \int_0^T \frac{C_{vF}(T',x)}{T'} \, dT' = \int_0^{T/T_F} \frac{C_{vF}(t)}{t} \, dt \quad . \tag{8}$$

The entropy at absolute zero is independent of the ^{3}He concentration, in accordance with the Third Law, and is taken equal to zero. With equation (6) the entropy of the mixture can be written as:

$$S_m = xS_F + (1-x)S_4^0 \quad . \tag{9}$$

where S_4^0 is the molar entropy of pure ^{4}He. From equations (4), (5) and (9) it follows that:

$$S_3 = S_F + x(1-x)(\partial S_F/\partial x)_{T,p} \qquad (10)$$

and

$$S_4 = S_4^0 - x^2(\partial S_F/\partial x)_{T,p} \quad . \qquad (11)$$

In Fig. 1 a graphical construction of the different entropies is given. In this figure S_m is plotted as a function of x at constant temperature. According to equations (4) and (5) the partial entropies can be found as the intersections of the tangent to this curve with both vertical axes. The entropy of pure ^{4}He is the value of S_m at $x = 0$. The straight line connecting this point with the point $(x = 1$; $S = 0)$ is $(1-x)S_4^0$. Hence, using equation (9), the value of xS_F can be found.
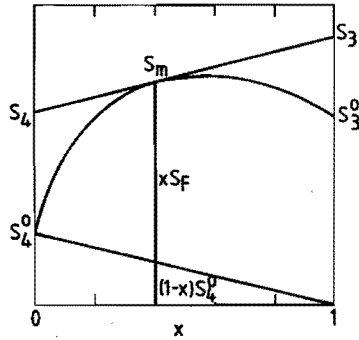
Fig. 1 *Graphical construction of the partial entropies S_3 and S_4, and the entropy of the Fermi gas S_F, from the total entropy of the mixture as a function of x. The plotted curve does not correspond to the actual situation.*

The chemical potential of the ideal quasiparticle gas follows from

$$\mu_F = U_F + p_F V_F - T S_F \quad , \qquad (12)$$

where V_F is the molar volume (equal to V_m/x) and p_F the pressure of the quasiparticle gas; U_F is the molar internal energy, given by:

$$U_F = U_{OF}(x) + \int_0^T C_{vF}(T',x)dT' = U_{OF}(x) + T_F \int_0^{T/T_F} C_{vF}\, dt \quad . \quad (13)$$

where U_{OF} is the internal energy at zero temperature. Taking the potential energy of the quasiparticle gas equal to zero, p_F is related to U_F by [8]

$$p_F V_F = \frac{2}{3} U_F \quad . \tag{14}$$

Thus

$$\mu_F = \mu_{OF}(x) + \frac{5}{3} T_F \int_0^{T/T_F} C_{vF}\, dt - TS_F(T,x) \quad , \tag{15}$$

where $\mu_{OF} = \frac{5}{3} U_{OF}$ can be identified as the chemical potential at zero temperature which is equal to

$$\mu_{OF} = RT_F \quad . \tag{16}$$

With equation (9) and $p = 0$, the Gibbs–Duhem relation (1) simplifies to

$$d\mu_3 = -\frac{1-x}{x} d\mu_4 - (S_F + \frac{1-x}{x} S_4^0)dT \quad . \tag{17}$$

There are various ways to define the osmotic pressure Π. The one commonly used is the implicit definition [2]

$$\mu_4(p,T,x) = \mu_4(p-\Pi,T,0) \quad . \tag{18}$$

At zero pressure and the temperatures and ^{3}He concentrations in consideration, the right hand side of equation (18) can be expanded, yielding

$$\mu_4(T,x) = \mu_4^0(T) - V_4^0\Pi(T,x) \quad , \tag{19}$$

13

where V_4^0 is the molar volume (which is constant in this temperature region [9]), and μ_4^0 the molar chemical potential of pure ^{4}He respectively. From the relation

$$(\partial\mu_4/\partial T)_x = -S_4 \qquad (20)$$

and equation (11), it follows that

$$(\partial\Pi/\partial T)_x = -\frac{x^2}{V_4^\sigma}(\partial S_F/\partial x)_T + \frac{1}{V_4^\sigma}(S_4^0 + \partial\mu_4^0/\partial T) \quad . \qquad (21)$$

The last term on the right hand side equals zero. Thus

$$(\partial\Pi/\partial T)_x = -\frac{x^2}{V_4^\sigma}(\partial S_F/\partial x)_T \quad . \qquad (22)$$

By differentiating equation (8) with respect to x, keeping T constant, it follows that

$$(\partial S_F/\partial x)_T = -\frac{1}{T_F}\frac{dT_F}{dx}C_{vF} \quad . \qquad (23)$$

Substitution in equation (22) and integration over T yields

$$\Pi(T,x) = \Pi_0(x) + \frac{x^2}{V_4^\sigma}\frac{dT_F}{dx}\int_0^{T/T_F}C_{vF}\,dt \quad , \qquad (24)$$

where $\Pi_0(x)$ is the osmotic pressure at zero temperature. This expression shows that the osmotic pressure at nonzero temperatures can be calculated from the osmotic pressure at zero temperature and the specific heat of the quasiparticle gas, if the x-dependence of T_F is known.

The chemical potential of the ^{4}He component follows from equations (19) and (24).

Substitution of equation (19) in (17) yields an equation for the total differential of the ^{3}He chemical potential:

$$d\mu_3 = \frac{1-x}{x} V_4^0 \, (\partial\Pi/\partial x)_T \, dx + \left[\frac{1-x}{x} V_4^0 (\partial\Pi/\partial T)_x - S_F\right] dT \quad . \tag{25}$$

The chemical potential of the ^{3}He component follows by integration, first at zero temperature from x_0, the ^{3}He concentration of the saturated solution at $T = 0$, to x and then at constant ^{3}He concentration from $T = 0$ to temperature T. The result is

$$\mu_3(T,x) = \mu_3(0,x_0)$$

$$+ V_4^0 \left[\frac{1-x}{x} \Pi_0(x) - \frac{1-x_0}{x_0} \Pi_0(x_0) + \int_{x_0}^{x} \frac{1}{x'^2} \Pi_0(x')dx'\right]$$

$$- TS_F(T,x) + \left\{(1-x)x \frac{dT_F}{dx} + T_F\right\} \int_0^{T/T_F} C_{vF} \, dt \quad , \tag{26}$$

where integration by parts has been used to write

$$\int_0^T S_F \, dT' = TS_F - \int_0^T T' (\partial S_F/\partial T)_x dT' \quad .$$

In general the zero points of the chemical potentials of two components can be chosen independently, as long as no chemical reactions between the two components take place (see the appendix). In the presentation of the numerical results this freedom of choice is used to set the chemical potentials of the pure liquids of ^{3}He and ^{4}He equal to zero at zero temperature. As a result, $\mu_3(0,x_0)$ is equal to zero.

The molar Gibbs free energy is given by

$$G_m = x\mu_3 + (1-x)\mu_4 \quad . \tag{27}$$

If G_m is known as a function of T and x, all other thermodynamic quantities can be calculated. The molar enthalpy of the mixture H_m is given by

$$H_m = G_m + TS_m \quad . \tag{28}$$

Using equations (19),(24) and (26), H_m can be written as

$$H_m = xV_4^o \left\{ \int_{x_0}^{x} \frac{1}{x'^2} \Pi_0(x')dx' - \frac{1-x_0}{x_0} \Pi_0(x_0) \right\}$$

$$+ xT_F \int_0^{T/T_F} C_{vF} \, dt + (1-x)H_4^o(T) \quad , \tag{29}$$

where H_4^o is the molar enthalpy of pure ^{4}He.

In chapter IV it is derived that conservation of energy in adiabatic ^{3}He flow experiments leads to a conserved quantity [4,9,10], given by

$$H_3^{os}(T,x) = \mu_3(T,x) + TS_F(T,x) + \frac{1-x}{x} TS_4^o(T) \quad . \tag{30}$$

Following Ebner and Edwards [9] this quantity is called the osmotic enthalpy per mole ^{3}He. For low temperatures and not too low ^{3}He concentrations the last term on the right hand side is negligible. Then H_3^{os} is equal to the enthalpy of the quasiparticle gas, H_3^x, introduced in reference 11 and to the quantity H_3, introduced by Radebaugh [1]. When one component of a classical mixture flows with respect to the rest of the fluid, the conserved quantity is the partial enthalpy of the flowing component. In ^{3}He–^{4}He II mixtures the superfluid component carries no entropy. Hence, the conserved quantity differs from the partial ^{3}He enthalpy which is normally indicated by H_3, and given by

$$H_3 = \mu_3 + TS_3 \quad . \tag{31}$$

From equations (10) and (11) it can be seen that the two enthalpies H_3 and H_3^{os} differ by a term

$$H_3^{os} - H_3 = \frac{1-x}{x} TS_4 \quad . \tag{32}$$

which is generally not negligible (see equations (11) and (23)).

16

The quantity μ_3' is defined as [1,12]

$$\mu_3'(T,x) = \mu_3(T,x) - \mu_F(T,x) \quad . \tag{33}$$

Since μ_F is the chemical potential of a noninteracting Fermi gas of quasiparticles with the same effective mass and density as the ^{3}He quasiparticle gas, μ_3' can be interpreted as the potential energy of the ^{3}He due to interactions.

With the molar specific heat of pure ^{3}He, C_{v3}^0, the thermodynamic quantities of pure ^{3}He can be calculated. The entropy is given by

$$S_3^0 = \int_0^T \frac{C_{v3}^0(T')}{T'} \, dT' \quad ; \tag{34}$$

the internal energy by

$$U_3^0 = \int_0^T C_{v3}^0 \, dT' \quad . \tag{35}$$

The enthalpy and internal energy are equal, since the pressure equals zero. Hence,

$$H_3^0 = U_3^0 \quad . \tag{36}$$

The chemical potential equals

$$\mu_3^0 = U_3^0 - TS_3^0 \quad . \tag{37}$$

Analogous relations hold for pure ^{4}He.

The excess enthalpy H^E is defined as the increase in enthalpy when the mixture is produced from the pure components at constant temperature and pressure:

$$H^E = H_m(T,x) - xH_3^0(T) - (1-x)H_4^0(T) \quad . \tag{38}$$

It follows from the condition of thermodynamic equilibrium that in a saturated solution the chemical potential of the ^{3}He component is

17

equal to the ^{3}He chemical potential of the concentrated phase at the same temperature. At low temperatures the concentrated phase mainly consists of pure ^{3}He and the ^{4}He in it will be neglected (see chapter I). The equation of the phase separation curve, $x_s(T)$, then follows from

$$\mu_3\{T,x_s(T)\} = \mu_3^0(T) \quad . \tag{39}$$

It follows, as noted before, that

$$\mu_3(0,x_0) = \mu_3^0(0) = 0 \quad . \tag{40}$$

Since the ^{3}He chemical potential is by definition the partial Gibbs free energy of the ^{3}He component [6]

$$\mu_3 = G_m + (1-x)(\partial G_m/\partial x)_T \quad , \tag{41}$$

the concentration of a saturated solution can be found from the graph of $G_m(x)$, as shown in Fig. 2. Similar as in Fig. 1, the partial chemical potentials μ_3 and μ_4 can be found from the intersections of this curve with both vertical axes. Furthermore, μ_3^0 is the value of $G_m(x)$ at $x = 1$. From equation (39) it follows that x_s is the value of x, where μ_3 equals μ_3^0 and hence where the tangent to $G_m(x)$ intersects the line $x = 1$ at μ_3^0.
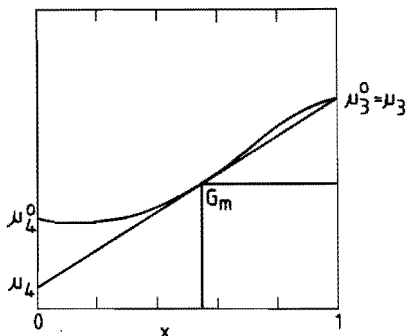
Fig. 2 *Graphical construction of the concentration of the saturated solution. The value of x_s corresponds with the concentration where the tangent to G_m intersects the line $x = 1$ in μ_3^0.*

2.3 *Calculation scheme and experimental data*

With the relations derived in the preceding section a scheme is constructed, according to which all thermodynamic quantities can be calculated. It is shown in Fig. 3a. The quantities on the top line were deduced from experiments. The dependence of C_{vF} on the reduced temperature t was calculated and tabulated by Stoner [13]. It is not possible to approximate these tabulated values by a simple polynomial over the whole t region. Radebaugh [1] has divided the domain of the reduced temperature into three regions and fitted a power series in t to Stoner's values in each region. His fit is, however, not continuously differentiable at the boundaries of the regions. In this work Radebaugh's results for t < 0.15 and t > 0.7 are used. Another polynomial is fitted to Stoner's values in the intermediate region, requiring that the specific heat is continuously differentiable at the boundaries. This requirement is necessary to avoid discontinuities in derived quantities. The result is:

$$\frac{C_{vF}}{R} = \sum_{j=0}^{4} A_{1j} t^{2j+1} \qquad \text{for } t \leq 0.15,$$

$$\frac{C_{vF}}{R} = \sum_{j=0}^{6} A_{2j} t^{j} \qquad \text{for } 0.15 \leq t \leq 0.7,$$

and

$$\frac{C_{vF}}{R} = \sum_{j=0}^{3} A_{3j} t^{-3j/2} \qquad \text{for } 0.7 \leq t, \qquad (42)$$

where R is the molar gas constant. The coefficients A_{ij} are given in Table I.
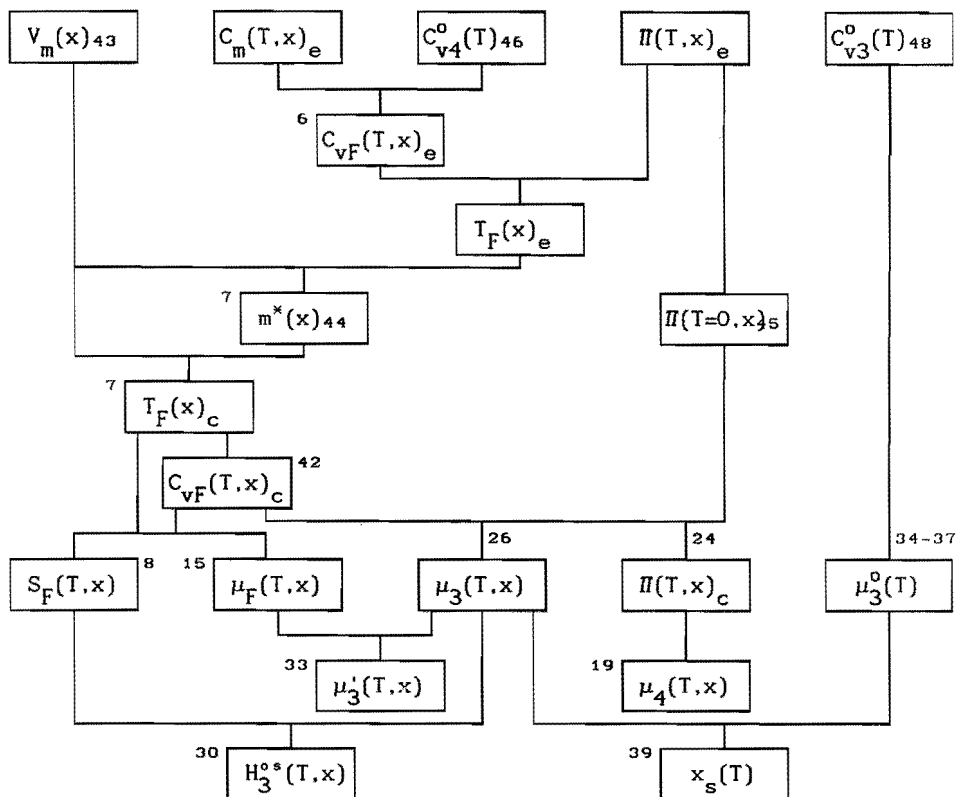
Fig. 3a *The calculation scheme used in this work. The quantities on the top line are the input data. The subscripts e and c refer to quantities deduced from experiments and calculated quantities respectively. The numbers correspond with the equations in this chapter. For some quantities the dependence on the thermodynamic properties of pure* ^{4}*He is not indicated.*
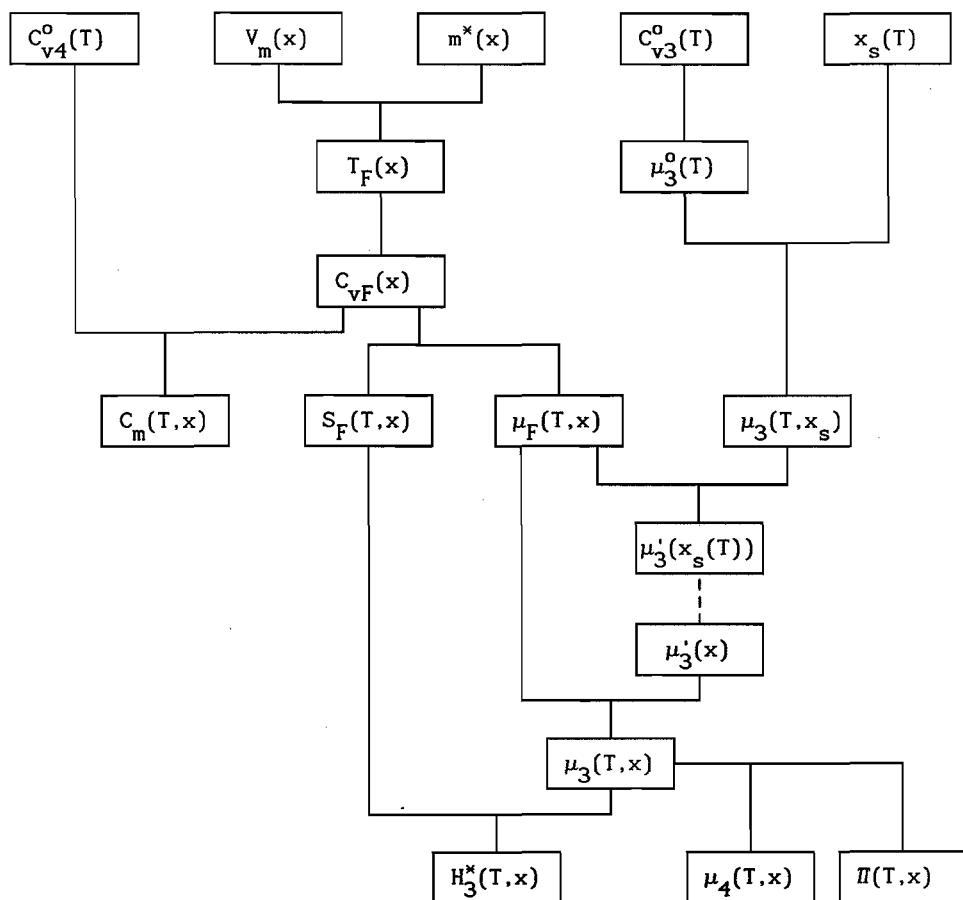
Fig. 3b The calculation scheme used by Radebaugh [1]. The dashed line
means that a theoretical extrapolation has been used.

Table I.

The coefficients A_{ij} from equation (42).

i	A_{1i}	A_{2i}	A_{3i}
0	4.934802	-0.201414	1.5
1	-14.400636	8.910152	-0.09973557
2	-167.8453	-27.147564	0.00560236
3	-4313.1735	56.254979	-0.00024872
4	203138.64	-77.719454	-
5	-	62.61363	-
6	-	-21.64979	-

As mentioned before, the molar volume of the mixture is tempera-ture independent at low temperatures. The concentration dependence is given by [3]

$$V_m(x) = V_4^0(1+\alpha x) \quad , \tag{43}$$

where the molar volume of pure ^{4}He, $V_4^0 = 27.58 \times 10^{-6}$ m^{3}mol^{-1} and $\alpha = 0.286$.

The value of the effective quasiparticle mass has been determined experimentally by measuring the specific heat [5,7], the osmotic pres-sure [2] or the velocity of second sound [5]. From these measurements it was found that m^x is slightly x-dependent. However, the results are not consistent [5]. In this calculation a concentration independent value of the effective mass is used:

$$m^x = 2.46 \ m_3 \quad , \tag{44}$$

where m_3 is the mass of the bare ^{3}He atom. This value is consistent with specific-heat measurements at concentrations of 1-5% [7] and fits the specific-heat measurements at low concentrations [5] within 1%. Also, as will turn out later, it fits the measurements of the osmotic pressure and the T-x dependence of the phase separation curve. This choice of the value of the effective mass will be discussed in more detail in section 2.7.

22

With equations (7) and (42) to (44) the specific heat of the quasiparticle gas can be calculated as a function of T and x.

Measurements of the osmotic pressure were performed by Landau *et al.* [2,14] and by Ghozlan *et al.* [3]. The fit to a theoretical formula of Varoquaux [15] of Landau's results for T = 0, yields:

$$\Pi_0(x) = 3.092 \times 10^5 \left[\frac{x}{1+\alpha x}\right]^{5/3} - 1.32 \times 10^5 \left[\frac{x}{1+\alpha x}\right]^2$$

$$- 6.91 \times 10^5 \left[\frac{x}{1+\alpha x}\right]^{8/3} \text{Pa.} \tag{45}$$

This formula is based on measurements for concentrations below x_0. In principle it might not be valid at higher concentrations. However, the calculated phase separation curve agrees with measurements up to x = 8%. Therefore, equation (45) will be used for concentrations up to 8%. The osmotic pressure at temperatures above zero can be obtained, using equations (24) and (45). The results fit Landau's data [2] within 1%.

The molar specific heat of pure ^{4}He was measured by Greywall for 0.14 K < T < 0.86 K [16]. He fitted a polynomial to his data for low temperatures, yielding:

$$C_{v4}^0 = \sum_{i=0}^{4} B_i T^{i+3} \qquad \text{for } T < 0.4 \text{ K.} \tag{46}$$

The coefficients B_i are given in Table II. From a theoretical formula for the phonon contribution to the specific heat it is expected that this formula will be valid for temperatures down to zero kelvin [16].

Different measurements of x_0 do not give the same result [17]. The value used here,

$$x_0 = 0.066 \quad , \tag{47}$$

is consistent with the measurements of Ref. 19.

The specific heat of pure ^{3}He at zero pressure was measured by Greywall [18]. He fitted mathematical expressions to his measurements,

dividing the temperature domain into two regions. However, the fit at higher temperatures cannot be integrated analytically. Therefore, a polynomial is fitted to the data for temperatures between 100 and 450 mK, imposing the condition that C_{v3}^0 is continuously differentiable at T = 100 mK. The result is

$$\frac{C_{v3}^0}{R} = \sum_{j=1}^{5} C_{ij} T^j \qquad \begin{array}{l} i = 1 \text{ for } T \leq 0.1 \text{ K} \\ i = 2 \text{ for } 0.1 \text{ K} \leq T \leq 0.45 \text{ K}. \end{array} \qquad (48)$$

The coefficients C_{ij} are given in Table II. This formula fits the measurements within 1%.

The concentration of the saturated solution, x_s, was obtained as a function of temperature by solving equation (39) numerically. To the values of x_s obtained in this way, a polynomial fit in T results in:

$$x_s(T) = x_0 + \sum_{i=2}^{5} D_i T^i \quad , \qquad (49)$$

The coefficients D_i are given in Table II. For concentrations up to 8% equation (49) agrees within experimental error with measurements of Abraham et al. [19]. For higher concentrations there are deviations

Table II.
The coefficients B_i, C_{ij} and D_i from equations (46), (48) and (49).

i	B_i	C_{1i}	C_{2i}	D_i
0	0.08137	–	0.0245435	–
1	0	2.7415	1.85688	–
2	-0.0528	0	9.39988	0.5056
3	0.05089	-61.78929	-117.910	-0.2488
4	0.019	-177.8937	440.368	18.22
5	–	2890.0675	-735.836	-74.22
6	–	0	468.741	–

between equation (49) and experiment. This is to be expected, since equation (45) yields for higher concentrations a decreasing value for $\Pi_0(x)$, which is not consistent with measurements. Therefore, equation (49) is in good agreement with measurements for temperatures below 150 mK.

2.4 *Applications to dilution refrigeration*

In chapter IV the basic properties of a ^{3}He circulating dilution refrigerator are explained. Consider a ^{3}He–^{4}He dilution refrigerator in which $\dot{n}_3$ moles of pure ^{3}He are circulated per second. The mixing chamber is sketched in Fig. 4. The temperature in the mixing chamber is T_m, the temperature of the incoming ^{3}He is T_i and the cooling power is $\dot{Q}$. As will be shown in chapter IV, the enthalpy balance of the mixing chamber can be written as

$$\dot{Q} + \dot{n}_3 H_3^0(T_i) = \dot{n}_3 H_3^{0s}\{T_m, x_s(T_m)\} \quad . \tag{50}$$

Furthermore,

$$\mu_3^0(T_m) = \mu_3\{T_m, x_s(T_m)\} \quad . \tag{51}$$
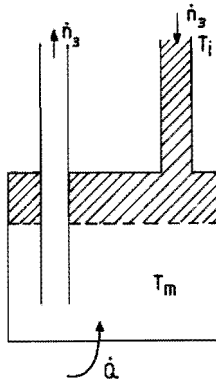
Fig. 4 *The mixing chamber of a ^{3}He circulating dilution refrigerator. The temperatures of the incoming ^{3}He and of the mixing chamber are T_i and T_m respectively. The cooling power is $\dot{Q}$.*

The maximum cooling power of the dilution refrigerator is reached in the limit that $T_i = T_m = T$. There holds

$$H_3^0(T) = \mu_3^0(T) + TS_3^0(T)$$

and

$$H_3^{os}\{T,x_s(T)\} = \mu_3\{T,x_s(T)\} + TS_F\{T,x_s(T)\}$$

$$= \mu_3^0(T) + TS_F\{T,x_s(T)\} \quad ,$$

where equation (51) has been used. A measure for the cooling power is the quantity γ, defined as:

$$\gamma = \frac{\dot{Q}}{\dot{n}_3 T^2} = \frac{H_3^{os}\{T,x_s(T)\} - H_3^0(T)}{T^2} \quad . \tag{52}$$

It follows that

$$\gamma = \frac{S_F\{T,x_s(T)\} - S_3^0(T)}{T} \quad . \tag{53}$$

The minimum mixing chamber temperature is reached if $\dot{Q} = 0$. Equation (50) then reads:

$$H_3^0(T_i) = H_3^{os}\{T_m,x_s(T_m)\} \quad . \tag{54}$$

Some thermodynamic properties will be calculated in the low temperature limit, where terms of higher order than T^2 and $x-x_0$ can be neglected.

First the equation of the phase separation curve is calculated. The chemical potentials in equation (51) can be expanded in the following way:

26

$$\mu_3(T,x) = V_4^0 \frac{1-x_0}{x_0} \frac{d\Pi_0}{dx}\bigg|_{x_0} (x-x_0)$$

$$+ \frac{1}{2}\left\{(1-x_0)x_0 \frac{dT_F}{dx}\bigg|_{x_0} - T_F(x_0)\right\} RA_{10} \frac{T^2}{T_F^2(x_0)}$$

$$= 17.58 \ (x-x_0) - 20.28 \ T^2 \tag{55}$$

and

$$\mu_3^0(T) = -\frac{1}{2} C_{11} RT^2 = -11.40 \ T^2 \quad, \tag{56}$$

with A_{10} and C_{11} given in Table I. Substitution in equation (51) yields:

$$x_s(T) = x_0 + 0.5056 \ T^2 \quad. \tag{57}$$

in accordance with equation (49).

    In the same limit it follows from equation (53):

$$\gamma = R\left[\frac{A_{10}}{T_F(x_0)} - C_{11}\right] = 81.54 \ \text{J mol}^{-1} \ \text{K}^{-2} \quad. \tag{58}$$

When the first order terms of the enthalpies are substituted, equation (54) yields

$$\left[\frac{T_i}{T_m}\right]^2 = \frac{2A_{10}}{C_{11}T_F(x_0)} - 1 = 8.156 \quad.$$

Thus the minimum temperature is directly related to the temperature of the incoming ^{3}He, according to:

$$T_i = 2.856 \ T_m \quad. \tag{59}$$

As follows from equation (46), in the low temperature limit the ^{4}He contribution to the osmotic enthalpy can be neglected. This quantity is given by

$$H_3^{os}(T,x) = 17.58\ (x-x_0) + 84.06\ T^2 \quad . \tag{60}$$

The T-x dependence of the isenthalps is given by

$$T^2 + \beta x = \text{constant}, \tag{61}$$

where $\beta = 0.209\ K^2$. In the low temperature limit the osmotic enthalpy is equal to Radebaugh's H_3. Therefore, the same linear relationship between T^2 and x must hold for lines of constant H_3.

As a last property the osmotic pressure along the phase separation curve is computed. From the approximation for the osmotic pressure:

$$\Pi(T,x) = \Pi_0(x_0) + \left.\frac{d\Pi_0}{dx}\right|_{x_0} (x-x_0) + \frac{1}{2}\ A_{10}R\ \frac{x_0^2}{V_4^0}\left.\frac{dT_F}{dx}\right|_{x_0}\ \frac{T^2}{T_F^2(x_0)} \quad ,\tag{62}$$

and equation (57) for the phase separation curve, it follows that

$$\Pi_s(T) = 2209 + 1.044 \times 10^5\ T^2\ \text{(Pa)}. \tag{63}$$

This result agrees with the experimental values of Varoquaux [15] and of Landau et al. [2], within experimental accuracy.

2.5 Results

In reference 20 the thermodynamic quantities, defined above and calculated according to the scheme described above are listed as functions of x and T, together with the fountain pressure of pure ^{4}He, defined as:

$$P_f = -\ \{\mu_4^0(T)-\mu_4^0(0)\}/V_4^0 \quad . \tag{64}$$
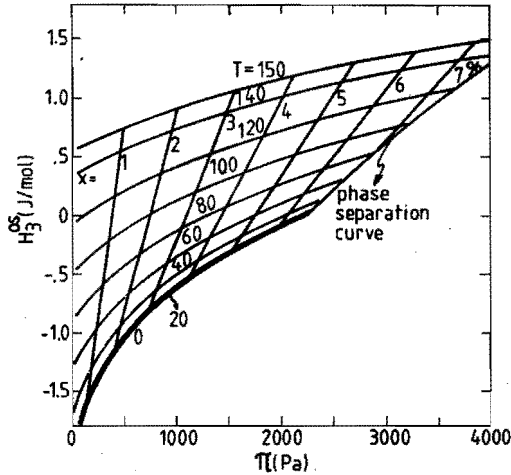
Fig. 5   The H_3^{os}-Π diagram with isotherms (T in mK), lines of constant
         ^{3}He concentration and the phase separation curve, resulting
         from the calculations described here.

In Fig. 5 the H_3^{os}-Π diagram with isotherms, lines of constant x
and the phase separation curve is shown. Figure 6 is the inverse dia-
gram: a T^2-x diagram with lines of constant osmotic pressure (iso-
tones), isenthalps and the phase separation curve. From the latter
diagram it can be seen that the linear relationship between T^2 and x
of the isenthalps, as expressed by equation (61), is in good approxi-
mation valid in a large T-x region: x > 0.02 and T < 100 mK.

2.6 _Thermodynamics of ^{3}He-^{4}He mixtures at nonzero pressures_

In this section the calculation of the thermodynamics of ^{3}He-^{4}He
mixtures is extended to nonzero pressures. In the results only the
first order terms in the pressure will be maintained. This restricts
the validity to pressures below about 10^4 Pa, which is the region of
interest for the following chapters. At these pressures ^{3}He-^{4}He
mixtures do not undergo a phase transition in the region of interest.
Therefore, the thermodynamic quantities are smooth functions of the
pressure and can be obtained from an expansion in powers of p.
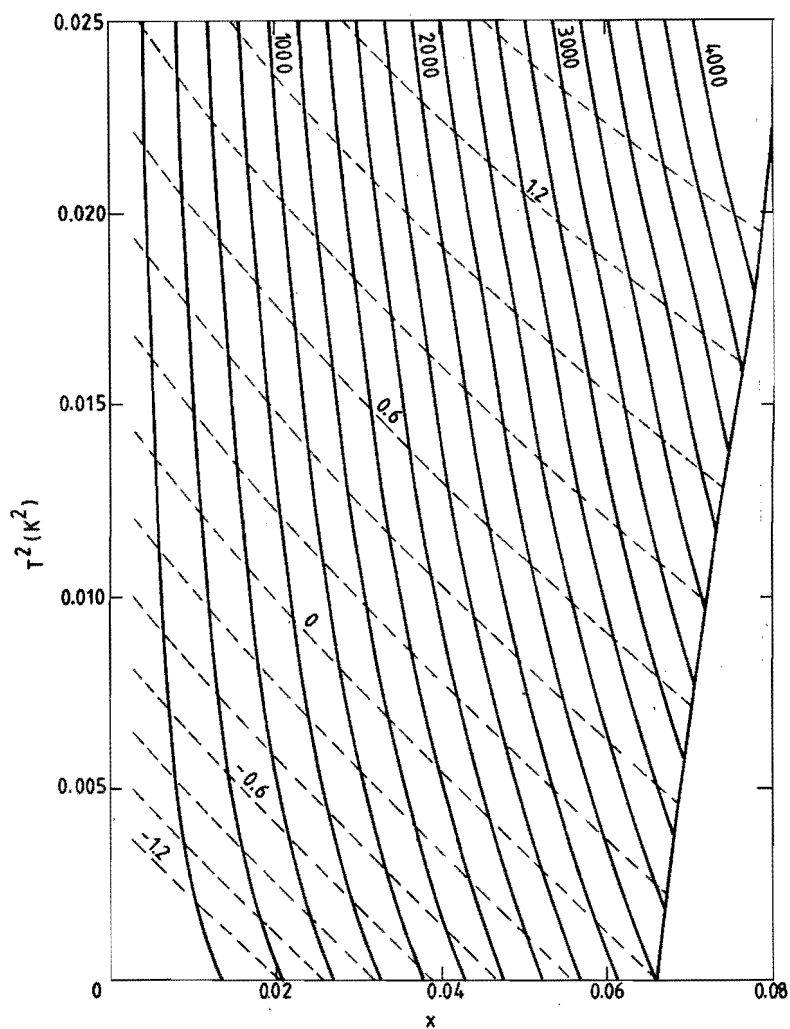
Fig. 6 The T^2-x diagram with isenthalps (dashed), isotones (full) and
the phase separation curve (fat). (Π in Pa and $H_3^{o\,s}$ in J/mol).

As a first example the ^{4}He chemical potential satisfies [6]

$$(\partial\mu_4/\partial p)_{T,x} = V_4 \quad . \tag{65}$$

where V_4 is the partial volume of the ^{4}He component, defined in the same way as S_4. The expansion of μ_4 in powers of p follows as

$$\mu_4(p,T,x) = \mu_4(0,T,x) + V_4(0,T,x)p + \frac{1}{2}\left.\frac{\partial V_4}{\partial p}\right|_{p=0} p^2 + .. \tag{66}$$

The partial volume of the ^{4}He component can be derived from the molar volume of the mixture, which is given by [2]

$$V_m(p,T,x) = V_4^0(p)\{1 + x\alpha(p)\} \quad . \tag{67}$$

In this equation the thermal expansion and the x-dependence of α, which both are small at low temperature and ^{3}He concentration [2], have been neglected. From equation (67) V_4 follows as

$$V_4(p,T,x) = V_4^0(p) \quad . \tag{68}$$

So, to first order in the pressure the ^{4}He chemical potential equals

$$\mu_4(p,T,x) = \mu_4(0,T,x) + V_4^0(0)p \quad . \tag{69}$$

The second order term equals

$$\frac{1}{2}(\partial V_4^0/\partial p)_{p=0} p^2 = -\frac{1}{2}V_4^0(0)\kappa_4(0)p^2 \quad , \tag{70}$$

where $\kappa_4(p)$ is the compressibility of pure ^{4}He, which equals 1.2×10^{-7} Pa^{-1} at zero pressure [21]. Hence, neglecting the second order term in p is valid if $p \ll 1/\kappa_4(0) \simeq 8\times10^6$ Pa.

The osmotic pressure at arbitrary pressure follows from its definition (equation (18)) as

$$\mu_4(p,T,x) = \int_0^{-\Pi(p,T,x)} V_4^0(p',T)dp' + \mu_4^0(p,T) \quad . \tag{71}$$

In the region of interest Π is of the order of 1000 Pa. Hence, equation (71) can be approximated by the first order term in Π, yielding

$$\Pi(p,T,x) = -\frac{1}{V_4^0(p)} \{\mu_4(p,T,x) - \mu_4^0(p,T)\} \quad . \tag{72}$$

Using equation (69) and (19) this gives to first order in p

$$\Pi(p,T,x) = \Pi(0,T,x)\{1 + \kappa_4(0)p\} \quad . \tag{73}$$

In this case the first order term is negligible in all situations of interest.

For the ^{3}He chemical potential the following relation holds

$$(\partial\mu_3/\partial p)_{T,x} = \mathcal{V}_3 \quad , \tag{74}$$

where $\mathcal{V}_3$ is the partial volume of the ^{3}He component, equal to

$$\mathcal{V}_3(p,T,x) = V_4^0(p)\{1 + \alpha(p)\} \quad . \tag{75}$$

So to first order in p the ^{3}He chemical potential equals

$$\mu_3(p,T,x) = \mu_3(0,T,x) + V_4^0(0)\{1+\alpha(0)\}p \quad . \tag{76}$$

The expansion of the molar entropy can be found from the Maxwell relation

$$(\partial S_m/\partial p)_{T,x} = -(\partial V_m/\partial T)_{p,x} \quad . \tag{77}$$

The right hand side of equation (77) is proportional to the cubic expansion coefficient, which is negligible at low temperatures. Hence, to first order the molar entropy is independent of pressure. Without any approximation equation (77) yields a differential equation for the effective mass as a function of pressure in the following way. From equation (9) follows

$$(\partial S_m/\partial p)_{T,x} = (1-x)(\partial S_4^o/\partial p)_T + x(\partial S_F/\partial p)_{T,x} \quad . \tag{78}$$

Furthermore

$$(\partial S_4^o/\partial p)_T = -(\partial V_4^o/\partial T)_p \tag{79}$$

and

$$(\partial S_F/\partial p)_{T,x} = -C_{vF} \frac{1}{T_F} (\partial T_F/\partial p)_{T,x} \quad . \tag{80}$$

where T_F is a function of p through V_m and $m^{\times}$. From equation (67), where in general V_4^o and α also depend on T follows

$$(\partial V_m/\partial T)_{p,x} = (\partial V_4^o/\partial T)_p + x \left[\frac{\partial}{\partial T}(\alpha V_4^o)\right]_{p,x} \quad . \tag{81}$$

Substitution in equation (77) yields, using (7)

$$-C_{vF} \left\{\frac{1}{m^{\times}} \frac{\partial m^{\times}}{\partial p} + \frac{2}{3} \frac{1}{V_m} \frac{\partial V_m}{\partial p}\right\} = \frac{\partial}{\partial T}\{V_4^o(1 + \alpha)\} \quad . \tag{82}$$

In principle, with this equation it is possible to calculate $m^{\times}$ at arbitrary pressure, if it is known at zero pressure and the equation of state is known.

The molar Gibbs free energy can be calculated from equation (27). Substitution of equations (69) and (76) for the chemical potentials yields to first order in p

$$G_m(p,T,x) = G_m(0,T,x) + V_4^o(0)\{1+\alpha(0)x\}p \quad . \tag{83}$$

In the same way the molar enthalpy equals

$$H_m(p,T,x) = H_m(0,T,x) + V_4^o(0)\{1+\alpha(0)x\}p \quad . \tag{84}$$

The molar Helmholtz free energy, defined as $F_m = G_m - pV_m$, is in first order independent of pressure, since the first order term of the

molar Gibbs free energy equals pV_m. This can be seen directly from the relation

$$dF_m = -S_m dT - p dV_m + (\partial F_m/\partial x)_{V_m,T} dx, \qquad (85)$$

which gives

$$(\partial F_m/\partial p)_{T,x} = -p(\partial V_m/\partial p)_{T,x} = pV_m \kappa, \qquad (86)$$

where κ is the compressibility of the mixture. This leads in second order to

$$F_m(p,T,x) = F_m(0,T,x) + \frac{1}{2} V_m \kappa p^2 \quad . \qquad (87)$$

From equation (38) and (84) follows for the molar excess enthalpy

$$H^E(p,T,x) = H^E(0,T,x) + x\{V_4^o(0)[1+\alpha(0)]-V_3^o(0)\}p \quad . \qquad (88)$$

Finally, the osmotic enthalpy is in first order equal to

$$H_3^{os}(p,T,x) = H_3^{os}(0,T,x) + V_4^o(0)\{1+\alpha(0)\}p \quad . \qquad (89)$$

With these results, the ^{3}He concentration of a saturated solution, x_s, can be calculated at low pressures. As follows from the condition for thermodynamic equilibrium, the chemical potentials of the concentrated and dilute phases are equal. Hence, x_s satisfies the relation

$$\mu_3\{p,T,x_s(p,T)\} = \mu_3^o(p,T) \quad , \qquad (90)$$

where μ_3^o is the molar chemical potential of pure ^{3}He. Expansion in powers of p yields to first order

$$\mu_3(0,T,x_s(0,T)) + \left[\frac{\partial\mu_3}{\partial p} + \frac{\partial\mu_3}{\partial x}\bigg|_{x=x_s} \frac{\partial x_s}{\partial p}\right]p = \mu_3^o(0,T) + \frac{\partial\mu_3^o}{\partial p}p \quad . \qquad (91)$$

34

Substitution of equations (39) and (76) gives

$$\frac{\partial x_s}{\partial p} = \frac{V_3^o - V_4^o(1+\alpha)}{\partial \mu_3/\partial x} \quad . \tag{92}$$

The molar volumes of pure ^{3}He and ^{4}He have been measured by Greywall [16,18]. At zero temperature the low temperature approximation of section 4 can be used, yielding $(\partial\mu_3/\partial x)_{T=0,p=0} = 17.58$ J/mol [22]. The result is:

$$(\partial x_s/\partial p)_{T=0} = 7.70\times10^{-8} \ Pa^{-1}. \tag{93}$$

This is in good agreement with the experimentally determined values of 8.6×10^{-8} Pa^{-1} [2] and 6.6×10^{-8} Pa^{-1} [17].

In section 4 the cooling power and the minimum mixing chamber temperature of a ^{3}He circulating dilution refrigerator are calculated at zero pressure. It is possible to extend these calculations to non-zero pressures. However, the terms of first order in the pressure are smaller than the terms of higher order than T^2 and $x-x_0$, which are neglected in section 4. Therefore, the corrections due to the small pressures in the practical situation are not important for the calculated values of the cooling power and minimum temperature.

2.7 Discussion

In this section the results of our calculation are compared with the calculations of Radebaugh [1] and with experimental results.

First the choice of the value of 2.46 for the ratio m^x/m_3 is discussed. The values deduced by Greywall [5] from measurements of the second-sound velocity and the specific heat, range from 2.34 at $x = 0$ to 2.425 at $x = 0.01$. However, these specific-heat measurements were performed at high reduced temperatures: $T \gtrsim T_F$, where C_{vF} is not sensitive to the effective mass. Although the values of m^x of Greywall differ up to 5% from the values obtained from equation (44), the calculated values for the specific heat agree with the values of Greywall within 1%. This should be compared with the estimated precision of the measurements of 0.1%. On the other hand, a small

change in the value of m^x causes a larger change in the values of the osmotic pressure in the T-x region of Landau's measurements; the strong dependence of m^x on x, as found by Greywall, would lead to osmotic pressures that differ from the measurements of Landau *et al.* [2] up to 10%. Values of the effective mass that lead to consistency within 1% with both types of measurements are preferable. The value, given by equation (44) satisfies this requirement.

The specific heat data of Anderson *et al.* [7] were refitted by Landau *et al.* [2] who deduced $m^x/m_3 = 2.42 \pm 0.04$ at 1.3% and $m^x/m_3 = 2.47 \pm 0.04$ at 5%, consistent with equation (44).

The excess enthalpy at zero temperature was measured by Seligmann *et al.* [23]. These measurements are compared with the calculations in Fig. 7. The differences are systematic and increase with increasing ^{3}He concentration. This may be due to the measuring method which leads to systematic and cumulative errors in the excess enthalpy [23]. In Fig. 8 the calculated results for μ_3 at zero temperature are compared with the values calculated from the excess enthalpy in reference 23. It can be seen that the values of μ_3 are almost the same at low concentrations and deviate at higher concentrations. Since μ_3, determined in reference 23, does not satisfy the requirement that $\mu_3(0,x_0) = 0$, the osmotic-pressure data of Landau *et al.* [2] are a better starting point for the calculations than the data on the excess enthalpy.
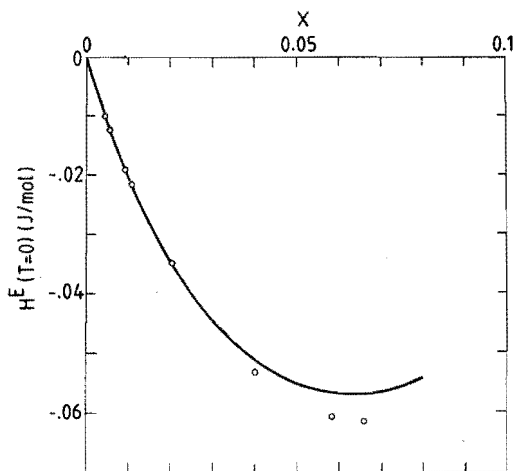
Fig. 7 *Comparison of the excess enthalpy between this calculation (full curve) and measurements of Seligmann et al. [23] (o).*
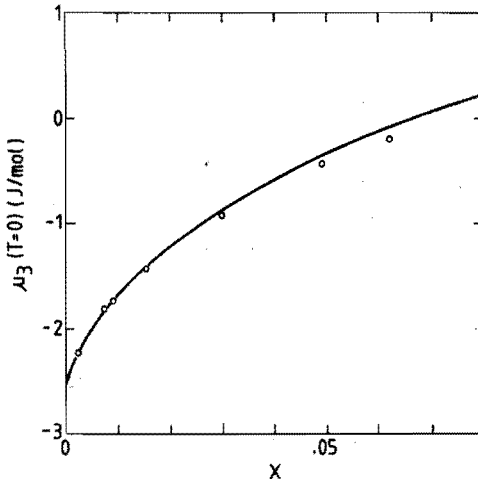
Fig. 8 *Comparison of the* ^{3}*He chemical potential between this (full curve) and Seligmann's [23] calculation (o).*

Finally the results are compared with the work of Radebaugh [1]. In Fig. 3b the calculation scheme of the latter is shown. This has to be compared with the calculation scheme given in Fig. 3a. The results of the two calculation schemes should be the same, as the same thermo-dynamic relations are used. The values of the specific heat of an ideal Fermi gas, the effective mass and the molar volume are nearly the same in both calculations and do not lead to significant differ-ences. This can be verified by comparing the two results on the specific heat, the entropy and the chemical potential of the quasiparticle gas, which agree within 2% for $x > 0.01$.

However, the differences are more significant for the other tabu-lated quantities. This is caused by the difference in input data. Radebaugh used data on μ_3 at the phase separation curve. For ^{3}He con-centrations lower than x_0 he extrapolated the potential energy μ_3', using a theoretical expression of Bardeen, Baym and Pines [24]. This expression, however, gives the difference between μ_3 and the chemical potential of an ideal Fermi gas of mass m_0, the quasiparticle mass at zero concentration, where Radebaugh used the concentration-dependent quasiparticle mass. Recent measurements [3,25] give a value for m_0/m_3
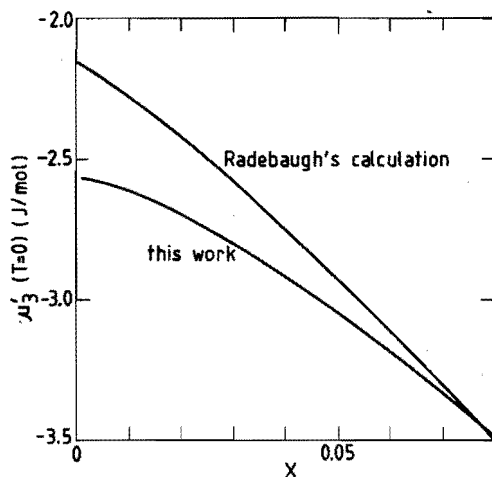
Fig. 9 Comparison of the quantity μ_3' at zero temperature between this
and Radebaugh's calculation [1].

of 2.25, which leads to an appreciable difference in μ_3' at zero
concentration. Furthermore, the theoretical expression for μ_3' contains
the interaction potential between two ^{3}He atoms, which was not well
known in 1967. These two facts explain the difference between μ_3',
calculated by Radebaugh, and the values calculated in this work, which
follow directly from measured quantities (see Fig. 9).

   A similar difference also shows up in the values of the osmotic
pressure and the osmotic enthalpy, which Radebaugh calculated using
μ_3'. In Fig. 10 Radebaugh's values of the osmotic pressure at zero
temperature are compared with measurements and with the fit to these
measurements given in equation (45). Since the osmotic enthalpy is
equal to Radebaugh's H_3 at low temperatures, the differences between
the two calculations also become evident by comparing the values of
the constant β, defined in equation (61). The value of 0.209 K^2 calcu-
lated here agrees very well with the measured value [4] of 0.21 K^2.
Radebaugh's $\beta = 0.14$ K^2, on the other hand, is too low. This can also
be seen from Fig. 11, where an isenthalp for both calculations and a
measured isenthalp [26] are given in the T^2-x diagram.

   The results of the calculations presented here are in good agree-
ment with the measurements. However, at present there is a lack of
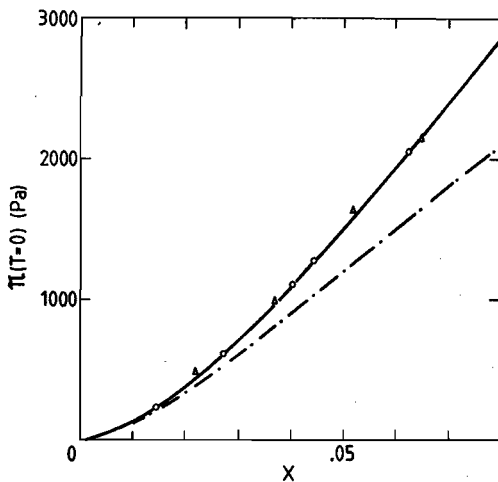
Fig. 10 *Comparison between the measurements of the osmotic pressure by Landau et al. [2] (○), Ghozlan et al [3] (△) and the calculations of Radebaugh [1] (chained line). The full curve represents equation (45).*
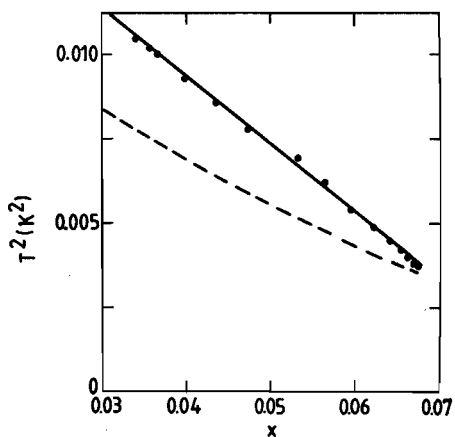
Fig. 11 *Comparison between the calculated isenthalps of Radebaugh [1], this work, and measurements of Zeegers [26];*
full curve: $H_3^{o\,s}$ = 0.33 J/mol as calculated in this work;
dashed curve: $H_3^{o\,s}$ = 0.33 J/mol as calculated by Radebaugh.

accurate measurements of the specific heat at low temperatures and ^{3}He concentrations higher than 1%. New measurements will result in a more precise determination of the effective quasiparticle mass, from which the thermodynamic properties can be derived with more precision than given here.

Appendix

In this appendix it will be shown that the zero points of the chemical potentials of two substances can be chosen independently, if no chemical reactions between the two components occur. This can be understood as follows. Following the argument of Guggenheim [6], the system drawn schematically in Fig. 12 is considered. Vessel A contains the mixture at temperature T_A and concentration x_i of component i. Vessel B contains the component i in the pure form. The two vessels are connected through a thermally-insulating, semi-permeable membrane which can only be passed by component i. The temperature in vessel B can be chosen in such a manner that the system is in equilibrium. This is the case if the chemical potentials of i in both vessels are the
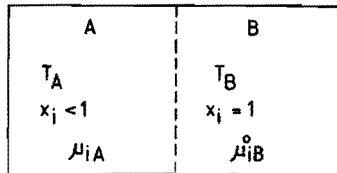
Fig. 12 *Illustration used in the proof that the zero points of the partial chemical potentials of the components in a mixture can be chosen arbitrarily. Vessel A contains the mixture at temperature T_A; the concentration of component i in A is x_i. Vessel B contains the component i in pure form at temperature T_B. The boundary between the two vessels is a semi-permeable membrane, through which only component i can pass. The chemical potentials of component i in both vessels are the same.*

40

same. The zero point of the chemical potential of any *pure* substance
may be chosen independent of the zero points of other pure substances
provided that no chemical reactions take place. Since $\mu_i = \mu_i^0$, the
zero point of the chemical potential of the component i in the mixture
can also be chosen independent of the zero point of component j. All
thermodynamic expressions for observable quantities, such as the
specific heat and the osmotic pressure, are independent of the choices
of the zero points of the two chemical potentials.

References

[1]   R. Radebaugh, NBS Technical Note 362 (1967).

[2]   J. Landau, J.T. Tough, N.R. Brubaker, and D.O. Edwards,
      Phys. Rev. **A2**, 2472 (1970).

[3]   A. Ghozlan, and E. Varoquaux, Ann. de Phys. **3**, 239 (1979).

[4]   A.T.A.M. de Waele, J.C.M. Keltjens, C.A.M. Castelijns, and
      H.M. Gijsman, Phys. Rev. **B28**, 5350 (1983).

[5]   D.S. Greywall, Phys. Rev. **B20**, 2643 (1979).

[6]   E.A. Guggenheim, Thermodynamics (North Holland Publishing
      Company, Amsterdam, 1967).

[7]   A.C. Anderson, D.O. Edwards, W.R. Roach, R.E. Sarwinski, and
      J.C. Wheatley, Phys. Rev. Lett. **17**, 376 (1966).

[8]   For a treatment of ideal Fermi gases see for example
      K. Huang, Statistical Mechanics (John Wiley & Sons, New York,
      1963).

[9]   C. Ebner, and D.O. Edwards, Phys. Reports **2C**, 77 (1971).

[10] J.C. Wheatley, Am. J. Phys. **36**, 181 (1968).

[11] J.G.M. Kuerten, C.A.M. Castelijns, A.T.A.M. de Waele, and
      H.M. Gijsman, Physica **128B**, 197 (1985).

[12] J. Bardeen, G. Baym, and D. Pines, Phys. Rev. **156**, 207 (1967).

[13] E.C. Stoner, Phil. Magz. **25**, 899 (1938).

[14] J. Landau, and R.L. Rosenbaum, J. Low Temp. Phys.
      11, 483 (1973).

[15]   E. Varoquaux, Thesis, Orsay, (1971).

[16]   D.S. Greywall, Phys. Rev. **B18**, 2127 (1978).

[17]   G.W. Watson, J.D. Reppy, and R.C. Richardson, Phys. Rev.
       188, 384 (1969).

[18]   D.S. Greywall, Phys. Rev. **B27**, 2747 (1982).

[19]   B.M. Abraham, O.G. Brandt, Y. Eckstein, J. Munarin, and
       G. Baym, Phys. Rev. **188**, 309 (1969).

[20]   J.G.M. Kuerten, C.A.M. Castelijns, A.T.A.M. de Waele, and
       H.M. Gijsman, Cryogenics **25**, 419 (1985).

[21]   The compressibility κ_4 of pure ^{4}He is equal to $V_4^0/M_4 s_4^{0^2}$, where
       M_4 is the molar mass of ^{4}He and s_4^0 is the velocity of sound,
       that equals 238 ms^{-1} (see reference 3).

[22]   C.A.M. Castelijns, J.G.M. Kuerten, A.T.A.M. de Waele, and
       H.M. Gijsman, Phys. Rev. **B32**, 2870 (1985).

[23]   P. Seligmann, D.O. Edwards, R.E. Sarwinski, and J.T. Tough,
       Phys. Rev. **181**, 415 (1969).

[24]   J. Bardeen, G. Baym, and D. Pines, Phys. Rev. **156**, 207 (1967).

[25]   R.M. Bowley, J. Low Temp. Phys. **61**, 291 (1985).

[26]   J. Zeegers, unpublished.

III HYDRODYNAMIC PROPERTIES OF ^{3}He–^{4}He MIXTURES

3.1 *Introduction*

Until some years ago it was generally assumed that there would only be a dissipative interaction between ^{3}He and ^{4}He if the relative velocity is high enough to create rotons. This assumption has its origin in a paper by Landau and Pomeranchuk [1], and is called the Mechanical Vacuum Model. Khalatnikov used it to derive the hydrodynamic equations for ^{3}He–^{4}He II mixtures [2]. Wheatley and his coworkers [3,4] calculated the properties of a ^{3}He circulating dilution refrigerator, using this model.

This hydrodynamic description leans heavily on the hydrodynamics of pure superfluid ^{4}He, developed by Landau [5]. It is based on the idea that in order to describe the macroscopic properties, ^{4}He II can be viewed of as consisting of two components: a superfluid and a normal component. This two-fluid model is not appropriate for microscopic properties, as it is not possible to call a single atom normal or superfluid. Below the critical relative velocity for roton excitation (58 m/s) no friction should occur. However, only a few years after the proposal of this model the experiments of Gorter and Mellink showed the existence of a frictional force between the two components above a critical velocity of the order of a few cm/s [6].

In the same year Onsager conjectured besides phonons and rotons a third kind of elementary excitations [7], namely vortices with quantized circulation. Following a suggestion of Feynman [8], Vinen developed a model in which the frictional force between the two components is caused by the interaction of the normal fluid with vortices. These vortices are assumed to form a tangle throughout the fluid when a critical relative velocity between the two components is exceeded [9]. This flow situation is generally called superfluid turbulence.

Since the work of Mazur and Prigogine [10,11], who did consider a mutual frictional force between ^{3}He and ^{4}He, the existence of a vortex tangle in ^{3}He–^{4}He II mixtures as a possible origin for the interaction has not been considered for a long time. However, in studying the properties of ^{3}He circulating dilution refrigerators, where ^{3}He flows

through superfluid ^{4}He, discrepancies from the Mechanical Vacuum Model have been reported occasionally [12,13]. A more extensive study on these discrepancies was initiated by the observations of Coops et $al.$ [14,15], and continued by Castelijns et $al.$ [16,17]. It was found that the interaction between ^{3}He and ^{4}He could be described by a mutual frictional force which, if the ^{4}He velocity is small, varied with the cube of the relative velocity, like in the Gorter-Mellink experiment. In the course of the investigation a new difficulty showed up: in the experiments where the mutual friction was measured, no pressure difference over the tube in which ^{3}He flows through ^{4}He was detected. Hence, it was assumed that there is no viscous force. The solution to this problem was presented recently [18]. It turned out that the early experiments by Wheatley et $al.$ [19] were performed in a region in which the mutual frictional force is outweighed by the viscous force, whereas in the experiments of Castelijns et $al.$ the former is dominant. In chapter V the results of an experiment in the intermediate region, where both forces can be detected, will be presented.

In section 3.2 some aspects of the microscopic theory of super-fluid ^{4}He and ^{3}He-^{4}He mixtures that are useful for this chapter are reviewed. In section 3.3 the hydrodynamics of ^{3}He-^{4}He II including mutual friction is developed in the region $T < 0.5$ K and $x < 8\%$.

3.2 $Microscopic$ $theory$ of $superfluid$ ^4He and ^3He-^4He $mixtures$

3.2.1 $Pure$ ^4He

Liquid ^{4}He exhibits a second-order phase transition at the λ point. It has been proposed that, in spite of the large interatomic forces in ^{4}He, the transition results from the same effect as the condensation of an ideal Bose gas [20]. Feynman has shown that this effect would indeed explain the λ transition [21].

In order to explain the properties of ^{4}He, Landau [5] introduced the two-fluid model mentioned above. The densities of the normal and superfluid component are denoted by ρ_n and ρ_s respectively. At zero temperature ρ_n equals zero, since there are no excitations. Above the λ point the whole fluid is normal: $\rho_s = 0$. The two components have

44
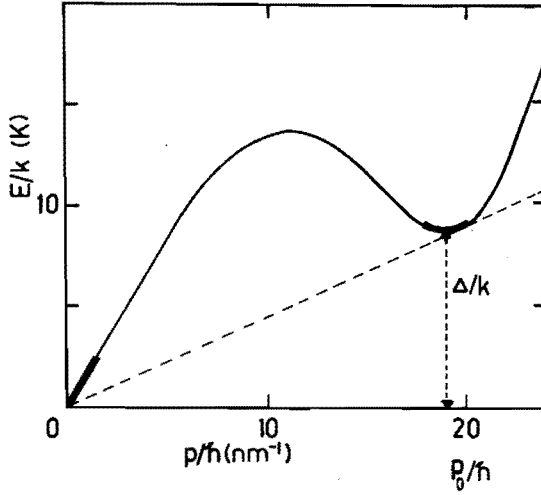
Fig. 1 *The dispersion curve for elementary excitations in He II. The thickened regions of the curve indicate the phonon- and roton excitations. The slope of the dashed line corresponds with the critical velocity for roton excitation, as explained in the text.*

velocities v_n and v_s respectively. The total momentum density j can be written as

$$j = \rho_n v_n + \rho_s v_s \quad . \tag{1}$$

It should be noted that the two-fluid model is a phenomenological model, which was set up to describe the macroscopic observations. It is certainly *not* true, that some atoms belong to the normal component and others to the superfluid.

The unusual properties below the λ point can be explained by studying the elementary excitations. On basis of measured thermodynamic properties, Landau [22] proposed the energy spectrum of the excitations given in Fig. 1. At low values of the energy there are two parts in the energy spectrum with different behaviour. At low values of the momentum p the excitations are phonons with energy equal to

$$\epsilon = cp \quad , \tag{2}$$

45

where c is the velocity of sound in ^{4}He, which at zero pressure equals 239.6 m/s [23]. At values of the momentum near the minimum in the spectrum a second kind of excitations occurs, called rotons. Their energy is given by

$$\epsilon = \Delta + (p-p_0)^2/2\mu \quad . \tag{3}$$

where $\Delta/k = 8.6$ K, $p_0/\hbar = 1.91$ Å^{-1}, and $\mu = 0.16m_4$ [2], and m_4 is the mass of a ^{4}He atom.

It is possible to explain superfluidity from the energy spectrum and conservation of energy and momentum [5,24]. It follows that the fluid velocity **v** needed to create an excitation of momentum **p** and energy ϵ equals

$$v = \frac{\epsilon}{p \cos \vartheta} \quad . \tag{4}$$

where ϑ is the angle between **v** and **p**. Equation (4) can only be satisfied, if

$$v \geq \epsilon/p \quad . \tag{5}$$

From the excitation spectrum it can be seen that ϵ/p has a minimum in the point where $d\epsilon/dp = \epsilon/p$, near the roton minimum. If the velocity is lower than this value of ϵ/p, it is not possible to create phonons and rotons. The critical velocity is equal to 58 m/s and is called the Landau critical velocity. This would imply that superfluid ^{4}He can flow without friction through very narrow channels with velocities up to 58 m/s.

Feynman has shown from first principles that the excitations of lowest energy are phonons [25], and that there exists a minimum in the energy spectrum corresponding with rotons [26]. However, as stated in the introduction, there are other possible excitations with higher momentum. Experiments show that the critical velocity for creation of these excitations is of the order of a few centimeter per second, far below the Landau critical velocity. Furthermore, the critical velocity measured in circular tubes is dependent on the diameter of the flow tube [27]. This observation suggests that the energy spectrum of these excitations depends on the geometry of the flow channel.

From the experiments in rotating superfluid ^{4}He it is known that above a certain angular velocity quantized vortex lines, parallel to the axis of rotation, are created [28,29]. The properties of these vortex lines have been explained by Feynman [8]. He showed that at absolute zero the many-particle wave function of a uniformly moving superfluid is given by

$$\Psi = \Phi \exp (iS) \quad , \tag{6a}$$

where the phase of the wave function equals

$$S = \mathbf{k} \cdot \sum_j \mathbf{R}_j \quad , \tag{6b}$$

Φ is the wave function of the ground state and $\mathbf{R}_j$ is the position of the jth particle. The wave vector $\mathbf{k}$ is related to the total momentum $\mathbf{P}$ of the system, through

$$\mathbf{P}\Psi = \sum_j \frac{\hbar}{i} \nabla_j \Psi = N\hbar \mathbf{k}\Psi \quad , \tag{7}$$

where N is the total number of particles and the property that Ψ is an eigenfunction of the momentum operator has been used. On the other hand the total momentum equals $Nm_4\mathbf{v}_s$, if $\mathbf{v}_s$ is the velocity of the superfluid. Thus:

$$S = \hbar^{-1}m_4\mathbf{v}_s \cdot \sum_j \mathbf{R}_j \quad , \tag{8}$$

if $\mathbf{v}_s$ is uniform. If $\mathbf{v}_s$ varies only little over distances of the order of the atomic spacing, a function s of r can be introduced by

$$S = \sum_j s(\mathbf{R}_j) \quad . \tag{9}$$

Here, s is evaluated at the position of each particle. The local velocity of the superfluid is given by

$$\mathbf{v}_s = \hbar m_4^{-1}\nabla s \quad . \tag{10}$$

From this relation an important equation for superfluid flow follows at once:

$$\nabla \times \mathbf{v}_s = 0 \quad . \tag{11}$$

Hence, the flow of a superfluid is irrotational.

Next, consider a very long chain of atoms each of which is a nearest neighbour of the next in line, and together lying on a closed contour C. If all the atoms are displaced over small distances $\Delta \mathbf{R}_j$, then the change in the phase ΔS of the wave function equals

$$\Delta S = \hbar^{-1} m_4 \sum_j \mathbf{v}_s(\mathbf{R}_j) \cdot \Delta \mathbf{R}_j \quad , \tag{12}$$

apart from small changes in the wave function of the ground state. If the displacements are such that each atom moves to its nearest neighbour next in line, the change in phase equals

$$\hbar^{-1} m_4 \sum_j \mathbf{v}_s(\mathbf{R}_j) \cdot \Delta \mathbf{R}_j = \hbar^{-1} m_4 \oint_C \mathbf{v}_s \cdot d\boldsymbol{\ell} = \hbar^{-1} m_4 k \quad , \tag{13}$$

where k is by definition the circulation around the contour[1]. Since the final situation is indistinguishable from the initial situation (the spin of a ^{4}He atom equals zero), the change in phase has to be equal to 2π times an integer. Hence, the circulation is quantized:

$$k = \frac{h}{m_4} n \quad , \tag{14}$$

with n an integer.

By changing a contour in the fluid the circulation can only change in discrete steps, so it was proposed that there may be lines

---

[1]The transition from the summation to an integration is only allowed, if the superfluid velocity does not vary appreciably over distances of the order of the atomic spacing.

in the fluid (vortex lines) around which the circulation is quantized [8]. Outside these lines the flow is irrotational. It can be shown [2] that vortex lines with n = ±1 are energetically favourable. When the angular velocity of a rotating bucket of ^{4}He II is increased, gradually more vortex lines appear. At higher angular velocities the density of the vortex lines is so high, that the superfluid seems to be in a state of solid body rotation.

Quantized vortex lines are also created in other situations where the normal component moves with respect to the superfluid. From equation (11) and Stokes's theorem follows that they form a closed loop or end on natural boundaries, such as walls and liquid-vapour interfaces. For the onset of vorticity in flow through channels, circular vortex rings with their axes aligned along the axis of the channel appear to be important. Apart from logarithmic terms, the energy of a vortex ring is proportional to its radius, while its impulse[2] varies as the square of the radius [31]. Thus the relative velocity between the two components needed to create a vortex ring of radius R is inversely proportional to R (see equation (5)). So the larger the vortex ring, the smaller the velocity needed to create it. However, the radius of the vortex ring is bounded by the dimension of the channel. It is thus not surprising that the critical velocity depends on the geometry of the channel. For a cylindrical flow channel the critical velocity would in first approximation be inversely proportional to the diameter of the tube [28]. This picture is far too simple to explain the measured critical velocities quantitatively [27].

One of the aspects that has not been taken into account yet, is the structure of the vortex core. The detailed structure is still a subject of investigation. A review of the various models has been given recently by Glaberson and Donnelly [32]. However, a few general remarks can be given. The superfluid velocity varies inversely proportional to the distance to the vortex line, r:

$$v_s = k/2\pi r \quad .$$ (15)

---

[2]The impulse of a vortex ring is defined as $\int \mathbf{F} dt$, where $\mathbf{F}$ is the force needed to create it. This impulse is immediately transmitted to infinity. Therefore, the momentum of a vortex ring equals zero and one has to use the impulse [30].

In order to keep the kinetic energy of the superfluid motion finite, the superfluid density should approach zero at the center of the vortex line. Furthermore, in a region where $\nabla \times \mathbf{v}_s = 0$, the pressure is in a stationary situation and at constant temperature related to the superfluid velocity by Bernoulli's law according to [28]

$$p + \frac{1}{2}\rho_s v_s^2 = \text{constant.} \tag{16}$$

Hence, the pressure decreases near a vortex line, so that the normal component is attracted towards the center of a vortex line. In one of the proposed models [32], the vortex core is considered as a region filled with the normal component, around which the superfluid rotates. Since the diameter of the core region is of atomic size ($\simeq$ 1Å) [32], quantummechanical effects will play an important role in the description of the core of quantized vortices.

Since the normal part of the fluid is attracted towards the vortex line, the concentration of excitations is higher near the vortex line. It is conceivable that in a steady state at a temperature above 1 K the excitations are continually trapped into the vortex core and emitted again. Moreover, the energy of the excitations depends on the local superfluid velocity, which varies strongly near the vortex core. These two effects lead to an interaction between the vortex lines and the phonons and rotons, which is responsible for the mutual frictional force. A microscopic calculation for the force between rotons and a vortex line has been given by Hillel and Vinen [33,34]. A more detailed description of the interaction between vortices and excitations will be given in chapter VI.

3.2.2 ^{3}He-^{4}He mixtures

From a theoretical point of view ^{3}He-^{4}He II mixtures are of special interest, since these are the only known mixtures of bosons (^{4}He) and fermions (^{3}He) that are liquid down to absolute zero at ambient pressure. This opens the possibility to study the interaction between ^{4}He and quasiparticles in the range where the quasiparticles vary from a classical gas to a degenerate Fermi gas, by varying both temperature and ^{3}He concentration.

50

In the hamiltonian of a ^{3}He–^{4}He mixture there are several contributions from the ^{3}He particles. In the first place a moving ^{3}He atom can excite phonons and rotons. However, the momentum of the ^{3}He atom needed is, even at the concentration of a saturated solution, much higher than the Fermi momentum (see section 3.2.1). Thus the excitation of *real* phonons and rotons does not occur at ^{3}He velocities below the Landau critical velocity. In the second place a ^{3}He atom is able to excite and absorb *virtual* ^{4}He phonons and rotons [35]. In this way it is always surrounded by a cloud of virtual excitations. This leads to the notion of effective mass. When a ^{3}He atom moves through the fluid, the virtual excitations are moving with it, thus increasing the inertia of the ^{3}He atom. The most sophisticated microscopic calculation until now yields a value of the effective mass of 2.37 times the bare mass of a ^{3}He atom [36]. This value is close to the experimentally determined $m/m_3 = 2.34$ [37]. In the third place there is an interaction between the ^{3}He particles. Since ^{3}He and ^{4}He are isotopes, the interatomic force between ^{3}He atoms is almost the same as that between ^{4}He atoms. However, since the bare mass of a ^{3}He atom is smaller than the mass of a ^{4}He atom, the zero point motion of a ^{3}He atom will be bigger, leading to a larger atomic volume [35].

If the superfluid velocity is unequal to zero, for example by the presence of a thermal excitation or a vortex line, the energy of a ^{3}He quasiparticle is changed. This affects the effective interaction between two ^{3}He atoms. The origin of the dependence of the quasiparticle energy on the local superfluid velocity can be explained as follows. Consider a system of ^{4}He with a single ^{3}He quasiparticle. The hamiltonian of this system can be written as

$$\mathcal{H} = \sum_i \frac{\mathbf{p}_i^2}{2m_4} + \sum_{i<j} V(\mathbf{r}_i - \mathbf{r}_j) + \frac{\mathbf{p}^2}{2m_3} + \sum_i U(\mathbf{r}_i - \mathbf{r}) \quad , \tag{17}$$

where $\mathbf{p}_i$ and $\mathbf{r}_i$ are the momentum and position of the ^{4}He particles and $\mathbf{p}$ and $\mathbf{r}$ of the ^{3}He particle, V is the interatomic ^{4}He potential, and U the ^{3}He–^{4}He interatomic potential. On the other hand the total energy in the superfluid rest frame equals

$$\mathcal{H} = \mathcal{H}_0 + \epsilon_\mathbf{p}\{0\} \quad , \tag{18}$$

where $\mathcal{H}_0$ is the hamiltonian of pure ^{4}He and $\epsilon_p\{0\}$ the energy of a quasiparticle with momentum $\mathbf{p}$ in the superfluid rest frame. At low values of the momentum this quantity equals [38]

$$\epsilon_p\{0\} = \epsilon_0 + \frac{p^2}{2m} \quad , \tag{19}$$

where ϵ_0 is the binding energy of a ^{3}He particle to pure ^{4}He and m the effective mass in the limit of zero concentration. Greywall has measured the deviations from this equation at high values of the momentum [37].

In a frame where the superfluid velocity equals $\mathbf{v}_s$ (denoted by primes), the momenta of the particles are related to the momenta in the superfluid rest frame by

$$\mathbf{p}_i' = \mathbf{p}_i + m_4 \mathbf{v}_s \tag{20a}$$

and

$$\mathbf{p}' = \mathbf{p} + m_3 \mathbf{v}_s \quad . \tag{20b}$$

Substitution in equation (17) gives the energy in this frame as

$$\mathcal{H}' = \sum_i \frac{(\mathbf{p}_i + m_4 \mathbf{v}_s)^2}{2m_4} + \sum_{i<j} V(\mathbf{r}_i - \mathbf{r}_j) + \frac{(\mathbf{p} + m_3 \mathbf{v}_s)^2}{2m_3} + \sum_i U(\mathbf{r}_i - \mathbf{r})$$

$$= \mathcal{H} + \sum_i \mathbf{p}_i \cdot \mathbf{v}_s + \frac{1}{2} N m_4 \mathbf{v}_s^2 + \mathbf{p} \cdot \mathbf{v}_s + \frac{1}{2} m_3 \mathbf{v}_s^2 \quad . \tag{21}$$

where N is the number of ^{4}He particles, and it has been assumed that the interatomic potentials are independent of momentum. Substitution of equation (18) and (19) yields

$$\mathcal{H}' = \mathcal{H}_0' + \epsilon_0 + \frac{p^2}{2m} + \mathbf{p} \cdot \mathbf{v}_s + \frac{1}{2} m_3 \mathbf{v}_s^2 \quad . \tag{22}$$

On the other hand this energy equals

$$\mathcal{H}' = \mathcal{H}_0' + \epsilon_{p + m_3 \mathbf{v}_s}\{\mathbf{v}_s\} \quad . \tag{23}$$

52

By comparing these equations an expression for the energy of a quasi-particle in the frame with superfluid velocity $\mathbf{v}_s$ can be obtained as:

$$\epsilon_p\{\mathbf{v}_s\} = \epsilon_0 + \frac{(\mathbf{p}-m_3\mathbf{v}_s)^2}{2m} + (\mathbf{p}-m_3\mathbf{v}_s)\cdot\mathbf{v}_s + \frac{1}{2}m_3\mathbf{v}_s^2$$

$$= \epsilon_0 + \frac{\mathbf{p}^2}{2m} + \frac{\delta m}{m}\,\mathbf{p}\cdot\mathbf{v}_s - \frac{\delta m}{2m}\,m_3\mathbf{v}_s^2 \quad , \tag{24}$$

where δm is the difference between the effective mass and the bare mass of a ^{3}He atom:

$$\delta m = m - m_3 \tag{25}$$

Equation (24) describes the most important contribution to the interaction between ^{3}He and vortices.

At temperatures below about 500 mK ^{3}He-^{4}He mixtures can be described by considering only one kind of excitations: the ^{3}He quasiparticles. In the appendix it is shown that the momentum density of ^{3}He-^{4}He mixtures at these temperatures can be written as

$$\mathbf{j} = \rho_n\mathbf{v}_3 + (\rho-\rho_n)\mathbf{v}_s \quad , \tag{26}$$

where ρ_n is the density of the normal component due to the quasiparticles, which exceeds the ^{3}He density ρ_3.

The velocity $\mathbf{v}_3$ is the hydrodynamic ^{3}He velocity which appears in the equation for ^{3}He number conservation

$$\frac{\partial\rho_3}{\partial t} + \nabla\cdot(\rho_3\mathbf{v}_3) = 0 \quad . \tag{27}$$

Conservation of total mass can be written as

$$\frac{\partial\rho}{\partial t} + \nabla\cdot\mathbf{j} = 0 \quad . \tag{28}$$

It turns out that part of the ^{4}He mass is carried along by the ^{3}He quasiparticles and is not counted as superfluid density, which is defined as

$$\rho_s = \rho - \rho_n \quad . \tag{29}$$

In a quantummechanical point of view the effective mass is caused by the fact that a [3]He particle is surrounded by a cloud of virtual phonons and rotons. This phenomenon has a simple classical analogon. It is known that if a rigid sphere moves through a perfect fluid, part of the fluid flows with the sphere, so that the inertia of the sphere in the fluid exceeds the bare mass of the sphere [39].

Equation (26) is the basis for the Landau two-fluid model, for it shows that the total momentum density consists of one part proportional to the superfluid velocity and another part caused by the excitations, constituting the normal fluid which at low temperatures consists only of quasiparticles.

It is known from experiment that the presence of [3]He atoms in superfluid [4]He has a large effect on properties related to quantized vortices. Recently, it has been found that below 0.5 K the critical center-of-mass velocity above which vorticity occurs in pure [4]He, decreases with the addition of only a very small amount of [3]He ($x \simeq 10^{-7}$) [40,41]. Other experiments indicate that the mobility of positively charged helium clusters and electrons in superfluid [4]He is affected strongly by the presence of [3]He (for x of the order of a few percent and T < 0.5 K) [32,42,43].

There are two major contributions to the interaction between [3]He and vortices. One results from the pressure decrease towards a vortex line (equation (16)), as the binding energy of quasiparticles in superfluid [4]He is a function of the pressure, and the other contribution results from the fact that the energy of a quasiparticle is a function of the local superfluid velocity (equation (24)).

Several authors have calculated the hamiltonian of a [3]He quasiparticle as a function of its momentum and its distance to the center of a rectilinear vortex line, and calculated the energy spectrum [44-46]. The most sophisticated calculation results in the existence of states in which the [3]He quasiparticle is bound to the vortex, the lowest of which has a nonzero angular momentum and a binding energy of 3.51 K at zero external pressure [44]. Using scattering theory, Titus [47] found the possibility of trapping of quasiparticles onto the vortex core. Thus the [3]He will be attracted towards a vortex line and

condenses onto it. If the ambient ³He concentration is high enough, the ³He concentration in the vortex core will exceed the value of a saturated solution, so that phase separation occurs [48,49]. This explains the observation that below a certain temperature ions do not condense onto vortex lines [32] in the presence of ³He. The diameter of the vortex core will increase with increasing ³He concentration and decreasing temperature, thus changing the properties of the quantized vortices.

In a situation where ³He flows through superfluid ⁴He, the ³He particles will be attracted towards the vortex lines, which they create themselves, be absorbed by them and re-emitted. This leads to a mutual frictional force between ³He and ⁴He, like in pure ⁴He when the normal component flows with respect to the superfluid component. At present, the properties of vortices are not sufficiently understood to calculate this force microscopically.

3.3 *Hydrodynamics of ³He-⁴He II mixtures*

The hydrodynamic equations for pure ⁴He II and for ³He-⁴He II mixtures have been derived by Khalatnikov [2]. He supposed, however, that no interaction between the normal fluid and the superfluid is present. If interactions between the two components or between the superfluid component and the wall are present, extra terms in the hydrodynamic equations appear. In this section it will be assumed that there is a mutual frictional force between ³He and the superfluid. A force between the superfluid and the wall will not be incorporated, since there is no experimental evidence for the existence of such a force.

The hydrodynamic equations can be derived starting from the conservation laws. In the case of ³He-⁴He mixtures the total mass, total momentum, the number of ³He particles and total energy are conserved quantities. The equation of motion of the superfluid component is extended to include a mutual frictional force. Finally, from the condition that the entropy production is positive, expressions for the dissipative terms in the conservation laws can be found. This treatment is analogous to the one given in Ref. 50 for a classical multi-component fluid. In the derivation it will be assumed that the

temperature is low enough to neglect the normal component of ^{4}He entirely, apart from its effect on the quasiparticle mass, as described above.

The equation for conservation of mass has been given in equation (28). In Khalatnikov's derivation a dissipative ^{3}He flux appears in the equation for ^{3}He number conservation. However, this term is negligible at temperatures where thermal excitations are negligible, because the normal component of the mixture contains only ^{3}He. So, there is no difference between $\mathbf{v}_n$ and $\mathbf{v}_3$. The equation describing conservation of ^{3}He particle number is therefore

$$\frac{\partial \rho_3}{\partial t} + \nabla \cdot (\rho_3 \mathbf{v}_n) = 0 \quad . \tag{30}$$

It is convenient to introduce the mass concentration of ^{3}He particles, defined as

$$c = \frac{N_3 M_3}{N_3 M_3 + N_4 M_4} = \frac{\rho_3}{\rho} \quad , \tag{31}$$

where N_3 and N_4 are the number of moles ^{3}He and ^{4}He and M_3 and M_4 the respective molar masses. Combining equations (28), (30) and (31) yields

$$\frac{\partial c}{\partial t} = \frac{1}{\rho} \nabla \cdot (\rho c \mathbf{v}_n) + \frac{c}{\rho} \nabla \cdot \mathbf{j} \quad . \tag{32}$$

The law of conservation of total momentum reads [2]

$$\frac{\partial j_i}{\partial t} + \frac{\partial \Pi_{ik}}{\partial r_k} = \frac{\partial \tau_{ik}}{\partial r_k} \quad , \tag{33}$$

where Π_{ik} is the stress tensor equal to

$$\Pi_{ik} = p \delta_{ik} + \rho_n v_{ni} v_{nk} + \rho_s v_{si} v_{sk} \quad , \tag{34}$$

and τ_{ik} is the viscous stress tensor. The viscous stress tensor takes into account the dissipation caused by a possible difference in normal

56

velocity between two neighbouring layers of fluid. As the mutual frictional force acts only between the two components and not on the total fluid, it does not show up in equation (33). The stress tensor (34) accounts for the force acting on the fluid through a pressure gradient, and the momentum densities transported by the normal and superfluid components respectively.

The equation for energy conservation reads

$$\frac{\partial E}{\partial t} + \nabla \cdot \mathbf{Q} = 0 \quad , \tag{35}$$

where E is the energy density and $\mathbf{Q}$ the energy flux, still to be determined. The energy density consists of the kinetic energy of the motion of the fluid and of the internal energy. From equation (22) follows that the energy density equals

$$E = E_0 + \mathbf{J}_0 \cdot \mathbf{v}_s + \frac{1}{2}\rho v_s^2 \quad . \tag{36}$$

where E_0 and $\mathbf{J}_0$ are the energy and momentum densities in the superfluid rest frame. If the relative ^{3}He-^{4}He velocity equals zero, the energy density in the superfluid rest frame follows from thermodynamics. For the total energy U the following relation holds

$$dU = TdS - pdV + \mu_3 dN_3 + \mu_4 dN_4 \quad . \tag{37}$$

where S is the entropy and V the volume of the system. From an elementary but tedious calculation it follows that

$$dE_0 = Td\sigma + \mu d\rho + Zdc \quad , \tag{38}$$

where σ is the entropy per unit volume, and μ and Z are related to the chemical potentials through (see [2])

$$\mu = c \frac{\mu_3}{M_3} + (1-c) \frac{\mu_4}{M_4} \tag{39}$$

and

$$Z = \rho \left[\frac{\mu_3}{M_3} - \frac{\mu_4}{M_4} \right] \quad . \tag{40}$$

If the normal fluid has a nonzero velocity in the superfluid rest frame, there is a contribution to the energy density due to the kinetic energy of the relative motion [2,28]:

$$dE_0 = Td\sigma + \mu d\rho + Zdc + (\mathbf{v}_n - \mathbf{v}_s) \cdot d\mathbf{J}_0 \quad . \tag{41}$$

Equation (37) can be used to calculate the pressure, since

$$p = -\left[\frac{\partial (E_0 V)}{\partial V} \right]_{S, N_3, N_4, J_0} \quad , \tag{42}$$

where J_0 is the total momentum in the superfluid rest frame. Combining equations (42) and (41) yields

$$p = -E_0 + T\sigma + \mu\rho + (\mathbf{v}_n - \mathbf{v}_s) \cdot \mathbf{J}_0 \quad . \tag{43}$$

The equation for the entropy production is

$$\frac{\partial \sigma}{\partial t} + \nabla \cdot (\sigma \mathbf{v}_n + \mathbf{q}/T) = R/T \quad , \tag{44}$$

where $\mathbf{q}$ is the dissipative heat flux and R the dissipative function. In this equation is incorporated that the superfluid component does not carry entropy, so that entropy is transported with velocity $\mathbf{v}_n$.

Finally, the equation of motion for the superfluid component reads

$$\frac{\partial \mathbf{v}_s}{\partial t} + (\mathbf{v}_s \cdot \nabla)\mathbf{v}_s + \nabla(\varphi + h) = \mathbf{f} \quad , \tag{45}$$

where $\nabla\varphi$ is the non-dissipative force on the superfluid and h the dissipative term, both still to be determined. The right hand side of equation (45) is the mutual frictional force per unit mass of the superfluid component, that is exerted by the normal component on the superfluid. Taking the curl of equation (45) and using $\nabla \times \nabla = 0$ gives

$$\frac{\partial}{\partial t}(\nabla \times \mathbf{v}_s) = \nabla \times \mathbf{f} + \nabla \times (\mathbf{v}_s \times (\nabla \times \mathbf{v}_s)) \quad . \tag{46}$$

Equation (46) shows that the mutual frictional force creates vorticity. If $\nabla \times \mathbf{f}$ equals zero, and $\nabla \times \mathbf{v}_s = 0$ initially, the superfluid stays irrotational. If $\nabla \times \mathbf{f}$ is unequal to zero, equation (45) is in conflict with equation (11), which states that the flow of the superfluid is irrotational. However, vorticity is possible if restricted to lines on which $\rho_s \to 0$. If the velocity is averaged over a volume containing many vortex lines, this average velocity field may be rotational. So the hydrodynamic equations derived here, are averaged over volumes with dimensions larger than the typical distance between vortices.

Now it is possible to determine the unknown terms in the hydrodynamic equations, since there is one equation more than variables. Differentiating equation (36) with respect to time and using (41) and equations (28), (32), (33), (44) and (45) yields after a time-consuming calculation

$$\frac{\partial E}{\partial t} + \nabla \cdot \{(\mu - \frac{Zc}{\rho} + \frac{1}{2}v_s^2)\mathbf{J} + Zc\mathbf{v}_n + \sigma T \mathbf{v}_n + h(\mathbf{J} - \rho \mathbf{v}_n) + \mathbf{v}_n(\mathbf{v}_n \cdot \mathbf{J}_0) + \mathbf{q} + \mathbf{v}_n \cdot \tau\} =$$

$$\rho_s(\mathbf{v}_n - \mathbf{v}_s) \cdot \nabla(\varphi - \mu + \frac{Zc}{\rho}) + R + h\nabla \cdot (\mathbf{J} - \rho \mathbf{v}_n) + \frac{1}{T}\mathbf{q} \cdot \nabla T - \rho_s(\mathbf{v}_n - \mathbf{v}_s) \cdot \mathbf{f} + \tau : \nabla \mathbf{v}_n \quad . \tag{47}$$

With equation (35) the energy flux $\mathbf{Q}$ can be identified as

$$\mathbf{Q} = (\mu - \frac{Zc}{\rho} + \frac{1}{2}v_s^2)\mathbf{J} + Zc\mathbf{v}_n + \sigma T \mathbf{v}_n + h(\mathbf{J} - \rho \mathbf{v}_n) + \mathbf{v}_n(\mathbf{v}_n \cdot \mathbf{J}_0) + \mathbf{q} + \mathbf{v}_n \cdot \tau \quad . \tag{48}$$

and the right hand side of equation (47) equals zero. Since the first term on the right hand side of (47) is non-dissipative it cannot give a contribution to the dissipative function R, and must equal zero for all values of $\mathbf{v}_n$ and $\mathbf{v}_s$. Therefore,

$$\varphi = \mu - \frac{Zc}{\rho} = \frac{\mu_4}{M_4} \quad . \tag{49}$$

where equations (39) and (40) have been used. The driving force on the

superfluid is thus the ^{4}He chemical potential. The other terms in equation (47) are the contributions to the dissipative function:

$$R = - h \, \nabla \cdot (\mathbf{J} - \rho \mathbf{v}_n) - \frac{1}{T} \mathbf{q} \cdot \nabla T + \rho_s (\mathbf{v}_n - \mathbf{v}_s) \cdot \mathbf{f} - \tau : \nabla \mathbf{v}_n \geq 0 \quad . \quad (50)$$

At this point, the theory of the thermodynamics of irreversible processes can be applied. The dissipative function is a sum of four terms, each of which is the product of a generalized thermodynamic force and a flux. In thermodynamic equilibrium all these forces and fluxes are equal to zero. For a large class of irreversible processes there exist linear relations between the fluxes and forces [50], but in general, higher order relationships are allowed, provided that the dissipative function is positive. By writing

$$\tau_{ik} = \tau \delta_{ik} + \mu_{ik} \quad . \quad (51)$$

where the indices refer to components of the tensors and μ_{ik} is a traceless symmetric tensor, it is possible to write down the linear relations between the fluxes and forces:

$$\tau = -\zeta_1 \nabla \cdot (\mathbf{J} - \rho \mathbf{v}_n) - \zeta_2 \nabla \cdot \mathbf{v}_n \quad . \quad (52a)$$

$$h = -\zeta_3 \nabla \cdot (\mathbf{J} - \rho \mathbf{v}_n) - \zeta_4 \nabla \cdot \mathbf{v}_n \quad , \quad (52b)$$

$$\mu_{ik} = -\eta \left[\frac{\partial v_{ni}}{\partial r_k} + \frac{\partial v_{nk}}{\partial r_i} - \frac{2}{3} \delta_{ik} \nabla \cdot \mathbf{v}_n \right] \quad , \quad (52c)$$

$$\mathbf{q} = -\kappa \nabla T + \alpha \rho_s (\mathbf{v}_n - \mathbf{v}_s) \quad . \quad (52d)$$

and

$$\mathbf{f} = -\frac{\beta}{T} \nabla T + \gamma \rho_s (\mathbf{v}_n - \mathbf{v}_s) \quad , \quad (52e)$$

where v_{ni} is the ith component of the vector $\mathbf{v}_n$. The Onsager relations, which follow from time reversal invariance read

$$\zeta_1 = \zeta_4 \quad (53)$$

and

60

$$\alpha = -\beta \quad , \tag{54}$$

where the minus-sign in equation (54) appears, because ∇T is invariant under time reversal, whereas $\rho_s(\mathbf{v}_n - \mathbf{v}_s)$ changes sign. The coefficient η can be recognized as the coefficient of first viscosity, and the ζ_i as coefficients of second viscosity. The heat conduction coefficient is denoted by κ.

Equations (52a)-(52d) are verified experimentally, but from experiments, both in pure ^{4}He [6] and in mixtures [18], it is known, that the relationship between the mutual frictional force f and the velocity difference is nonlinear. The most important contribution to the frictional force is proportional to the cube of the relative velocity:

$$\mathbf{f} \simeq B\rho_n |\mathbf{v}_n - \mathbf{v}_s|^2 (\mathbf{v}_n - \mathbf{v}_s) \quad , \tag{55}$$

where B may be a positive function of temperature and ^{3}He concentration. This equation has been verified for ^{3}He-^{4}He mixtures below 150 mK, ^{3}He concentrations between 2% and 7% and small values of v_s.

The reason for this nonlinear dependence is the following. The normal component can interact with the superfluid only by creating excitations. For low velocities the only possible excitations are quantized vortices. The vortices form a tangle in the fluid, due to the interaction with the quasiparticles and with each other. The total force on the superfluid is proportional to L, the density of vortex-line-length and to the averaged relative velocity. However, L itself is a function of the relative velocity. The higher the relative velocity, the larger L. From a dimensional argument it can be seen that L is proportional to the square of the relative velocity. If the turbulence is homogeneous, L is independent of volume and has dimension $[length]^{-2}$. There are two relevant quantities connected with the flow of ^{3}He through a tangle of quantized vortices: the absolute value of the relative velocity $|\mathbf{v}_n - \mathbf{v}_s|$ and the circulation around a vortex line h/m_4. The only way to make a quantity with dimension $[length]^{-2}$ with these quantities is the combination $(m_4 |\mathbf{v}_n - \mathbf{v}_s|/h)^2$. Using the Π-theorem [51], it follows that L is proportional to $|\mathbf{v}_n - \mathbf{v}_s|^2$.

In writing down equation (55) the effect of a temperature gradient on the mutual frictional force has been neglected. In the same approximation the effect of a relative velocity on the dissipative heat flux is negligible.

There have been several derivations of the hydrodynamic equations of pure ^{4}He in the presence of quantized vortices. Bekarevich and Khalatnikov [2,29] have derived these for a rotating superfluid. In that case the vortex lines all have the same direction, parallel to the axis of rotation. The number of vortex lines is directly related to the angular momentum of the system and to the value of $\nabla \times \mathbf{v}_s$ averaged over a volume containing many vortex lines. Khalatnikov used this average of $\nabla \times \mathbf{v}_s$ as an independent hydrodynamic variable and calculated the mutual frictional force using the conservation laws. Since a vortex line implies a known superfluid velocity profile, a definite amount of energy can be assigned to a unit vortex line.

Nemirovskii and Lebedev [52] have extended this approach to the situation of superfluid turbulence. They chose L as a hydrodynamic variable and used the Vinen equation [9] to account for the time dependence of L. However, they also needed experimental results to obtain the right expression for the mutual frictional force and their result is essentially the same as the one obtained here, in the case that the ^{3}He concentration equals zero everywhere.

Geurst [53,54] used the expression of Bekarevich and Khalatnikov for the mutual frictional force to describe ^{4}He flow through capillaries. His results agree with measurements for small velocities. They are not applicable to the situation of homogeneous superfluid turbulence, the situation in which the average vortex line density is uniform in the capillary. In a later paper [55] he used an averaging procedure to describe homogeneous superfluid turbulence. If certain assumptions about the shape and the order of the vortex lines are satisfied, his calculations produce equation (55) for the frictional force.

Schwarz [56] used the equation of motion for a vortex line, which will be given in chapter VI, to calculate the evolution of homogeneous superfluid turbulence numerically. The motion of a vortex line consists of a self-induced part and a contribution from the friction by the normal component. For the latter term he used an expression obtained from measurements in rotating ^{4}He. He calculated L and the

frictional force from the configuration of the vortex tangle in the steady state. The dependence on the relative velocity follows from a dimensional analysis, and the numerical values of both quantities agree with measurements on homogeneous superfluid turbulence within a few percent. A more detailed analysis of these numerical simulations will be given in chapter VI.

Yamauchi and Yamada [57] introduced a boundary force due to the interaction of a vortex line with the wall, in order to explain the measured excess pressure difference for flow through capillaries in pure ^{4}He. A result of their calculation is a form of the Vinen equation which implies a critical velocity in the case of thermal counterflow. An assumption in their derivation is, that the boundary force is uniform in a cross-section of the capillary, while one would think that it is only present in the neighbourhood of the walls.

Equation (55) is certainly not valid under all circumstances. In pure ^{4}He II experiments have been performed for many different combinations of v_n and v_s [58,59]. The cubic relationship (55) seems to be valid only in situations where v_s is small compared to v_n. Furthermore, for small velocities no mutual friction is present and the flow is laminar. If the velocity is gradually increased, at some value suddenly the extra dissipation appears. It seems that the turbulent state just above this critical velocity is not homogeneous. Above a second critical velocity a state of homogeneous superfluid turbulence exists in which the cubic relationship (55) holds [27]. In pure ^{4}He II the values of the critical velocities have been measured in many experiments [60-62] and have been calculated by numerical simulations [63].

It seems reasonable to assume that the situation in superfluid ^{3}He-^{4}He mixtures is similar. Until now, however, there have not been enough measurements to derive a general expression for the frictional force. All experimental evidence suggests that f is proportional to the cube of v_n in the case that the superfluid velocity is small [18]. Furthermore, recent investigation [64] showed that below some critical ^{3}He velocity the mutual frictional force is zero. In most situations discussed in the next section, the ^{3}He velocity is higher than the critical value and the superfluid velocity small enough to assume the validity of equation (55).

In this appendix it will be shown, using microscopic theory, that the contribution to the momentum density that moves with the ^{3}He velocity is not equal to $\rho_3 \mathbf{v}_3$, but has a contribution from the ^{4}He mass, that has to be counted to the normal fluid, as stated in equation (26). It will be assumed that the temperature is so low, that the thermal excitations can be neglected. In reference 38 a general derivation is given.

When E is the density of internal energy, the variation of E is given by

$$\delta E = \mu_4 \delta n_4 + \sum_{\mathbf{p}} \epsilon_{\mathbf{p}} \delta n_{\mathbf{p}} \quad , \tag{56}$$

where μ_4 is the ^{4}He chemical potential per particle, n_4 the ^{4}He number density, $n_{\mathbf{p}}$ the number density of quasiparticles with momentum $\mathbf{p}$ and $\epsilon_{\mathbf{p}}$ their energy:

$$\epsilon_{\mathbf{p}} = (\delta E / \delta n_{\mathbf{p}})_{n_{\mathbf{p}'}, n_4} \quad , \tag{57}$$

In this equation the difference between the two spin states of the quasiparticles is neglected. The total ^{3}He number density can be found from the $n_{\mathbf{p}}$ as

$$n_3 = \sum_{\mathbf{p}} n_{\mathbf{p}} \quad . \tag{58}$$

The Boltzmann equation for the quasiparticles reads

$$\frac{\partial n_{\mathbf{p}}}{\partial t} + (\nabla_{\mathbf{p}} \epsilon_{\mathbf{p}}) \cdot \nabla_r n_{\mathbf{p}} - (\nabla_r \epsilon_{\mathbf{p}}) \cdot \nabla_{\mathbf{p}} n_{\mathbf{p}} = I(\mathbf{p}) \quad , \tag{59}$$

where ∇_r and $\nabla_{\mathbf{p}}$ are the gradients in co-ordinate space and in momentum space respectively, and $I(\mathbf{p})$ is the collision integral, equal to the increase in number density of quasiparticles with momentum $\mathbf{p}$ due to collisions with other quasiparticles. The only property of the collision integral needed is the conservation of quasiparticles:

$$\sum_{\mathbf{p}} I(\mathbf{p}) = 0 \quad . \tag{60}$$

The equation for conservation of ^{3}He particles can be found by summing the Boltzmann equation over all momenta:

$$\sum_{\mathbf{p}} \frac{\partial n_{\mathbf{p}}}{\partial t} + \sum_{\mathbf{p}} (\nabla_{\mathbf{p}} \epsilon_{\mathbf{p}}) \cdot \nabla_{\mathbf{r}} n_{\mathbf{p}} - \sum_{\mathbf{p}} (\nabla_{\mathbf{r}} \epsilon_{\mathbf{p}}) \cdot \nabla_{\mathbf{p}} n_{\mathbf{p}} = 0 \quad . \tag{61}$$

By changing the order of summation and differentiation, the first term yields $\partial n_3 / \partial t$. The other terms can be written as a divergence by integrating by parts. This is allowed as the summation over $\mathbf{p}$ is equivalent to an integral over $\mathbf{p}$:

$$\sum_{\mathbf{p}} (\nabla_{\mathbf{r}} \epsilon_{\mathbf{p}}) \cdot \nabla_{\mathbf{p}} n_{\mathbf{p}} \stackrel{\wedge}{=} \frac{V}{(2\pi\hbar)^3} \int d\mathbf{p} \ (\nabla_{\mathbf{r}} \epsilon_{\mathbf{p}}) \cdot \nabla_{\mathbf{p}} n_{\mathbf{p}} \quad . \tag{62}$$

The result is

$$\frac{\partial n_3}{\partial t} + \nabla_{\mathbf{r}} \cdot \sum_{\mathbf{p}} n_{\mathbf{p}} \nabla_{\mathbf{p}} \epsilon_{\mathbf{p}} = 0 \quad . \tag{63}$$

The second term is equal to $\nabla_{\mathbf{r}} \cdot n_3 \mathbf{v}_3$, where $\mathbf{v}_3$ is the hydrodynamic ^{3}He velocity:

$$\mathbf{v}_3 = \frac{1}{n_3} \sum_{\mathbf{p}} n_{\mathbf{p}} \nabla_{\mathbf{p}} \epsilon_{\mathbf{p}} \quad . \tag{64}$$

Conservation of total mass can be written as

$$\frac{\partial \rho}{\partial t} + \nabla \cdot \mathbf{j} = 0 \quad , \tag{65}$$

According to equation (20b) the momentum density in the superfluid rest frame equals

$$\mathbf{j}_0 = \sum_{\mathbf{p}} (\mathbf{p} - m_3 \mathbf{v}_s) n_{\mathbf{p}} \quad . \tag{66}$$

So in the frame with superfluid velocity $\mathbf{v}_s$

$$\mathbf{j} = \sum_{\mathbf{p}} (\mathbf{p} - m_3 \mathbf{v}_s) n_{\mathbf{p}} + \rho \mathbf{v}_s = \sum_{\mathbf{p}} \mathbf{p} n_{\mathbf{p}} + (\rho - m_3 n_3) \mathbf{v}_s \quad . \tag{67}$$

In equation (24) the energy of a quasiparticle in a superfluid velocity $\mathbf{v}_s$ is calculated in the case that only one quasiparticle is present. If more quasiparticles are present, the interactions alter the mass of a quasiparticle and it is possible to define a concentration dependent effective mass $m_3^{\times}$, so that

$$\epsilon_{\mathbf{p}} \{\mathbf{v}_s\} = \frac{\mathbf{p}^2}{2m_3^{\times}} + \mathbf{p} \cdot \mathbf{v}_s (1 - \frac{m_3}{m_3^{\times}}) - \frac{1}{2}(1 - \frac{m_3}{m_3^{\times}}) m_3 \mathbf{v}_s^2 \quad . \tag{68}$$

This effective mass is larger than m, the effective mass at zero concentration [38]. Substitution of equation (68) in (64) yields

$$n_3 \mathbf{v}_3 = \sum_{\mathbf{p}} [\mathbf{p} + \mathbf{v}_s (m_3^{\times} - m_3)] \, n_{\mathbf{p}} / m_3^{\times} = \frac{1}{m_3^{\times}} \sum_{\mathbf{p}} \mathbf{p} n_{\mathbf{p}} + n_3 \frac{\Delta m}{m_3^{\times}} \mathbf{v}_s \quad . \tag{69}$$

where Δm is the difference between the concentration dependent effective mass and the bare mass of a ^{3}He particle:

$$\Delta m = m_3^{\times} - m_3 \quad . \tag{70}$$

Equation (69) can be used to calculate the momentum density. The result is

$$\mathbf{j} = m_3^{\times} n_3 \mathbf{v}_3 + (\rho - m_3^{\times} n_3) \mathbf{v}_s \quad . \tag{71}$$

By defining the normal mass density ρ_n as

$$\rho_n = m_3^{\times} n_3 \quad , \tag{72}$$

equation (26) follows.

References

[1] L.D. Landau, and I. Pomeranchuk, Dokl. Akad. Nauk. SSR **59**, 668 (1948).

[2] I.M. Khalatnikov, An Introduction to the Theory of Superfluidity (W.A. Benjamin, Inc., New York, 1965).

[3] J.C. Wheatley, Am. J. Phys. **36**, 181 (1968).

[4] J.C. Wheatley, O.E. Vilches, and W.R. Abel, Physics **4**, 1 (1968).

[5] L.D. Landau, J. Phys. USSR **5**, 71 (1941).

[6] C.J. Gorter, and J.H. Mellink, Physica **15**, 185 (1949).

[7] L. Onsager, Nuov. Cim. **6**, Supp. **2**, 249 (1949).

[8] R.P. Feynman, in Progress in Low Temperature Physics, Vol I, C.J. Gorter, ed. (North-Holland, Amsterdam, 1955), Ch. 2.

[9] W.F. Vinen, Proc. Roy. Soc. **A242**, 493 (1957).

[10] I. Prigogine, and P. Mazur, Physica **17**, 661 (1951).

[11] P. Mazur, and I. Prigogine, Physica **17**, 680 (1951).

[12] T.O. Niinikoski, Nucl. Instrum. Methods **97**, 95 (1971).

[13] G. Frossati, H. Godfrin, B. Hebral, G. Schumacher, and D. Thoulouze, in Physics at Ultralow Temperatures, Proceedings of the International Symposium at Hakone, P. Sugawara, ed. (Physical Society of Japan, Tokyo, 1977), p. 205.

[14] G.M. Coops, A.T.A.M. de Waele, and H.M. Gijsman, Phys. Rev. **B25**, 4879 (1982).

[15] G.M. Coops, Thesis, Eindhoven University of Technology, (1981).

[16] C.A.M. Castelijns, J.G.M. Kuerten, A.T.A.M. de Waele, and H.M. Gijsman, Phys. Rev. **B32**, 2870 (1985).

[17] C.A.M. Castelijns, Thesis, Eindhoven University of Technology, (1986).

[18] J.G.M. Kuerten, C.A.M. Castelijns, A.T.A.M. de Waele, and H.M. Gijsman, Phys. Rev. Lett. **56**, 2288 (1986).

[19] J.C. Wheatley, R.E. Rapp, and R.T. Johnson, J. Low. Temp. Phys. **4**, 1 (1971).

[20] F. London, Phys. Rev. **54**, 947 (1938).

[21] R.P. Feynman, Phys. Rev. **91**, 1291 (1953).

[22] L.D. Landau, J. Phys. USSR **11**, 91 (1947).

[23] D.S. Greywall, Phys. Rev. **B18**, 2127 (1978).

[24] J. Wilks, The Properties of Liquid and Solid Helium (Clarendon Press, Oxford, 1967).

[25] R.P. Feynman, Phys. Rev. **91**, 1301 (1953).

[26] R.P. Feynman, Phys. Rev. **94**, 262 (1954).

[27] J.T. Tough, in Progress in Low Temperature Physics, Vol VIII, D.F. Brewer, ed. (North-Holland, Amsterdam, 1982), Ch. 3.

[28] S.J. Putterman, Superfluid Hydrodynamics (North-Holland, Amsterdam, 1974).

[29] I.L. Bekarevich, and I.M. Khalatnikov, Sov. Phys. JETP **13**, 643 (1961).

[30] C.C. Lin, in Liquid Helium, G. Careri, ed. (Academic Press, New York, 1963), p. 93.

[31] C.F. Barenghi, R.J. Donnelly, and W.F. Vinen, J. Low Temp. Phys **52**, 189 (1983).

[32] W.I. Glaberson, and R.J. Donnelly, in Progress in Low Temperature Physics, Vol VIII, D.F. Brewer, ed. (North-Holland, Amsterdam, 1982), Ch. 1.

[33] A.J. Hillel, J. Phys. **C14**, 4027 (1981).

[34] A.J. Hillel, and W.F. Vinen, J. Phys **C16**, 3267 (1983).

[35] J. Bardeen, G. Baym, and D. Pines, Phys. Rev. **156**, 207 (1967).

[36] C.W. Woo, H.T. Tan, and W.E. Massey, Phys. Rev. **185**, 287 (1969).

[37] D.S. Greywall, Phys. Rev. **B20**, 2643 (1979).

[38] G. Baym, and C. Pethick, in The Physics of Liquid and Solid Helium, part 2, K.H. Benneman, and J.B. Ketterson, eds. (Wiley, New York, 1978), Ch. 2.

[39] L.D. Landau, and E.M. Lifshitz, Fluid Mechanics (Pergamon Press Ltd., Oxford, 1959).

[40] E. Varoquaux, M.W. Meisel, and O. Avenel, Phys. Rev. Lett. **57**, 2291 (1986).

[41] R.M. Bowley, G.G. Nancolas, and P.V.E. McClintock, Phys. Rev. Lett. **52**, 659 (1984).

[42]   R.M. Ostermeier, and W.I. Glaberson,
       J. Low Temp. Phys. 21, 191 (1975).

[43]   R.M. Ostermeier, and W.I. Glaberson,
       J. Low Temp. Phys. 25, 317 (1976).

[44]   C.M. Muirhead, W.F. Vinen, and R.J. Donnelly,
       Proc. Roy. Soc. A402, 225 (1985).

[45]   L.S. Rent, and I.S. Fisher, Sov. Phys. JETP 28, 375 (1969).

[46]   L. Senbetu, J. Low Temp. Phys. 32, 571 (1978).

[47]   W.J. Titus, Phys. Rev. A2, 206 (1970).

[48]   T. Ohmi, T. Tsuneto, and T. Usui,
       Prog. Theor. Phys. 41, 1395 (1969).

[49]   T. Ohmi, and T. Usui, Prog. Theor. Phys. 41, 1401 (1969).

[50]   S.R. de Groot, and P. Mazur, Nonequilibrium Thermodynamics,
       (North-Holland, Amsterdam, 1962).

[51]   L.I. Sedov, Similarity and Dimensional Methods in Mechanics,
       (Academic Press Inc., New York, 1959), p. 19.

[52]   S.K. Nemirovskii, and V.V. Lebedev,
       Sov. Phys. JETP 57, 1009 (1983).

[53]   J.A. Geurst, Phys. Lett. 71A, 78 (1979).

[54]   J.A. Geurst, in Proceedings of the XVth International
       Conference of Theoretical and Applied Mechanics, Toronto, 1980.

[55]   J.A. Geurst, unpublished.

[56]   K.W. Schwarz, Phys. Rev. Lett. 49, 283 (1982).

[57]   J. Yamauchi, and K. Yamada, Physica 128B, 45 (1985).

[58]   M.L. Baehr, and J.T. Tough, Phys. Rev. B32, 5632 (1985).

[59]   G. Marees, and H. van Beelen, Physica 133B, 21 (1985).

[60]   K.P. Martin, and J.T. Tough, Phys. Rev. B27, 2788 (1983).

[61]   M.L. Baehr, and J.T. Tough, Phys. Rev. Lett. 53, 1669 (1984).

[62]   C.E. Swanson, and R.J. Donnelly,
       J. Low Temp. Phys. 61, 363 (1985).

[63]   K.W. Schwarz, Phys. Rev. Lett. 50, 364 (1983).

[64]   J. Zeegers, J.G.M. Kuerten, A.T.A.M. de Waele, and H.M.
       Gijsman, to be published.

IV APPLICATIONS TO DILUTION REFRIGERATION

4.1 *Introduction*

In 1951 London suggested that the thermal properties of ^{3}He–^{4}He mixtures could be used to reach very low temperatures [1]. In 1962 he and his coworkers proposed three versions of a continuous refrigerator [2]. These proposals and all later dilution refrigerators are based on the fact that the molar enthalpy of pure ^{3}He is smaller than the molar enthalpy of ^{3}He in a saturated mixture at the same temperature (see chapter II). With the discovery of the finite solubility of ^{3}He in ^{4}He at zero temperature, it became clear that this cooling method can be used down to very low temperatures.
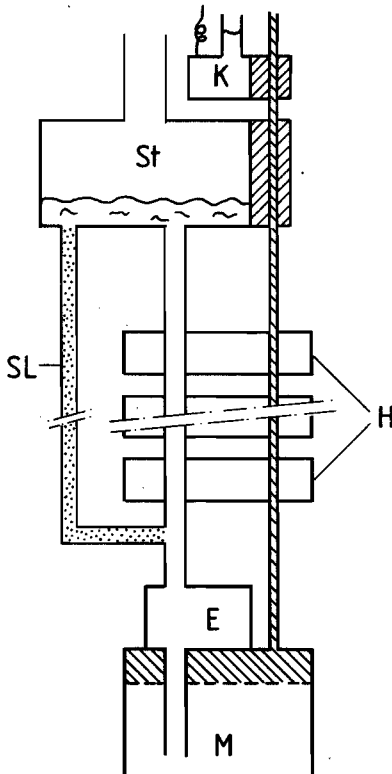
Fig. 1
Schematic drawing of the low-
temperature part of a ^{3}He
circulating dilution refrigerator.
M: mixing chamber; E: experimental
cell; H: heat exchangers;
St: still; K: 1-K plate;
SL: Optional superleak. The dilute
exit tube is the connection
between the mixing chamber and the
still, through which the ^{3}He
flows, after its dilution in the
mixing chamber.

A schematic drawing of the essential parts of a ^{3}He circulating dilution refrigerator is given in Fig. 1. The ^{3}He is circulated using the property that at 0.7 K and x = 1% the partial vapour pressure of

^{3}He is much higher than of ^{4}He. Thus, if the vapour is withdrawn from the liquid mixture in a still, pressurized by a pump at room temperature, and recondensed into the system before it enters the mixing chamber again, almost pure ^{3}He will be circulated. The heat exchangers provide a cooling of the ^{3}He by the cold mixture before it enters the mixing chamber.

The first ^{3}He circulating dilution refrigerator was built in 1964 by Das, de Bruyn Ouboter, and Taconis [3]. This prototype of a ^{3}He circulating dilution refrigerator was improved many times in the following decades, for example by improving the heat exchangers [4,5], the dimensions of the dilute exit tube [6], or by using a multiple mixing chamber device [7]. In other types of dilution refrigerators ^{4}He is circulated by injection through a superleak [8], or both components are circulated [9]. Reviews on dilution refrigerators have been given by Frossati [10] and by Taconis [11].

All types of dilution refrigerators have in common that they contain a tube in which the ^{3}He component flows with respect to the ^{4}He component. The description of the performance of a dilution refrigerator thus depends on the model about the flow properties of ^{3}He–^{4}He mixtures. In the pioneering years there has been some discussion about the presence of mutual friction, and in one of the proposals by London et al. [2] mutual friction is essential for the operation. However, since the properties of the existing ^{3}He circulating dilution refrigerators could satisfactorily be explained by assuming that no mutual friction is present, the Mechanical Vacuum Model was proposed [4]. Recently, measurements indicated that mutual friction can be important, depending on the geometry of the dilute exit tube, the flow rate and the temperature [12]. In this chapter the low temperature part of a ^{3}He circulating dilution refrigerator will be treated, using the hydrodynamic equations derived in the preceding chapter.

4.2 *General equations for ^{3}He circulating dilution refrigerators*

In Fig. 2 a schematic drawing of the low temperature parts of a ^{3}He circulating dilution refrigerator is given. Normally, the dilute exit tube, through which the diluted ^{3}He flows from the mixing chamber to the still, consists of a single cylindrical tube. In order to study

Fig. 2 *Schematic drawing of the mixing chamber* M, *experimental cell* E, *and heat exchangers* H. *Between* M *and* E *a flow impedance* Z_m *is installed. The molar* ^3He *flow rate is* $\dot{n}_3$, *and the temperature of the incoming* ^3He T_i. *The concentrations, temperatures and pressure difference can be measured.*

the properties of ^3He flowing through ^4He II, it is useful to consider more general geometries for this tube, such as a number of parallel tubes. This variable part of the dilute exit tube, on which the attention will be focussed in this chapter, will be called the impedance Z_m. In this impedance ^3He flows through ^4He II. So, the hydrodynamic equations of the preceding chapter can be applied to Z_m. In some situations there is also a ^4He flow through the impedance. The net ^4He molar flow rate will be denoted by $\dot{n}_4$. It will be assumed that the temperature is low enough to neglect thermal phonons and rotons, and that the velocities are so low that quadratic terms in the velocities may be neglected.

In the steady state the equation of continuity (III.28) yields

$$\nabla \cdot \mathbf{j} = 0 \quad , \tag{1}$$

or after integration over the cross section of the impedance

$$\dot{n}_3 M_3 + \dot{n}_4 M_4 = \text{constant}. \tag{2}$$

The equation of conservation of ^{3}He particle number (III.30) yields

$$\dot{n}_3 M_3 = \text{constant}. \tag{3}$$

Since ρ_n is not equal to ρ_3 (see chapter III), while $\mathbf{v}_n$ equals $\mathbf{v}_3$, these simple conservation laws have a rather unexpected effect. For, if the net flow rate of the ^{4}He component equals zero, the total momentum density $\mathbf{j}$ equals $\mathbf{j}_3$, the ^{3}He momentum density. Hence,

$$\rho_n \bar{\mathbf{v}}_n + \rho_s \bar{\mathbf{v}}_s = \rho_3 \bar{\mathbf{v}}_n \quad , \tag{4}$$

where a quantity with a dash denotes the quantity averaged over the cross section. As $\rho_n > \rho_3$, it follows that the average superfluid velocity is unequal to zero and directed opposite to $\bar{\mathbf{v}}_n$. This super- fluid flow compensates the flow caused by the ^{4}He that is moving with the ^{3}He quasiparticle gas.

In the following it will be assumed that the components of the velocities in the radial direction are negligible and that the temper- ature is uniform in a cross section of the impedance. For pure ^{4}He II deviations from these assumptions have been calculated [13]. It appeared that their magnitude depends on the boundary conditions. In pure ^{4}He there is a condition that the component of the mass velocity perpendicular to a wall equals zero at the wall, but there is no restriction on the individual normal and superfluid velocities. This implies that the radial component of both velocities may become large [13]. In ^{3}He-^{4}He mixtures on the other hand, both radial velocities equal zero at the boundaries, as there can be no flow of ^{3}He or ^{4}He into the wall. Furthermore, if there is no heat flow into the bound- ary, the radial temperature gradient equals zero at the boundary as well. This justifies the assumption. Hence, the continuity equation gives

$$\frac{\partial}{\partial\ell}(\rho_n v_n + \rho_s v_s) = 0 \qquad (5)$$

and

$$\frac{\partial}{\partial\ell}(\rho_3 v_n) = 0 \quad , \qquad (6)$$

where ℓ is the co-ordinate in the direction of the axis of the impedance, and v_n and v_s are the velocities in that direction.

Neglecting quadratic terms in the velocities and gradients in the equation for conservation of momentum (III.33) yields with substitution of (III.51) and (III.52c)

$$\frac{\partial p}{\partial\ell} = \eta \sum_{i=1}^{2} \frac{\partial^2}{\partial r_i^2} v_n \qquad (7)$$

and

$$\frac{\partial p}{\partial r_1} = \frac{\partial p}{\partial r_2} = 0 \quad , \qquad (8)$$

where r_1 and r_2 are the co-ordinates in the two directions perpendicular to the axis. Thus, the pressure is constant in a cross section of the impedance. It follows from equation (7) that $\sum_{i=1}^{2} \frac{\partial^2}{\partial r_i^2} v_n$ is also constant in a cross section of the impedance. The approximations made, are valid if the terms $\rho_n v_n^2 + \rho_s v_s^2$ and $\eta \partial v_n / \partial\ell$ in the stress tensor can be neglected with respect to p, which is the case at not too high velocities.

For a normal Fermi liquid the velocity at a boundary has been calculated by Højgaard Jensen et al. [14]. If the flow is stationary, the slip length, defined as the distance behind the wall at which the fluid velocity becomes zero when extrapolated from the bulk, equals approximately 0.6 l, where l is the mean free path of the Fermi gas. For ^{3}He-^{4}He II mixtures at low temperatures the mean free path of the ^{3}He quasiparticles is determined by their mutual interaction and is of the order of 0.1 μm [15]. Therefore, in the case under consideration the slip length is small compared to the dimensions of the impedance

and the no-slip approximation holds:

$$v_n = 0 \text{ at the boundaries.} \tag{9}$$

With this condition equation (7) and (8) can be solved for a cylindrical impedance, using the symmetry of the problem. The result is the familiar parabolic velocity profile for Poiseuille flow in a cylinder:

$$v_n = -\frac{1}{4\eta}\frac{dp}{d\ell}\left[\frac{D^2}{4} - r^2\right] \;, \tag{10}$$

where r is the distance from the tube axis and D the diameter of the tube. This result can be written as

$$\frac{dp}{d\ell} = -\eta\frac{128}{\pi D^4}\dot{n}_3 V_3 \;, \tag{11}$$

where V_3 is the volume of one mole of ^{3}He in the mixture (which is not equal to $\mathcal{V}_3$, the partial volume of ^{3}He, used in chapter II). For an impedance of arbitrary, uniform cross section, an impedance factor per unit length ζ, only dependent on the geometry, can be defined by [16]

$$\frac{dp}{d\ell} = -\eta\zeta\dot{n}_3 V_3 \;. \tag{12}$$

The equation of motion of the superfluid component (III.45) yields, when again quadratic terms in the gradients and velocities are neglected and with substitution of equations (III.49) and (III.55)

$$\frac{\partial\mu_4}{\partial\ell} = BM_4\rho_n(v_n-v_s)^3 \quad \text{for } |v_n-v_s| > v_c$$

$$\frac{\partial\mu_4}{\partial\ell} = 0 \qquad\qquad \text{for } |v_n-v_s| < v_c \tag{13}$$

and

$$\frac{\partial\mu_4}{\partial r_1} = \frac{\partial\mu_4}{\partial r_2} = 0 \;. \tag{14}$$

Below the critical velocity v_c which may depend on the geometry of the impedance and on the velocity of one of the components, no mutual friction is present [17]. Hence, the ^{4}He chemical potential is uniform in the impedance. If mutual friction is present, the ^{4}He chemical potential is uniform in a cross section of the impedance, and so is the relative velocity $v_n - v_s$. For a cylindrical tube this leads to a parabolic superfluid velocity profile. However, since the superfluid has a viscosity equal to zero, its velocity at the wall is not necessarily equal to zero. A parabolic velocity profile implies that the superfluid velocity is not irrotational ($\nabla \times v_s \neq 0$). However, as noted in chapter III, in the presence of quantized vortices the velocities in the hydrodynamic equations should be considered as averaged over a volume containing many vortices.

In the steady state the mutual frictional force can be obtained directly by determining the chemical potential difference over the impedance, which can be calculated from temperature, pressure and ^{3}He concentration (see chapter II). In the situation that the ^{4}He flow is small compared to the ^{3}He flow this has been done by Castelijns et al. [12,18] for several impedances as a function of $\dot{n}_3$. The results confirm the cubic dependence between the frictional force and the relative velocity and can be represented by

$$\frac{d\mu_4}{d\ell} = \chi \left[\frac{\dot{n}_3}{A} \right]^3 , \qquad (15a)$$

where

$$\chi = 1 \times 10^{-8} \text{ kg s m}^7 \text{mol}^{-4}, \qquad (15b)$$

and A is the cross-sectional area of the impedance. It is a rather unexpected result that χ does not vary much in a wide temperature and concentration range (10 mK $<$ T $<$ 150 mK and 0.02 $<$ x $<$ 0.07).

By measuring the temperature in the middle of the tube, it was verified that the quadratic terms in the equations of motion are very small indeed.

In the steady state the energy conservation law (III.35) reduces to

$$\nabla \cdot \mathbf{Q} = 0 \quad, \tag{16}$$

where the energy flux $\mathbf{Q}$ is given by (III.48). Neglecting again quadratic terms, using the approximation that the velocities are directed along the axis of the impedance, and integrating over the cross section yields with equation (III.52d)

$$\frac{d}{d\ell} \left\{ (\mu_3 + \frac{1}{x} S_m T) \dot{n}_3 + \mu_4 \dot{n}_4 - A\kappa \frac{dT}{d\ell} \right\} = 0 \quad, \tag{17}$$

or using (II.30)

$$\frac{d}{d\ell} \left\{ H_3^{os} \dot{n}_3 + \mu_4 \dot{n}_4 - A\kappa \frac{dT}{d\ell} \right\} = 0 \quad. \tag{18}$$

When the impedance connects two reservoirs with large cross-sectional area, a more general conservation law can be derived from equation (16). The cross sections of the reservoirs can be so big, that the velocities of both components are negligible there. If Ω is a volume consisting of the impedance and a part of both reservoirs, as
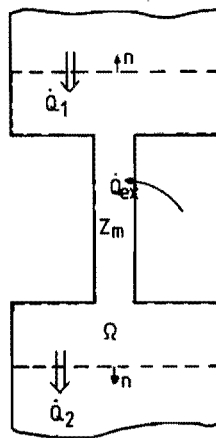

Fig. 3 *The energy conservation law applied to a volume consisting of two large reservoirs connected by an impedance. The energy flow* $\dot{Q}$ *denotes* $\dot{n}_3 H_3^{os} + \dot{n}_4 \mu_4 + \dot{Q}_c$. $\dot{Q}_{ex}$ *is an external heat load.*

indicated in Fig. 3, application of the divergence theorem gives

$$0 = \int_\Omega \nabla \cdot \mathbf{Q} \, d\mathbf{r} = \int_S \mathbf{Q} \cdot \mathbf{n} \, dS \quad , \tag{19}$$

where S is the closed surface bounding Ω, with area element dS and unit outward normal $\mathbf{n}$ at dS. At the natural boundaries there is no contribution from the energy flux to the surface integral, apart from an external heat flux $\dot{Q}_{ex}$, which is counted positively, if heat is supplied externally. Furthermore, at the other boundaries the velocities are so small, that all nonlinear terms can be neglected. As $\dot{n}_3$ and $\dot{n}_4$ are constants, the result is

$$\dot{n}_3 \Delta H_3^{\circ s} + \dot{n}_4 \Delta \mu_4 + \Delta \dot{Q}_c = \dot{Q}_{ex} \quad , \tag{20}$$

where the symbol Δ denotes the difference of a quantity between the exit and the entrance of the impedance, and $\dot{Q}_c$ is the heat flow caused by heat conduction:

$$\dot{Q}_c = -A\kappa \frac{dT}{d\ell} \quad . \tag{21}$$

This term cannot be made small by increasing the cross section of the reservoirs, since $dT/d\ell$ is inversely proportional to A.

Equation (18) can also be derived from the equation for the entropy production (III.44) using the expressions for the dissipative terms. This equation can be put in a more transparent form using the Gibbs–Duhem relation for the mixture (II.1). The result is

$$\left\{ T\frac{d}{d\ell}\left[\frac{S_m}{x}\right] + \frac{V_m}{x}\frac{dp}{d\ell} - \frac{1-x}{x}\frac{d\mu_4}{d\ell} \right\} \dot{n}_3 + \frac{d\mu_4}{d\ell} \dot{n}_4 - A\frac{d}{d\ell}\left[\kappa\frac{dT}{d\ell}\right] = 0 \quad . \tag{22}$$

From equations (12), (15) and (22) p, T and x can be calculated in principle as functions of ℓ. However, solution of these equations is complicated, for S_m, κ and the viscosity η are functions of temperature, ^{3}He concentration and pressure. The entropy is a well-known, but difficult function of these quantities. The viscosity and heat conduction are not well-known in the region of interest. This

makes an analytical solution of (22) impossible. In most situations, however, the impedance is placed just behind the mixing chamber. Hence, the temperature in the impedance is very low and the ^{3}He concentration close to x_0, the concentration of a saturated solution at zero temperature and pressure. In that situation S_m/x equals S_F (II.9). Furthermore, the following relations hold within 2% below 50 mK [18]

$$S_F = C_d T \quad , \text{ with } C_d = 104.3 \text{ J mol}^{-1}\text{K}^{-2}, \tag{23a}$$

$$\eta = \eta_d/T^2 \quad , \text{ with } \eta_d = 5\times10^{-8} \text{ Pa s K}^2, \tag{23b}$$

$$\kappa = \kappa_d/T \quad , \text{ with } \kappa_d = 3\times10^{-4} \text{ W m}^{-1} \tag{23c}$$

and

$$V_3 = V_{3d} = 4.26\times10^{-4} \text{ m}^3\text{mol}^{-1}. \tag{23d}$$

Substitution in equation (22) gives

$$\left\{\frac{1}{2}C_d \frac{dT^2}{d\ell} - \frac{\eta_d \zeta V_{3d}^2 \dot{n}_3}{T^2} - \frac{1-x_0}{x_0} \frac{d\mu_4}{d\ell}\right\} \dot{n}_3 + \frac{d\mu_4}{d\ell} \dot{n}_4 - \kappa_d A \frac{d}{d\ell}\left[\frac{1}{T}\frac{dT}{d\ell}\right] = 0 \quad . \tag{24}$$

This equation is generally valid, as it does not incorporate any assumption about mutual friction. Substitution of equation (15) makes it valid in the situation of the experiments by Castelijns et al. [18]. Substitution of $d\mu_4/d\ell = 0$, gives the results of the Mechanical Vacuum Model by Wheatley et al. [4]. In this case, equation (22) has been solved analytically by van Haeringen et al. [19] to calculate the temperature profile in the impedance and the intrinsic minimum temperature of a ^{3}He circulating dilution refrigerator.

In the derivation of equation (24) gravitation has not been taken into account. If the axis of the impedance is in the vertical direction, gravitation causes an extra contribution to the pressure- and chemical potential differences. However, these contributions cancel in equation (24), so that gravitation has no effect on the

temperature difference over the impedance. If the axis of the impedance does not coincide with the vertical direction, gravitation destroys the symmetry properties of the flow state. This weakens the basis for the assumption that the radial velocities and radial temperature gradient equal zero, and gives rise to radial pressure and chemical potential differences. Generally these effects are small and will not be considered here.

4.3 *The ^{3}He circulating dilution refrigerator in continuous operation*

In continuous operation a continuous flow of ^{3}He is maintained in a ^{3}He circulating dilution refrigerator. Under most circumstances the temperature in the still is low enough to neglect the amount of circulated ^{4}He. This reduces equation (24) to

$$\frac{1}{2} C_d \frac{dT^2}{d\ell} - \frac{\eta_d \zeta V_{3d}^2 \dot{n}_3}{T^2} - \frac{1-x_0}{x_0} \frac{d\mu_4}{d\ell} - \frac{\kappa_d}{\dot{n}_3} A \frac{d}{d\ell} \left[\frac{1}{T} \frac{dT}{d\ell} \right] = 0 \quad . \qquad (25)$$

This equation has been treated several times in the case $d\mu_4/d\ell = 0$ [18,19], but this relation is not valid in the presence of quantized vortices, where equation (15) has to be substituted. The result is an ordinary second-order differential equation for $T(\ell)$, which has a unique solution, if two boundary conditions are given. An analytical solution has not been found yet, but the equation has been solved numerically [16].

It is convenient to bring equation (25) in a dimensionless form by introducing the reduced temperature t and reduced length λ, defined by

$$t = T/T_0 \qquad\qquad\qquad\qquad (26)$$

and

$$\lambda = \ell/\ell_0 \quad , \qquad\qquad\qquad\qquad (27)$$

where

$$T_0 = \left[\frac{4\kappa_d \eta_d V_{3d}^2 A\zeta}{c_d^2}\right]^{1/6} \simeq 3.16\times10^{-4} \, (A\zeta)^{1/6} \text{ K} \tag{28}$$

and

$$\ell_0 = \left[\frac{2\kappa_d^2 A^2}{c_d \eta_d V_{3d}^2 \zeta}\right]^{1/3} \frac{1}{\dot{n}_3} \simeq 57.5 \frac{A}{\dot{n}_3}(A\zeta)^{-1/3} \text{ m} \tag{29}$$

are the characteristic temperature and length. Substitution in equation (25) yields

$$-\frac{d}{d\lambda}\left[\frac{1}{t}\frac{dt}{d\lambda}\right] + \frac{dt^2}{d\lambda} - \frac{1}{t^2} - \xi = 0 \quad , \tag{30}$$

where ξ is a dimensionless parameter equal to

$$\xi = \frac{1-x_0}{x_0} \chi \dot{n}_3^2 \left[\frac{4\kappa_d}{c_d^2 \eta_d^2 V_{3d}^4 A^8 \zeta^2}\right]^{1/3} \simeq 1.56 \left[\frac{\dot{n}_3}{A}\right]^2 (A\zeta)^{-2/3} \quad . \tag{31}$$

The parameter ξ measures the strength of the mutual frictional force. If no mutual friction is present, ξ equals zero. The ratio of the last two terms on the left of equation (30), ξt^2, is a measure for the ratio of the contributions to the temperature rise due to the viscous force and the mutual frictional force. It equals[1]

$$\xi t^2 = \frac{1-x_0}{x_0} \frac{\chi \dot{n}_3^2 T^2}{\eta_d V_{3d}^2 A^3 \zeta} \simeq 1.56\times10^7 \frac{\dot{n}_3^2 T^2}{A^3 \zeta} \quad . \tag{32}$$

For the experiments of Wheatley et al. [20] a value of ξt^2 of the order of 2.5×10^{-4} follows. Hence, the effect of mutual friction is negligible and the viscous force dominates. On the other hand, in the

---

[1] For dilution refrigeration it is often useful to work with mK, mm and mmol/s as units (milli-units). For one cylindrical tube with diameter D equation (32) yields

$$\xi t^2 \simeq 0.79 \, \dot{n}_3^2 T^2/D^2 \text{ (in milli-units)}.$$

flow situation of Castelijns *et al.* [18] ξt^2 is of the order of 200. This means that in these experiments the viscous force is dominated completely by the mutual frictional force. This work makes clear that both situations, which first seemed to be contradictory, are different limits of one theoretical description which incorporates both forces. If ξt^2 is of the order of 1, both forces are important. This will be called the combined-dissipation regime.

To solve equation (30), in analogy with Wheatley *et al.* [4], the function $f(t)$ is introduced as

$$f(t) = \frac{1}{t^3} \frac{dt}{d\lambda} \quad .$$ (33)

This quantity is the ratio of the enthalpy flow due to heat conduction and the total enthalpy flow. Substitution yields two first-order differential equations for f and λ as functions of t,

$$\frac{df}{dt} = \frac{2(1-f)}{t} - \frac{1}{t^7 f} - \frac{\xi}{t^5 f}$$ (34)

and

$$\frac{d\lambda}{dt} = \frac{1}{t^3 f} \quad ,$$ (35)

which can be solved, if f and λ are known for a certain value of t. In Fig. 4a-f the solutions are plotted for $\xi = 0$, $\xi = 1$ and $\xi = 10$. In these figures the solutions, in which f becomes negative for high values of t have been left out. Since these solutions correspond to cooling at the "warm" end of the dilute exit tube, they are impossible, unless the lowest heat exchanger is cooled somehow. This situation will not be considered here.

All solutions with $f < 1$ for high values of t tend to one asymptotic solution for low t (see Fig. 4). Outside the region of the asymptotic solution the derivative $dt/d\lambda$ is generally large. Hence, for a given temperature at the end of the tube, the temperature profile follows the asymptotic solution in the main part of the tube.
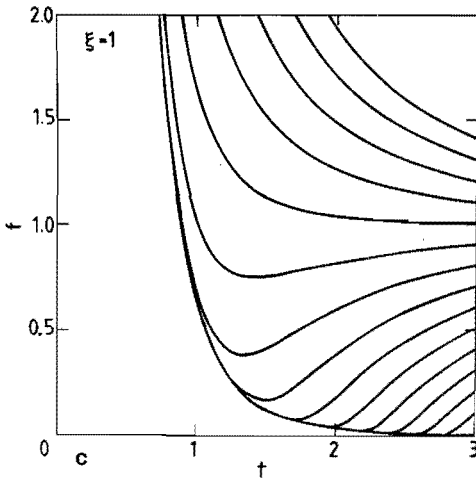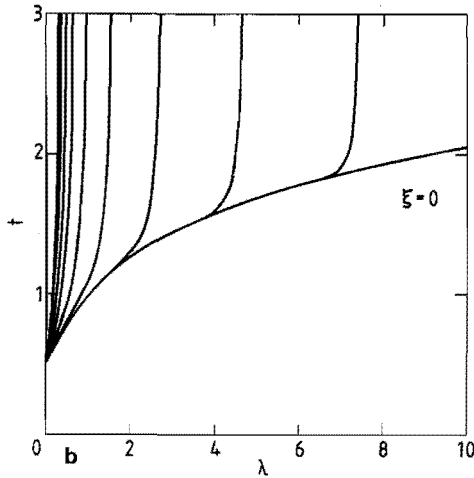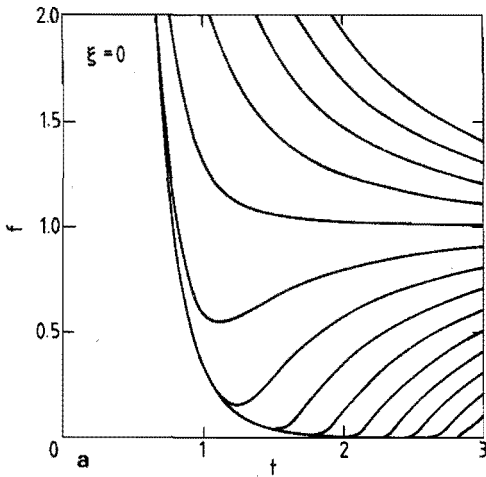
Fig. 4

The solutions of the differential equations (34) and (35).
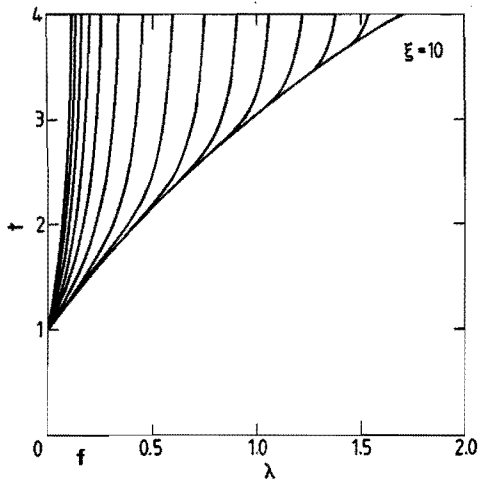
a,b: $\xi = 0$;

c,d: $\xi = 1$;

e,f: $\xi = 10$.

The solutions for which f becomes negative for high values of t are left out. Different curves correspond to different values of $f(t_h)$, where t_h is the highest value of the dimensionless temperature in the graph.

d,e,f: next page.
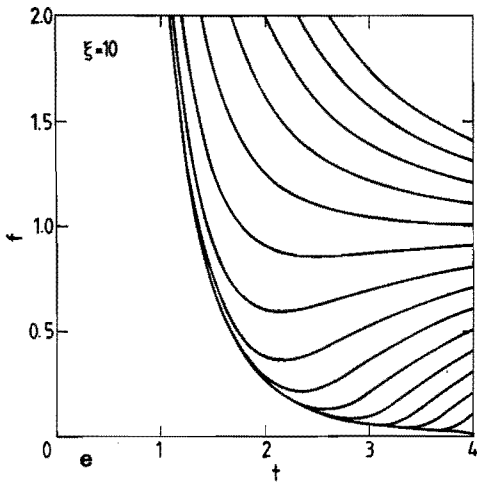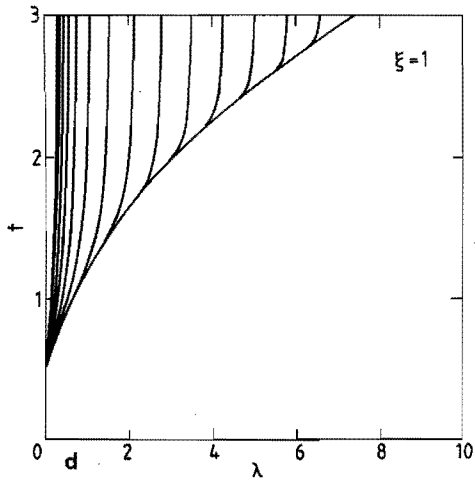
Fig. 5 *The asymptotic solutions of (34) and (35) for several values of ξ (full curves) and the solutions of the equations in which the heat conduction has been neglected, given in (42) and (43) (dashed curves).*

Only in a distance of order ℓ_0 near the exit, the profile will deviate from the asymptotic solution in order to obey the boundary condition. In Fig. 5a and 5b the asymptotic solutions $f(t)$ and $\lambda(t)$ are plotted for several values of ξ.
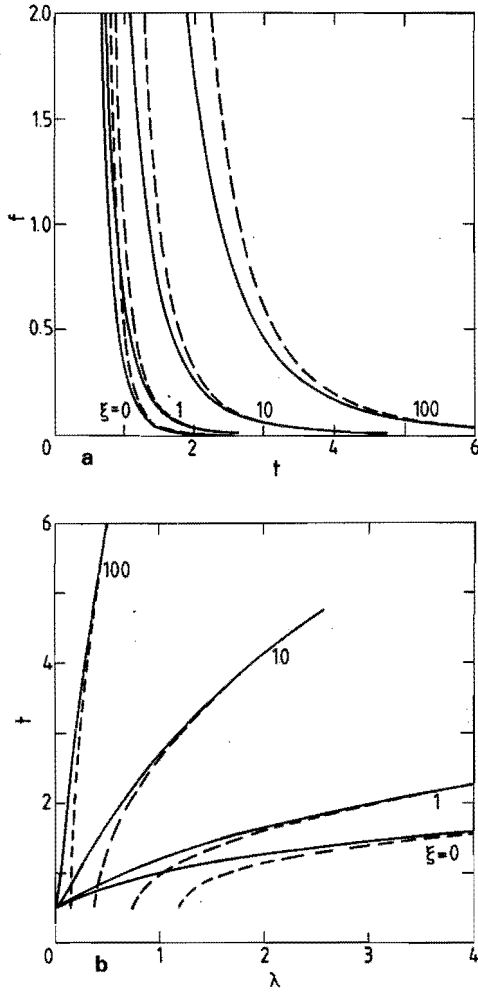
The temperature of the mixing chamber is a function of $\dot{n}_3$, the temperature T_i of the incoming ^{3}He, the sizes of the impedances of the inlet tube and the dilute exit tube and the external heat load on the mixing chamber $\dot{Q}_{ex}$. To calculate T_m, equation (30) has to be solved, for which two boundary conditions are needed.

The first boundary condition is a condition for the temperature at the end of the exit tube, T_e. Since the entrance of the inlet tube and the end of the exit tube are connected by a heat exchanger, T_e should be smaller than T_i. If T_e exceeds T_i, the incoming ^{3}He is heated by the mixture in the heat exchanger and T_i rises until a stationary situation is reached. So, the boundary condition reads in dimensionless form
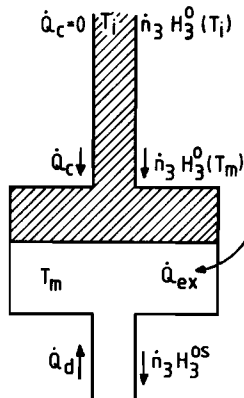
$$t_e \leq t_i \quad . \tag{36}$$

Fig. 6 Schematic drawing of the energy flows near the mixing chamber in continuous operation. The temperature T_i of the incoming ^{3}He at the entrance of the inlet tube is high enough to neglect the heat conduction there.

The second boundary condition is the energy balance in the mixing chamber (see Fig. 6), which reads, if the temperature in the mixing chamber is uniform

$$\dot{n}_3 H_3^0(T_m) + \dot{Q}_c + \dot{Q}_{ex} = \dot{n}_3 H_3^{os}(T_m, x_s(T_m)) - \dot{Q}_d \quad , \tag{37}$$

where $\dot{Q}_c$ and $\dot{Q}_d$ are the conductive heat flows towards the mixing chamber in the concentrated and dilute phase, respectively. The quantity $\dot{Q}_c$ involves the gradient of the temperature in the inlet tube, which can be found by solving the equation for the temperature profile in that tube. This equation has the same form as equation (30) with $\xi = 0$ [19], but different characteristic temperature and length. Thus, to calculate T_m, in principle two coupled differential equations should be solved. However, under normal conditions T_i is high enough to neglect the heat conduction at the entrance of the inlet tube. Hence, equation (37) can be replaced by

$$\dot{n}_3 H_3^0(T_i) + \dot{Q}_{ex} = \dot{n}_3 H_3^{os}(T_m, x_s(T_m)) - A\kappa \, (dT/d\ell)_m \quad , \tag{38}$$

or applying the low temperature limits

$$\dot{n}_3 H_{3c} T_i^2 + \dot{Q}_{ex} = \dot{n}_3 H_{3s} T_m^2 - A\kappa_d \frac{1}{T_m} \, (dT/d\ell)_m \quad , \tag{39}$$

where $H_{3c} = 11.4$ J/mol K^2, $H_{3s} = 93.0$ J/mol K^2 [14], and the suffix m denotes the mixing chamber values. With (33) equation (39) reads

$$f(t_m) = \frac{2H_{3s}}{C_d} - \frac{2H_{3c}}{C_d} \left[\frac{t_i}{t_m}\right]^2 - \frac{\dot{q}_{ex}}{t_m^2}$$

$$= 1.788 - 0.219 \left[\frac{t_i}{t_m}\right]^2 - \frac{\dot{q}_{ex}}{t_m^2} \quad , \tag{40}$$

where the dimensionless external heat load $\dot{q}_{ex}$ equals

$$\dot{q}_{ex} = \frac{2\dot{Q}_{ex}}{\dot{n}_3 C_d T_0^2} \quad . \tag{41}$$

The solutions of equation (30) depend very strongly on the boundary condition in the mixing chamber. This can be seen directly in Fig. 4 where many solutions tend to a single asymptotic solution for low values of t. A small change in the value of $f(t_m)$ leads to a completely different temperature profile. Therefore, a numerical integration from t_m to high values of t is impossible. There is, however, a way to cope with these numerical difficulties, namely by reversing the problem. First, for a given value of ξ and t_m equations (34) and (35) can be integrated in the negative λ-direction from several different high values of t and low values of f to t_m. In this way the asymptotic solution and $f(t_m)$ are found. Next, from equation (40) t_i can be found for a given value of $\dot{q}_{ex}$. Finally, the maximum dimensionless length of the tube Λ_u can be determined as the value of λ where the asymptotic solution $t(\lambda)$ equals t_i. Since for higher values of Λ cooling at the end of the tube should occur to reach t_i again, Λ_u is an upperbound for the length of the tube. For a shorter tube the t-profile does not have to follow the asymptotic solution. However, as the deviations from the asymptotic solution are restricted to a part near the end of the tube of length ℓ_0, this hardly affects the value of $f(t_m)$. Hence, for all values of $\Lambda \geq 2$, the value of t_i, found in this procedure, is reliable.

The values of t_i obtained in this way are plotted in Fig. 7 as functions of t_m for several values of ξ and $\dot{q}_{ex} = 0$. It turns out that if $t_i > 3$, the value of t_m is in good approximation independent of ξ for values of ξ up to 10. However, the maximum length of the tube decreases strongly with increasing ξ. Thus, the presence of mutual friction bounds the length of the dilute exit tube.

The intersections of the curves with the line $t_i = t_m$ obey the relation $f(t_m) = 1.788 - 0.219 = 1.569$, which follows from equation (40). The corresponding value of t_m can be called the intrinsic minimum temperature of a ^{3}He circulating dilution refrigerator in continuous operation. It can only be reached in the limit that Λ approaches zero, which corresponds to a very short or very wide dilute exit tube,
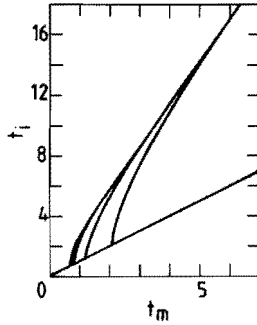
Fig. 7   *The maximum value of t_i as a function of t_m when the external heat load equals zero. The curves correspond from left to right with $\xi = 0, 1, 10$ and 100. The straight line represents $t_i = t_m$. The intersections of this line with the curves are the minimum t_m in continuous operation.*
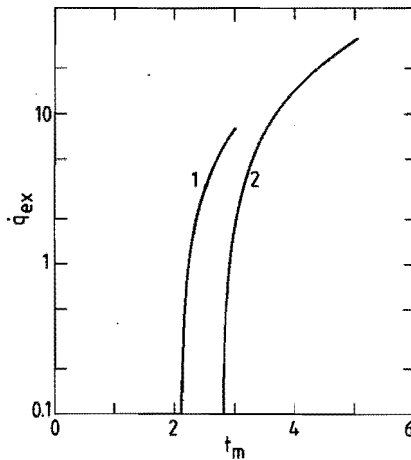
Fig. 8   *Two examples of $\dot{q}_{ex}$ as a function of t_m for fixed values of ξ and t_i; 1: $t_i = 6$, $\xi = 1$; 2: $t_i = 8$, $\xi = 10$.*

or a very small ^{3}He flow rate. This limiting temperature depends on ξ. In Table I some calculated values of t_m, t_i, $\dot{q}_{ex}$ and Λ_u are given for several values of ξ. In Fig. 8 two examples of graphs of $\dot{q}_{ex}$ as a function of t_m are plotted for fixed t_i and ξ. These examples show how a possible heat load on the mixing chamber influences its temperature.

90

Table I.

Calculated values of t_m, t_i, $\dot{q}_{ex}$ and Λ_u for several values of ξ.

ξ	t_i	t_m	$\dot{q}_{ex}$	Λ
0.0	0.777	0.71	0.0	0.130
0.0	0.906	0.72	0.0	0.401
0.0	1.209	0.75	0.0	1.344
0.0	2.571	1.0	0.0	21.98
0.0	3.459	1.25	0.0	70.86
0.0	4.237	1.5	0.0	158.95
1.0	0.993	0.8	0.0	0.281
1.0	2.294	1.0	0.0	3.461
1.0	4.133	1.5	0.0	13.315
1.0	5.654	2.0	0.0	26.20
1.0	7.114	2.5	0.0	42.47
1.0	8.556	3.0	0.0	62.25
10.0	1.193	1.17	0.0	0.00913
10.0	1.505	1.2	0.0	0.1247
10.0	3.329	1.5	0.0	0.9805
10.0	5.273	2.0	0.0	2.448
10.0	6.904	2.5	0.0	4.184
10.0	8.429	3.0	0.0	6.230
10.0	9.909	3.5	0.0	8.608
10.0	11.368	4.0	0.0	11.328
10.0	12.814	4.5	0.0	14.396
10.0	14.255	5.0	0.0	17.816
10.0	15.691	5.5	0.0	21.590
10.0	17.126	6.0	0.0	25.720
100.0	3.733	2.25	0.0	0.1179
100.0	5.170	2.5	0.0	0.240
100.0	7.363	3.0	0.0	0.485
100.0	9.196	3.5	0.0	0.751
100.0	10.867	4.0	0.0	1.044
100.0	12.451	4.5	0.0	1.367
100.0	13.984	5.0	0.0	1.722
100.0	15.484	5.5	0.0	2.109
100.0	16.964	6.0	0.0	2.529
1.0	6.0	3.0	8.147	25.74
1.0	6.0	2.75	5.564	27.03
1.0	6.0	2.5	3.200	28.19
1.0	6.0	2.25	1.053	29.22
1.0	6.0	2.15	0.253	29.59
1.0	6.0	2.1174	0.0028	29.71
10.0	8.0	5.0	30.49	3.903
10.0	8.0	4.5	21.95	4.380
10.0	8.0	4.0	14.28	4.809
10.0	8.0	3.7	10.10	5.044
10.0	8.0	3.5	7.488	5.191
10.0	8.0	3.2	3.821	5.397
10.0	8.0	3.0	1.543	5.526
10.0	8.0	2.87	0.134	5.606
10.0	8.0	2.8574	0.003	5.613

In the experiments of Castelijns et al. [18] an experimental cell was installed in the dilute exit tube between the mixing chamber and the lowest heat exchanger. In that case the steep part of the temperature profile, where heat conduction plays a role, is situated between the experimental cell and the heat exchangers. Hence, the asymptotic solution describes the temperature profile between the mixing chamber and the experimental cell. If the first term in equation (30), the heat conduction term, is negligible, equation (30) reduces to a first-order differential equation which can be solved implicitly. The result is

$$\lambda = \frac{1}{\xi} (t^2 - t_m^2) - \frac{1}{\xi^2} \ln\left[\frac{\xi t^2 + 1}{\xi t_m^2 + 1}\right] \quad \text{if } \xi > 0$$

and   (42)

$$\lambda = \frac{1}{2} (t^4 - t_m^4) \qquad \text{if } \xi = 0 .$$

Substitution of equation (42) in (33) yields for all values of ξ

$$f(t) = \frac{1 + \xi t^2}{2t^6} .$$ (43)

In Fig. 5a and 5b these functions are drawn for the same values of ξ as the asymptotic solutions. The parameter t_m in equation (42) has been chosen such that the temperatures of both solutions are the same at the high temperature side of the tube. It can be seen that the solutions of the equation without the heat conduction term follow the asymptotic solution with the same ξ down to low temperatures. Hence, if the temperature in the mixing chamber is not too low, heat conduction can be neglected in the part of the tube between the mixing chamber and the experimental cell.

In the situation of reference 18 the value of ξt^2 was always much greater than 1, so that the logarithmic term in equation (42) is negligible. Substitution of equations (28), (29) and (31) then yields

$$T_e^2 = T_m^2 + \frac{1-x_0}{x_0} \frac{2X}{C_d} \left[\frac{\dot{n}_3}{A}\right]^3 L \quad , \tag{44}$$

where T_e is the temperature in the experimental cell and L the length of the tube. In reference 18 the measured temperatures were represented by the relation

$$T_e^2 = T_m^2 + a\gamma \left[\frac{\dot{n}_3}{A}\right]^\alpha L \quad , \tag{45}$$

with $\alpha = 2.8 \pm 0.4$ and $a\gamma = (7.4 \pm 0.7) \times 10^{-9}$ in SI units. Refitting the measurements to a cubic dependence $\Delta(T^2) \sim (\dot{n}_3/A)^3 L$ yields good agreement with equation (44).

   If the heat conduction is negligible, the derivation of the temperature profile in the tube can be made much easier by leaving out the heat conduction term from the beginning and choosing other units of temperature and length. Neglecting the heat conduction term in the energy conservation law (25) leads to

$$C_d T \frac{dT}{d\ell} - \eta_d \frac{\dot{n}_3 V_{3d}^2}{T^2} \zeta - \frac{1-x_0}{x_0} X \left[\frac{\dot{n}_3}{A}\right]^3 = 0 \quad , \tag{46}$$

where equation (15) has been substituted for $d\mu_4/d\ell$. This equation can be made dimensionless by defining τ and λ' as

$$\tau = T/T_0' \tag{47}$$

and

$$\lambda' = \ell/\ell_0' \quad , \tag{48}$$

where

$$T_0' = \left[\frac{x_0}{1-x_0} \frac{\eta_d V_{3d}^2 \zeta A^3}{X}\right]^{1/2} \frac{1}{\dot{n}_3} \simeq 2.53 \times 10^{-4} \frac{A}{\dot{n}_3} (A\zeta)^{1/2} \text{ K} \tag{49}$$

93

and

$$
\ell_0^{\cdot} = \frac{1}{2} \left[\frac{x_0}{1-x_0} \right]^2 \frac{C_d \eta_d V_{3d}^2 A^6 \zeta}{\chi^2 \dot{n}_3^5} \simeq 23.61 \left[\frac{A}{\dot{n}_3} \right]^5 A \zeta \quad m \tag{50}
$$

are the characteristic temperature and length. In this temperature- and lengthscale equation (46) reads

$$
\frac{d\tau^2}{d\lambda'} - \frac{1}{\tau^2} - 1 = 0 \quad . \tag{51}
$$

from which follows the implicit relation for $\tau(\lambda')$

$$
\tau^2 - \tau_m^2 - \ln \left[\frac{1+\tau^2}{1+\tau_m^2} \right] = \lambda' \quad , \tag{52}
$$

where τ_m is the dimensionless temperature in the mixing chamber, where λ' equals zero. The pressure drop Δp over the impedance can be found from

$$
\Delta p = \int_0^L \left| \frac{dp}{d\ell} \right| d\ell = \dot{n}_3 V_{3d} \eta_d \zeta \int_0^L \frac{1}{T(\ell)^2} d\ell \quad . \tag{53}
$$

where equation (12) has been substituted. The integral in equation (53) can be calculated by substitution of (46). The result is

$$
\Delta p = p_0 (\tau_e^2 - \tau_m^2 - \Lambda') \quad . \tag{54}
$$

where τ_e is the temperature at the end of the impedance, Λ' the dimensionless length and p_0 the unit of pressure defined as

$$
p_0 = \frac{x_0}{1-x_0} \frac{\eta_d V_{3d} C_d A^3 \zeta}{2\chi \dot{n}_3^2} \simeq 7.85 \times 10^{-3} \left[\frac{A}{\dot{n}_3} \right]^2 A \zeta \quad Pa. \tag{55}
$$

94

From equation (40) and the shape of the asymptotic solution $f(t)$ it can be seen that the minimum attainable mixing chamber temperature in continuous operation is restricted by the temperature of the incoming ^{3}He. For high values of t_i, $f(t_m)$ is small which leads to a higher t_m. For low values of t_i the dissipation in the exit tube is important and restricts the dimensionless length of this tube to very small values.

A solution to this dilemma is the single-cycle mode. In this mode the circulation of ^{3}He is stopped at a certain moment, while ^{3}He is still extracted from the still, so that the amount of ^{3}He in the concentrated phase in the mixing chamber gradually decreases. The price to be paid is the finite duration of this process: when the ^{3}He in the concentrated phase is exhausted, the cooling in the mixing chamber comes to an end. Thus, the duration of the single cycle is determined by the amount of ^{3}He at the start and the molar ^{3}He flow rate.

At the start of a single cycle the situation in the exit tube is not stationary, but the temperature gradually decreases. At a certain time, however, a stationary situation in the exit tube begins to settle. From that time on, the amount of ^{3}He in the mixing chamber still decreases, but the temperature is constant. If the total amount of ^{3}He is diluted, the temperatures start rising again.

In this section only the situation during the time that the exit tube is in a stationary state will be considered. Hence, equation (24) for the conservation of energy in this tube still applies. However, although the temperature in the mixing chamber does not vary, the amount of ^{3}He, and thus the total energy in the mixing chamber, change. Hence, the time derivative in the energy conservation law (III.35), applied to the mixing chamber, does not equal zero.

During a single cycle, the ^{4}He flow cannot be neglected, since ^{4}He flows into the mixing chamber to compensate the ^{3}He flow out of the mixing chamber. If no mutual friction is present, this makes no difference, but in the presence of mutual friction, $\partial \mu_4 / \partial \ell$ is unequal to zero and this gives a contribution to the energy flux.

The net ^{4}He molar flow rate can be determined from the condition that the volume of the mixing chamber is constant. This volume is given by

$$V = N_{3c}V_3^o + N_{3d}V_{3d} \quad .$$

(56)

where N_{3c} and N_{3d} are the numbers of moles of ^{3}He in the concentrated and dilute phase in the mixing chamber, respectively, and V_3^o is the molar volume of pure ^{3}He, equal to 36.8×10^{-6} m^3/mol. The number of moles of ^{4}He in the mixing chamber equals

$$N_{4d} = \frac{1-x}{x} N_{3d} \quad .$$

(57)

and the molar flow rate of the ^{3}He leaving the mixing chamber equals

$$\dot{n}_3 = -(\dot{N}_{3d} + \dot{N}_{3c}) \quad .$$

(58)

where $\dot{n}_3$ is positive, if ^{3}He flows out of the mixing chamber.

From the time derivative of equation (56) follows that

$$\dot{N}_{3c}V_3^o + \dot{N}_{3d}V_{3d} = 0 \quad .$$

(59)

Hence

$$\dot{N}_{3c} = -\dot{n}_3 \frac{V_{3d}}{V_{3d} - V_3^o} \quad ,$$

(60)

$$\dot{N}_{3d} = \dot{n}_3 \frac{V_3^o}{V_{3d} - V_3^o} \quad ,$$

(61)

and

$$\dot{n}_4 = -\frac{1-x}{x} \dot{n}_3 \frac{V_3^o}{V_{3d} - V_3^o} \quad ,$$

(62)

where $\dot{n}_4$ is positive, if ^{4}He flows out of the mixing chamber.

Substitution in equation (24) and using (15) yields

$$\frac{1}{2}C_d \frac{dT^2}{d\ell} - \frac{\eta_d \zeta V_{3d}^2 \dot{n}_3}{T^2} - \frac{1-x_0}{x_0} \frac{V_{3d}}{V_{3d}-V_3^\sigma} \times \left[\frac{\dot{n}_3}{A}\right]^3 - \frac{\kappa_d}{\dot{n}_3} A\frac{d}{d\ell}\left[\frac{1}{T}\frac{dT}{d\ell}\right] = 0 \quad . \quad (63)$$

This equation can be written in dimensionless form in the same way as equation (25), by using the reduced temperature t and reduced length λ, defined in equations (26)-(29). The result is similar to equation (30):

$$-\frac{d}{d\lambda}\left[\frac{1}{t}\frac{dt}{d\lambda}\right] + \frac{dt^2}{d\lambda} - \frac{1}{t^2} - \xi' = 0 \quad , \quad (64)$$

where ξ' is a dimensionless parameter, which is due to the ^{4}He back-flow slightly different from ξ, and equal to

$$\xi' = \frac{V_{3d}}{V_{3d}-V_3^\sigma} \xi \simeq 1.71 \left[\frac{\dot{n}_3}{A}\right]^2 (A\zeta)^{-2/3} \quad . \quad (65)$$

As the structures of equations (64) and (30) are the same, the results of the foregoing section can also be used in the single-cycle mode: again the function f(t) of equation (33) can be introduced and the temperature profiles in the exit tube are given in Figs. 4 and 5. However, the boundary conditions at the entrance and exit of the tube are different.

The boundary condition in the mixing chamber can be found again from the law of conservation of energy. The internal energy of the mixing chamber equals

$$U = N_{3c}U_3^0 + (N_{3d}+N_{4d})U_m \quad , \quad (66)$$

where U_3^0 and U_m are the molar internal energies of pure ^{3}He and of the mixture, respectively. From equations (60)-(62) follows in the limiting situation in which T_m is constant

$$\frac{\partial U}{\partial t} = -\dot{n}_3 \frac{V_{3d}}{V_{3d}-V_3^\sigma} U_3^0 + \frac{\dot{n}_3}{x} \frac{V_3^0}{V_{3d}-V_3^\sigma} U_m \quad . \quad (67)$$

The increase of internal energy equals the sum of the external heat load and the energy flow from the exit tube into the mixing chamber, J_U, which can be found from equations (18) and (62) as

$$J_U = -\dot{n}_3 H_3^{os} + \dot{n}_3 \frac{1-x}{x} \frac{V_3^o}{V_{3d}-V_3^o} \mu_4 + A\kappa \left[\frac{dT}{d\ell}\right]_m + \dot{Q}_{ex} \quad . \tag{68}$$

Equating J_U and $\partial U/\partial t$, using the low temperature approximation, equation (II.30) for H_3^{os} and the equilibrium condition $\mu_3^o = \mu_3$, yields

$$\dot{n}_3 \frac{V_{3d}}{V_{3d}-V_3^o} (C_d-C_c) T_m^2 = A\kappa_d \frac{1}{T_m}\left[\frac{dT}{d\ell}\right]_m + \dot{Q}_{ex} \quad , \tag{69}$$

where it has been used that at low temperatures

$$S_3^o = C_c T \quad , \tag{70}$$

with $C_c = 22.8$ J/mol K^2.

In dimensionless units equation (69) with (33) and (41) reads

$$f(t_m) = 2\frac{V_{3d}}{V_{3d}-V_3^o} \frac{C_d-C_c}{C_d} - \frac{2\dot{Q}_{ex}}{\dot{n}_3 C_d T_m^2} = 1.711 - \frac{\dot{q}_{ex}}{t_m^2} \quad . \tag{71}$$

From the properties of the solutions of equation (64) it follows again that the boundary condition at the downstream end is not very important for the temperature profile near the mixing chamber. If the tube is long enough ($L \gg \ell_0$), the temperature profile will follow the asymptotic solution in the low temperature part of the tube for all reasonable boundary conditions at the exit of the tube.

The difference with the boundary conditions in continuous operation is that the temperature at the exit t_e is not coupled to t_i, as in equation (36). Thus, apart from the condition that the ^{3}He concentration in the still is high enough, there is no restriction on the length of the tube. Furthermore, as can be seen by comparing equations (40) and (71), $f(t_m)$ is larger in single-cycle operation. Hence, the temperature in the mixing chamber is lower. For arbitrary values of ξ'

equation (34) can be integrated along the asymptotic solution starting from a high value of t. The value of t_m where the solution obeys equation (71) for arbitrary $\dot{q}_{ex}$ is the limiting value of the mixing chamber temperature during the single cycle.
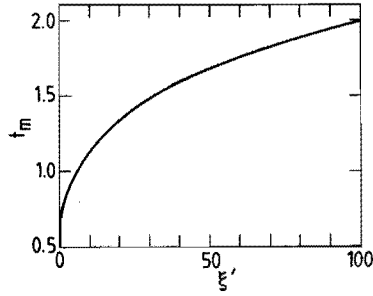

Fig. 9 *The minimum dimensionless mixing chamber temperature in single cycle operation as a function of ξ' for $\dot{q}_{ex} = 0$.*
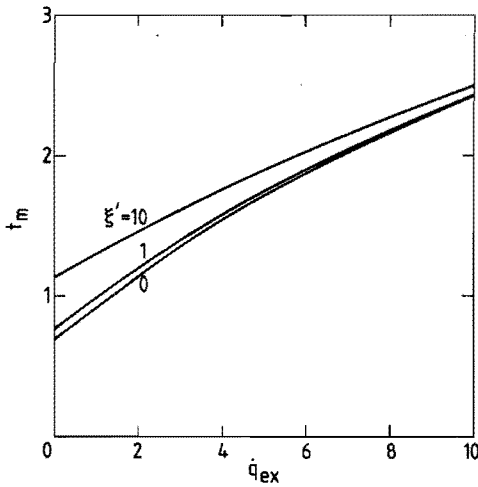

Fig. 10 *The minimum dimensionless mixing chamber temperature in a single cycle as a function of $\dot{q}_{ex}$ for $\xi' = 0$, 1 and 10.*
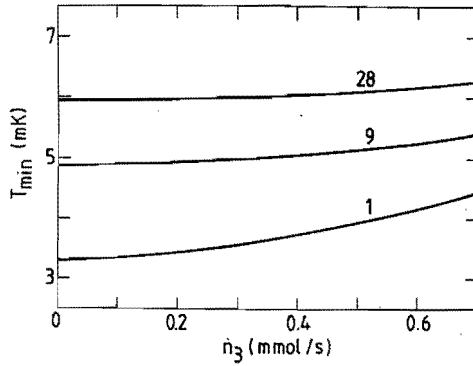
Fig. 11 *The minimum mixing chamber temperature in a single cycle as a*
function of the ^{3}He *molar flow rate for several impedances*
consisting of N parallel tubes with diameter D and length
23 mm. The values of N are indicated in the figure; N = 1:
D = 1.6 mm; N = 9: D = 0.5 mm; N = 28: D = 0.28 mm.

In Fig. 9 the thus obtained values of t_m are plotted as a func-
tion of ξ' in the case that $\dot{Q}_{ex} = 0$. In Fig. 10 t_m is plotted as a
function of $\dot{q}_{ex}$ for several values of ξ'. In Fig. 11 the mixing
chamber temperature is plotted as a function of the ^{3}He molar flow
rate for three different impedances, each consisting of N parallel
tubes with the same diameter D and the same length. The diameters are
chosen in such a way, that the total cross section of each impedance
is approximately the same. In each case the external heat load equals
zero. It follows from equations (28) and (65) that

$$T_0 = 5.63 \left[\frac{mm}{D}\right]^{1/3} mK \tag{72}$$

and

$$\xi' = 27.5 \left[\frac{\dot{n}_3}{mol/s}\right]^2 \frac{1}{N^2} \left[\frac{D}{mm}\right]^{8/3} . \tag{73}$$

100

It can be seen that the mixing chamber temperature is minimum in the limit of zero ^{3}He flow rate. This corresponds to $\xi' = 0$ and thus this temperature equals the intrinsic minimum temperature of a ^{3}He circulating dilution refrigerator in the Mechanical Vacuum Model, as calculated by Wheatley [5]. In the Mechanical Vacuum Model this temperature is independent of the ^{3}He flow rate. The presence of mutual friction leads to a higher minimum temperature for realistic values of the flow rate.

References

[1]   H. London, in Proceedings of the International Conference on Low temperature Physics, Oxford, 1951 (Clarendon Lab., 1951), p. 157.

[2]   H. London, G.R. Clarke, and E. Mendoza, Phys. Rev. **128**, 1992 (1962).

[3]   P. Das, R. de Bruyn Ouboter, and K.W. Taconis, in Proceedings of the IXth International Conference on Low Temperature Physics, Columbus, Ohio, 1964, J.G. Daunt, D.O. Edwards, F.J. Milford, and M. Yagub, eds. (Plenum, New York, 1965), p. 1253.

[4]   J.C. Wheatley, O.E. Vilches, and W.R. Abel, Physics **4**, 1 (1968).

[5]   G. Frossati, and D. Thoulouze, in Proceedings of the Fifth International Cryogenic Engineering Conference, Kyoto, 1974, K. Mendelssohn, ed. (IPC Business Press Ltd, 1974), p. 229.

[6]   A.T.A.M. de Waele, J.C.M. Keltjens, C.A.M. Castelijns, and H.M. Gijsman, Advances in Cryogenic Engeneering, **29**, (Plenum, New York, 1984), p. 565.

[7]   G.M. Coops, A.T.A.M. de Waele, and H.M. Gijsman, Cryogenics **19**, 659 (1979).

[8]   W. Griffioen, H.W. Jentink, and R. de Bruyn Ouboter, Physica **141B**, 137 (1986).

[9]   A.D. Severijns, and F.A. Staas, IFF meeting on advances in refrigeration at the lowest temperatures, Commision A1-2, Zürich (March 1978).

[10]   G. Frossati, J. de Physique, Colloq. C6, suppl. 8, **39**, 1578 (1978).

[11]   K.W. Taconis, Physica **109&110B**, 1753 (1982).

[12]   C.A.M. Castelijns, Thesis, Eindhoven University of Technology (1986).

[13]   R.J. Atkins, and N. Fox, Physica **142B**, 16 (1986).

[14]   H. Højgaard Jensen, H. Smith, P. Wölfle, K.Nagai, and T. Maack Bisgaard, J. Low Temp. Phys. **41**, 473 (1980).

[15]   J.C. Wheatley, Am. J. Phys. **36**, 181 (1968).

[16]   J.G.M. Kuerten, C.A.M. Castelijns, A.T.A.M. de Waele, and H.M. Gijsman, Phys. Rev. Lett. **56**, 2288 (1986).

[17]   J. Zeegers, J.G.M. Kuerten, A.T.A.M. de Waele, and H.M. Gijsman, to be published.

[18]   C.A.M. Castelijns, J.G.M. Kuerten, A.T.A.M. de Waele, and H.M. Gijsman, Phys. Rev. **B32**, 2870 (1985).

[19]   W. van Haeringen, F.A. Staas, and J.A. Geurst, Philips. J. Res. **34**, 107 (1979).

[20]   J.C. Wheatley, R.E. Rapp, and R.T. Johnson, J. Low Temp. Phys. **4**, 1 (1971).

V EXPERIMENTAL VERIFICATION IN THE ·COMBINED-DISSIPATION REGIME[1]

As stated in section 3.1, the results of the measurements of
Castelijns *et al*. [1] led to the existence of two contradicting theo-
retical models. In the Mechanical Vacuum Model [2] it was assumed that
mutual friction is absent and viscosity is the only dissipative term.
In the Mutual Friction Model viscosity is absent and the only dissi-
pative mechanism is mutual friction between ^{3}He and ^{4}He. The assump-
tion that viscosity is absent was inspired by measurements of the
pressure difference over a flow tube. Only in the situation where a
superleak parallel to the tube was installed, a nonzero pressure
difference was observed. However, in that case there is no mutual
friction, as the ^{4}He flows with the ^{3}He through the impedance and back
again through the superleak. Hence, the Mechanical Vacuum Model is
applicable. It seemed that two different models were needed to de-
scribe a general flow situation: one, the Mechanical Vacuum Model
leading to a small temperature increase and large pressure drop, holds
for small relative velocities, and the other, the Mutual Friction
Model, with large temperature increase and zero pressure drop, holds
for high relative velocities.

The measured pressure differences can be explained with the theo-
ry described in the preceding chapters. Since the viscosity of the
mixture decreases strongly with temperature, the pressure differences
in the experiments described in Reference 1 are of the order of 1 Pa.
Pressure differences of this order are difficult to measure accurate-
ly, because hydrostatic pressure differences due to density variations
in the liquid are of the same order of magnitude. Hence, in the exper-
iments by Castelijns *et al* [1]. the viscous force is dominated by
mutual friction. On the other hand, in the experiments by Wheatley
et al. [3], the ^{3}He flow rate is so low that the mutual friction is

---

outweighed by the viscous force. The value of ξt^2, introduced in chapter 4, determines the relative importance of both forces.

In the combined-dissipation regime, where $\xi t^2 \simeq 1$, the viscous force and the mutual frictional force play an equally important role. Therefore, an important verification of the theory is an experiment which measures the effects of both forces simultaneously in this regime. To satisfy $\xi t^2 \simeq 1$ with a ^{3}He flow rate in the range of the dilution refrigerator and a single flow tube, a large diameter is needed (see equation (IV.32)). This leads to negligibly small temperature differences over the tube. Therefore, a series of impedances was constructed consisting of a bundle of N parallel tubes each with the same diameter D_N and length L. The diameters D_N were chosen in such a way that the total cross-sectional area of the various impedances was approximately constant ($N \pi D_N^2/4 \simeq 2$ mm^2). The characteristics of the impedances are given in Table I.

Table I.
Properties of the flow impedances which were investigated in this work. The impedance factors Z of the bundles of tubes were calculated from the tube dimensions assuming Poiseuille flow ($Z = 128L/N \pi D_N^4$). The Z value of the sinter sponge was measured at room temperature. The properties of this sinter sponge are explained in the text. The ξ values are calculated for $\dot{n}_3 = 0.5$ mmol/s. The ξt^2 ranges are given for $\dot{n}_3$-T_m values of 0.7 mmol/s and 60 mK, and 0.2 mmol/s and 30 mK respectively.

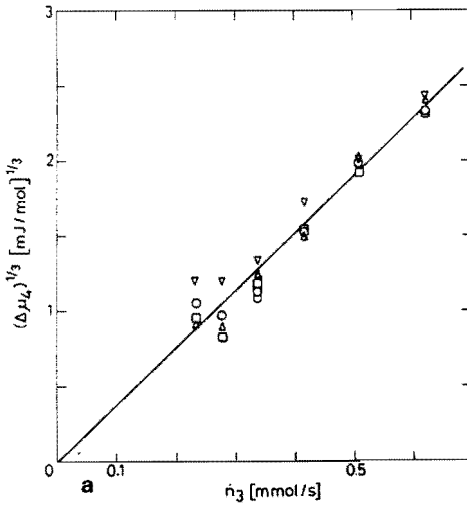| Kind of impedance	N	L (mm)	D_N (mm)	$Z/10^{12}$ (m^{-3})	ξ	ξt^2
bundle	1	23	1.6	0.14	1.8	11-540
bundle	9	23	0.5	1.7	0.49	1.4-70
bundle	28	23	0.28	5.4	0.24	0.46-23
sinter	–	–	0-0.1	183	–	–

Fig. 1

The cube root of the difference in chemical potential over the flow impedance as a function of the molar ^3He flow rate.

a: Data obtained with the flow impedance consisting of 28 tubes in parallel. The symbols correspond to different values of T_m ($\square$: 30 mK; $\circ$: 40 mK; $\triangle$: 50 mK; $\triangledown$: 60 mK).

The line obeys:

$$\Delta\mu_4 = 1.2 \times 10^{-8} \, (\dot{n}_3/A)^3 L.$$

b: Data obtained from four different flow impedances mentioned in Table I ($\triangle$: $N = 1$, $T_m = 30$ mK; $\square$: $N = 9$, $T_m = 30$ mK; $\circ$: $N = 28$, $T_m = 30$ mK; $\bullet$: sinter sponge, $T_m = 54$ mK).
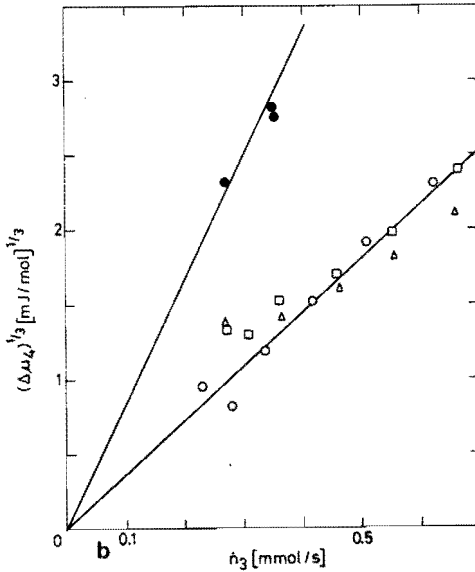
Fig. 2

a: The pressure difference Δp over the 28 parallel tubes, as a function of $\dot{n}_3$. The data were obtained for several constant values of T_m ($\square$: 30 mK; $\circ$: 40 mK; $\triangle$: 50 mK; ∇: 60 mK).

The lines are for visual aid only. The viscosity constant η_d is determined from the dashed parts of the curves.

b: Reduced pressure differences for the four flow impedances. The symbols refer to the same situations as in Fig. 1b. The straight line corresponds to the theoretical dependence given in equation (IV.12) for $\eta_d = 5 \times 10^{-8}$, which is valid at low flow rates. For higher ^{3}He flow rates the increasing temperature in the impedance results in deviations from the straight line. The differences between the tubes may be due to the inaccuracy in the values of the diameters of the tubes, leading to an uncertainty in the values of the impedance factor Z ($Z \sim D^{-4}$ for Poiseuille flow).
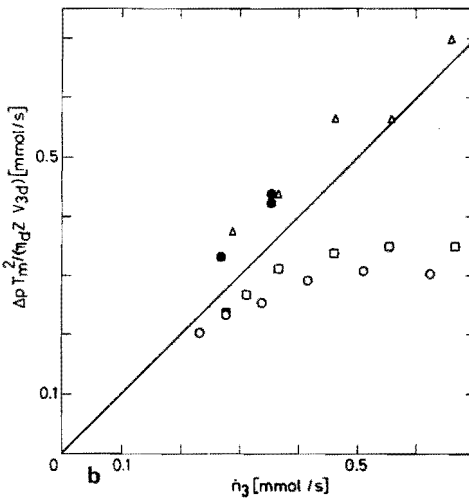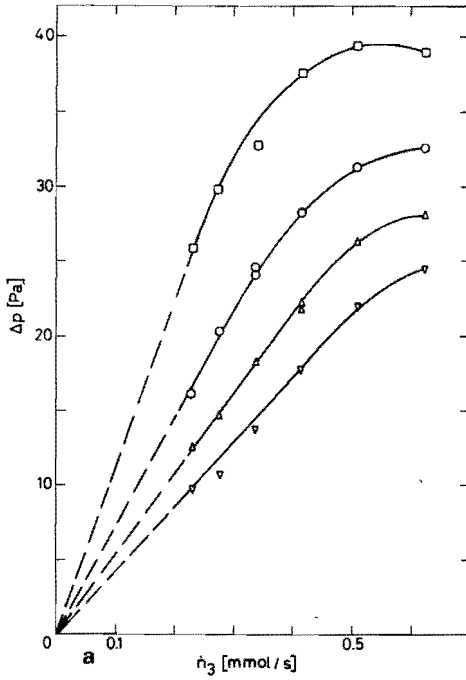
The pressure difference Δp was measured as a function of $\dot{n}_3$ for several values of the mixing chamber temperature, varying between 30 and 60 mK. Furthermore, from the measured temperature, pressure and ^{3}He concentration at the end of the impedance, the ^{4}He chemical potential is calculated. The ^{3}He concentration and the ^{4}He chemical potential in the mixing chamber follow from the measured T_m using the tabulated values at the coexistence curve [4].

In Fig. 1, some examples of the cube root of the difference in ^{4}He chemical potential between the exit and the entrance of the impedance, $\Delta\mu_4$, are plotted as functions of $\dot{n}_3$. It can be seen that mutual friction is present ($\Delta\mu_4 \neq 0$) and satisfies equation (IV.15). In Fig. 2 measured pressure differences for various values of T_m are plotted as functions of $\dot{n}_3$. The values of the constant η_d are derived from the linear part of these graphs. They vary from $(5\pm1)\times10^{-8}$ Pa s K^2 at $T_m = 30$ mK to $(6.5\pm1)\times10^{-8}$ Pa s K^2 at $T_m = 60$ mK. In view of the approximations made in deriving equation (IV.30), these values are in good agreement with the measurements of Kuenhold et al. [5], who found a value for η_d increasing with temperature and with a low temperature limit of 5×10^{-8} Pa s K^2. For higher flow rates the increasing temperature in the tube leads to a decreasing viscosity of the mixture. This effect results in a smaller pressure difference than expected from the linear Δp–$\dot{n}_3$ relationship in Fig. 2a and 2b.

Figures 1 and 2 also give the results of measurements using a porous plug as a flow impedance. The plug had a length of 33.8 mm and a circular diameter of 8 mm. It consisted of a sintered bronze sponge. The spherical particles had a diameter varying from 30 to 90 μm. The pore size was irregular and varied from 0 to 100 μm. The filling factor was 74 %. The values of the cross-sectional area A and the effective length L for this geometry are not well defined. From the results of Fig. 1 an effective area of 1 mm^2 is found, which is on the low side. A closed packed system of spheres would yield a free area for the flowing ^{3}He of the order of 3 mm^2. Using the value of the impedance factor $Z = \zeta L$ as determined at room temperature (see Table I), the results derived from the pressure measurements are in good agreement with equation (IV.12). This result shows the validity of the model described here for flow-impedance factors which differ by three orders of magnitude.

In conclusion, in this work a new description for the hydro-dynamics of ^{3}He-^{4}He mixtures is set up, which includes both a mutual frictional force and a viscous force. This description is in agreement with experiments, in which one force dominates the other, as well as with the measurements described here, in which both forces are equally important. With this description an important problem in ^{3}He-^{4}He hydrodynamics is solved.

References

[1]   C.A.M. Castelijns, J.G.M. Kuerten, A.T.A.M. de Waele, and H.M. Gijsman, Phys. Rev. **B32**, 2870 (1985).

[2]   J.C. Wheatley, O.E. Vilches, and R.T. Johnson, Physics **4**, 1 (1968).

[3]   J.C. Wheatley, J.C. Rapp, and R.T. Johnson, J. Low Temp. Phys., **4**, 1 (1971).

[4]   J.G.M. Kuerten, C.A.M. Castelijns, A.T.A.M. de Waele, and H.M. Gijsman, Cryogenics **25**, 419 (1985).

[5]   K.A. Kuenhold, D.B. Crum, and R.E. Sarwinski, Phys. Lett., **41A**, 13 (1972).

VI NUMERICAL SIMULATION OF THE MOTION OF QUANTIZED VORTICES

6.1 *Introduction*

In chapter III the phenomenological hydrodynamic equations for ^{3}He-^{4}He II mixtures, including mutual friction, were derived. From the analogy with flow in pure ^{4}He II it is expected, that mutual friction is due to the interaction of ^{3}He with quantized vortex lines. The adopted picture is that these vortex lines are created, if the average relative velocity between ^{3}He and ^{4}He exceeds a certain critical value. Due to their mutual interaction and the interaction with ^{3}He, the vortex lines will develop towards a complex structure, which is called a vortex tangle. Using a dimensional argument, the dependence of the mutual-frictional-force density on the relative velocity has been established (see equation (III.55) and below). The experimentally obtained frictional force of equation (IV.15) shows indeed this dependence on relative velocity, at least within the temperature and concentration region of the experiments.

What is still missing, is a theoretical derivation of the numerical value of the friction parameter χ, introduced in (IV.15). To make up for this deficiency, one would like to calculate the interaction between a vortex line and one ^{3}He particle, and subsequently the mutual-frictional-force density. In pure ^{4}He, where the normal fluid only consists of phonons and rotons, it is possible to calculate the interaction between a vortex line and the normal fluid in a semi-classical way [1,2]. On the other hand, in mixtures at low temperatures the ^{3}He constitutes a *degenerate* Fermi gas, so that a calculation of the interaction between ^{3}He and vortices involves quantummechanics. Furthermore, the vortex lines are of macroscopic size, and have a continually changing, irregular shape. Therefore, a calculation of the mutual-frictional-force density from first principles is an enormous task, which has not been accomplished as yet.

On the other hand, if the force between ^{3}He and a single straight vortex line is known, the equation of motion for a vortex line can be constructed. It is then possible to calculate the evolution of a vortex tangle numerically, starting from an arbitrary initial configuration. One may expect that after a transient time dynamical

equilibrium will be reached, in which macroscopic properties, like the line-length density L, and the mutual-frictional-force density F, fluctuate around an average value.

The procedure outlined above has been followed by Schwarz [3,4] for pure ^{4}He, where the force between the normal component and a straight vortex line is known from experiment [5]. Unfortunately, the force between ^{3}He and a vortex line is not known from experiment, nor from theory, although a theoretical calculation seems possible. It will be shown that it is possible to use a general expression for this force with only two unknown parameters, which may be dependent on temperature and ^{3}He concentration. Hence, the unknown quantities L and F can then be determined as functions of these two parameters and the relative velocity.

Especially for homogeneous turbulence a lot of work has been done by Schwarz, but many questions remain. Two of these are: what is the influence of walls on the mutual friction, and which effect does mutual friction have on the ^{3}He velocity profile. Both questions are related to the understanding of critical velocities. Furthermore, in the proposed treatment it will be possible to calculate the fluctuations of measurable quantities, such as the temperature and ^{3}He concentration, which are directly comparable with experimental results. To answer these questions an investigation on the numerical calculation of the evolution of a vortex tangle was started at the Eindhoven University of Technology. As a first step it is necessary to calculate the evolution in the case of homogeneous turbulence, as has been done before by Schwarz. The results can be compared with the experiments that led to equation (IV.15), so that an estimate of the accuracy of the calculations can be obtained. In a later stage, the open questions mentioned above will be studied. In this chapter the first results of the investigation on homogeneous turbulence are reported. Section 6.2 deals with the equation of motion of a vortex line. It turns out that in order to numerically simulate the evolution of a vortex tangle, serious problems arise, if two vortices approach closely. In those events Schwarz assumes that a reconnection of the two vortices occurs: they break at the point of closest approach and cross-connect (reconnection assumption). Similarly, he assumes that a vortex connects to a wall, if it approaches the wall closely. In

section 6.3 the latter process is studied in order to obtain a useful numerical procedure for a reconnection event in the simulation of a vortex tangle. The calculations described here, were performed on the supercomputer Cyber 205.

6.2 *The equation of motion of a vortex line*

As a first step towards the calculation of the evolution of a vortex tangle, the equation of motion of a vortex line should be known. This equation has been derived by Schwarz [6]. Two contributions can be distinguished. If there is no mutual friction, the vortices move along with the superfluid. This follows directly from the Kelvin circulation theorem [7] and equation (III.45) in the absence of f. So, the first contribution to the velocity of a point on the vortex line is the local superfluid velocity v_0. This *local* velocity v_0 differs from the hydrodynamic superfluid velocity v_s used in chapter III, which equals the *average* of v_0 over a volume containing many vortex lines. The other contribution stems from the force on the vortices due to the interaction with the normal component. Since the inertia of the vortex core is very small, this force has to be transferred to the superfluid as a Magnus force. This causes a difference between the local superfluid velocity and the velocity of the vortex line, as calculated by Schwarz [6].

He showed that this velocity difference is proportional to the velocity of the normal fluid with respect to the line. Generally, it has an arbitrary direction. However, the component in the direction of the line results in a displacement of a point on the vortex line along the line. As the resulting superfluid velocity field does not depend on the positions of the individual points on a vortex line, but only on the shape of the vortex as a whole, such a displacement has no physical significance. Therefore, the general expression for the velocity of a vortex line, v equals

$$v = v_0 + \alpha s' \times (v_n - v_0) - \alpha' s' \times [s' \times (v_n - v_0)] \quad , \qquad (1)$$

where v_n is the average normal fluid velocity, s' is the unit vector tangent to the vortex line (see Fig. 1), and α and α' are two friction

parameters, dependent on temperature and concentration. For pure ^{4}He II these parameters are known from experiments in rotating helium [5] and have been calculated theoretically [1,2]. The results are in reasonable agreement for temperatures below 2 K. For ^{3}He-^{4}He mixtures the friction parameters have not been measured in the same way.

For a given configuration of the vortices, equation (1) yields the time evolution, if $\mathbf{v}_0$ is known. This local superfluid velocity can be calculated in the following way. The vortex configuration is represented as a continuous curve by the parametric form $\mathbf{s}(\xi,t)$, where ξ is the arc length of the vortex and $\mathbf{s}(\xi,t)$ the position in three-dimensional space of the point ξ at time t. The local superfluid velocity obeys the relations

$$\nabla \times \mathbf{v}_0 = 0 \tag{2}$$

and

$$\oint_C \mathbf{v}_0 \cdot d\mathbf{l} = k = h/m_4 \quad . \tag{3}$$

if C is a contour around one vortex line with positive orientation. If the superfluid would be an incompressible fluid obeying

$$\nabla \cdot \mathbf{v}_0 = 0 \quad , \tag{4}$$

the equations are similar to the equations for a magnetic field in the presence of electric currents and give the Biot-Savart solution [8]:

$$\mathbf{v}_0(\mathbf{r},t) = \mathbf{v}_{s0} + \frac{k}{4\pi} \int_{\mathcal{L}} \frac{(\mathbf{s}-\mathbf{r}) \times d\mathbf{s}}{|\mathbf{s}-\mathbf{r}|^3} \quad , \tag{5}$$

where $\mathbf{r}$ is a position in three-dimensional space, $\mathbf{v}_{s0}$ is an arbitrary solution of equations (2) and (4) without vortices and the integral is taken over all vortex lines. As will be discussed later, $\mathbf{v}_{s0}$ can be found from the boundary conditions. Since the configuration of the vortex lines is a function of time, $\mathbf{v}_0$ depends on t.

In general $\nabla \cdot \mathbf{v}_0 \neq 0$, due to spatial variations in the normal and

112

superfluid densities, and equation (5) is not correct. However, it can be shown in the following way that in most cases the corrections to equation (5) are small. Suppose that

$$\nabla \cdot \mathbf{v}_0 = g(\mathbf{r}) \quad . \tag{6}$$

If $\mathbf{v}_0 = \mathbf{v}_{sa} + \mathbf{v}_{sb}$ in such a way that $\mathbf{v}_{sa}$ satisfies equations (3) and (4) and $\mathbf{v}_{sb}$ satisfies (2) and (6), then $\mathbf{v}_0$ satisfies equations (3) and (6) and is thus the general solution. The velocity field $\mathbf{v}_{sa}$ has already been given in equation (5), and $\mathbf{v}_{sb}$ can also be found from electrodynamics as the electric field in a static charge distribution [8]. By adding the two velocity fields the general solution for the local superfluid velocity follows as

$$\mathbf{v}_0(\mathbf{r},t) = \mathbf{v}_{s0} + \frac{k}{4\pi} \int_{\mathscr{L}} \frac{(\mathbf{s}-\mathbf{r}) \times d\mathbf{s}}{|\mathbf{s}-\mathbf{r}|^3} + \frac{1}{4\pi} \int_{\Omega} d^3r' g(\mathbf{r}') \frac{\mathbf{r}-\mathbf{r}'}{|\mathbf{r}-\mathbf{r}'|^3} \quad .\tag{7}$$

The region of integration of the second integral extends over the entire volume.

It is possible to estimate the last term, which will be denoted by I_2, with respect to the second as follows. Generally, the variations in the total density of the fluid are small, because the compressibility is small. Hence, the continuity equation (III.28), which also holds locally, yields

$$\nabla \cdot \mathbf{j} = 0 \quad , \tag{8}$$

or with $\mathbf{j} = \rho_n \mathbf{v}_n + \rho_s \mathbf{v}_0$ and equation (6)

$$g(\mathbf{r}) = -\frac{\mathbf{v}_0}{\rho_s} \cdot \nabla \rho_s - \frac{1}{\rho_s} \nabla \cdot (\rho_n \mathbf{v}_n) \quad . \tag{9}$$

Since the velocity of the normal component is generally small compared to the superfluid velocity, the second term will be neglected. Furthermore, the spatial variations of the superfluid density are small except near a vortex core, where $\rho_s \rightarrow 0$. Near a vortex core the superfluid velocity is large as well, but its important component is

in the azimuthal direction, perpendicular to $\nabla \rho_s$. Therefore, $g(r)$ is negligible except in the region of the vortex core, where it equals

$$g(r) \simeq - \frac{v_s^o(r)}{r_0} \quad , \tag{10}$$

where r_0 is of the order of the radius of the vortex core and v_s^o is the superfluid velocity at a vortex line due to boundary conditions and all other vortices. In this equation $|\nabla \rho_s(r)| \simeq \rho_s(r)/r_0$ has been substituted. The resulting estimate for I_2 is

$$I_2 \leq - \frac{r_0}{4} \int_{\mathscr{L}} v_s^o(s) \frac{r-s}{|r-s|^3} d\xi \quad . \tag{11}$$

Now, the two integrals in equation (7) can be compared. The result is that I_2 can be neglected, if

$$v_s^o \ll k/\pi r_0 \simeq 600 \text{ m/s} \quad , \tag{12}$$

where the core radius r_0 has been estimated as 0.5 Å. The superfluid velocity at a distance of 1 Å from the center of a vortex line equals 160 m/s. Hence, I_2 can be neglected, except if two vortex lines approach within a few ångström. It is to be expected, that if two vortex lines approach so closely, the structure of the vortex core, which is not known, plays an important role. Those situations, in which this classical calculation is not valid anyway, will be treated in a different way, and equation (5) can be used in all situations under consideration.

With expression (5) the velocity in the liquid, but also in a point on the vortex can be calculated. In the latter case equation (5) has to be evaluated for each point on the tangle:

$$v_0(s,t) = v_{s0} + \frac{k}{4\pi} \int_{\mathscr{L}} \frac{(s_1-s) \times ds_1}{|s_1-s|^3} \quad . \tag{13}$$

The integral diverges when $s_1 \to s$. This problem can be solved by taking

into account the finite structure of the vortex core. By comparison with the velocity of a classical vortex ring, the integral in equation (13) can be separated in two parts: a local contribution due to the part of the tangle near **s**, and a nonlocal contribution due to the rest of the tangle. The result is [4,9]

$$\mathbf{v}_0 = \mathbf{v}_{s0} + \frac{k}{4\pi} \mathbf{s}' \times \mathbf{s}'' \ln \left[\frac{2\sqrt{l_+ l_-}}{e^{1/4} a_0} \right] + \frac{k}{4\pi} \int_{\mathcal{L}}^{'} \frac{(\mathbf{s}_1 - \mathbf{s}) \times d\mathbf{s}_1}{|\mathbf{s}_1 - \mathbf{s}|^3} \quad , \qquad (14)$$

where a_0 is the diameter of the vortex core, l_+ and l_- are the lengths of the parts of the vortex line around **s** omitted from the integration in the second term, and the prime indicates that this local part is omitted. The second derivative of **s** with respect to ξ is denoted by **s"**. This vector points along the principle normal of the vortex line in **s** and has length R^{-1}, where R is the local radius of curvature. The cross product **s'×s"** is directed along the binormal and has the same length (see Fig. 1). Equation (14) yields the expression for the velocity of a classical vortex ring with radius R in an infinite fluid, independent of the choices of l_+ and l_- [10]:

$$\mathbf{v}_0 = \frac{k}{4\pi R} \ln \left[\frac{8R}{e^{1/4} a_0} \right] \quad , \qquad (15)$$

with direction perpendicular to the plane of the ring. In general, the separation in a local and nonlocal part in equation (14) is in good approximation valid, if l_+ and l_- are chosen in such a way, that $a_0 \ll l_+, l_- \ll R$. This follows by expansion of the integration variable in equation (13) around **s**.

There is still an unknown term in equation (14). As mentioned above, the velocity field $\mathbf{v}_{s0}$ is an arbitrary solution of equations (2) and (4). If boundaries are present, it can be calculated from the requirement that the local superfluid velocity satisfies a specified boundary condition. For the smooth plane surfaces considered here, the boundary condition that the component of the superfluid velocity perpendicular to the wall equals zero, can easily be incorporated. In that case $\mathbf{v}_{s0}$ equals the velocity field of the reflections of the tangle into each wall, with the direction of the reflections reversed.
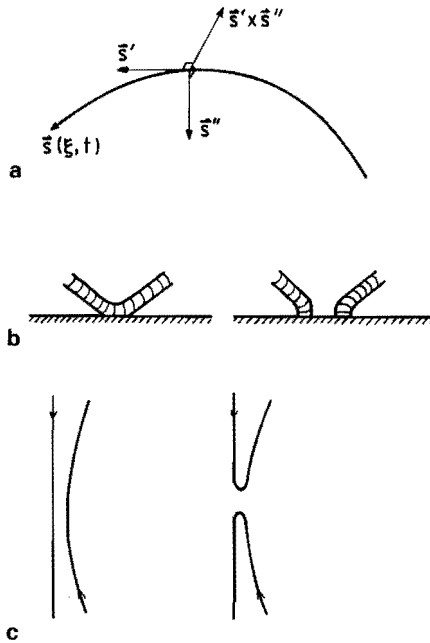
Fig. 1 *a. Part of a vortex line with parametric representation*
s(ξ,t), where ξ is the arc length. The derivatives of s with
respect to ξ are denoted by primes. The vectors s', s" and
s'×s" form a triad with lengths 1, R^{-1} and R^{-1}, where R is the
local radius of curvature of the vortex line.
b. Reconnection of a vortex line to a rigid smooth surface.
c. Reconnection of two vortex lines.

This implies that a vortex line ending on a wall should enter it at right angles. When considering homogeneous turbulence, periodic boundary conditions can be applied. Then v_{s0} equals the velocity field of the periodic continuation of the tangle. Another example is an open flow system. In that situation the boundary condition is the externally imposed superfluid velocity, which should be added to v_{s0}.

If equation (14) can be solved, the solution of equation (1) can easily be found, so that in principle it is possible to calculate the evolution of an arbitrary vortex tangle. There are, however, two serious problems. One arises when two parts of the tangle approach

each other. This approach takes place with increasing velocity, and the limit of the validity of the calculation will be reached soon. The same problem is encountered, if a vortex approaches a rigid wall. This problem will be dealt with later.

The second problem is the calculation time needed to solve the equation of motion numerically. To calculate the evolution, the tangle has to be discretized: a number of points on the line is defined, which together give a good representation of the tangle. The evolution of the tangle is followed by calculating the path of each point, using equations (1) and (14). If the distance between two neighbouring points on the tangle becomes too small or too large during the evolution, one point will be left out or a new point will be inserted in between, using a circular interpolation [4]. The points on the tangle are called discrete points. The most time-consuming contribution to **v** is the nonlocal term, which involves an integration over the entire tangle. Therefore, the time needed to calculate the velocity of all the points on the tangle is roughly proportional to N^2, were N is the number of discrete points. For simple configurations, like one or two loops, N may be of the order of 100 and the fully nonlocal calculation is possible. However, for a typical tangle N is of the order of 10^4, which makes the calculation even on a vector processor unfeasible.

To cope with these problems, some approximations are made. The local contribution is of the order of $10k/4\pi R$, where the logarithmic term has been estimated as 10, whereas the nonlocal contribution is of the order of $k/2\pi\Delta$, with Δ the distance to the nearest wall or other vortex line. Hence, except if two vortex lines approach very closely, the nonlocal contribution can be neglected. (This approximation is known from classical fluids as the localized induction approximation [9]). This is even more so for a random tangle, where nonlocal terms from different parts of the tangle tend to cancel. In the calculation of the evolution of a tangle, where not the exact shape of the tangle, but only average properties are of interest, the localized induction approximation would be sufficient. However, if $\Delta \ll R$, the nonlocal contribution is important. This is the case, if two vortices approach each other, or a vortex approaches a wall. The localized induction approximation would not take these events into account. An assumption

is needed to treat them. The results of Schwarz's calculations [3,4] suggest that in these events a reconnection takes place (see Fig. 1). With the localized induction approximation and reconnection at crossings of vortices a dynamically stable configuration develops.

This can be seen from the effect of friction on a curved vortex line. Consider a part of a vortex with radius of curvature R in the plane z = 0. In the localized-induction approximation the velocity of this part of the vortex equals

$$\mathbf{v}_0 = \mathbf{v}_{s0} + \frac{\beta}{R} \mathbf{e}_z \quad . \tag{16}$$

where $\mathbf{v}_{s0}$ is the superfluid velocity at infinity, $\mathbf{e}_z$ the unit vector in the z-direction and

$$\beta = \frac{\kappa}{4\pi} \ln \left[\frac{cR}{a_0} \right] \quad . \tag{17}$$

with c a constant of order unity. From equation (1) it can be seen that only the term with α is directed perpendicular to the local velocity, and thus gives the change of R. This change is given by

$$\frac{\partial R}{\partial t} = \alpha(v_{ns}\cos \vartheta - \beta/R) \quad . \tag{18}$$

where $\mathbf{v}_{ns}$ is the relative velocity $\mathbf{v}_n - \mathbf{v}_s$ at infinity and ϑ the angle between $\mathbf{v}_{ns}$ and $\mathbf{e}_z$. This equation can be elucidated by considering a transformation to the frame in which the part of the vortex under consideration is stationary. In this frame the velocity of the normal fluid equals $\mathbf{v}_{ns} - (\beta/R)\mathbf{e}_z$. Hence the sign of the z-component of the normal fluid velocity in this frame determines whether the part of the vortex shrinks or grows. If the z-component of the normal fluid velocity is positive, the normal fluid transfers energy to the vortex, so that it grows; if it is negative, energy is transferred from the vortex to the normal fluid. Only, if the vortex moves with the same velocity as the normal fluid, it retains its length. This can be put in the following mathematical form. A part of the vortex with $R < R_c$, where

$$R_c = \frac{R}{v_{ns}\cos \vartheta} \quad \text{if } \cos \vartheta > 0 \tag{19a}$$

and

$$R_c = \infty \quad \text{if } \cos \vartheta \leq 0, \tag{19b}$$

shrinks, whereas a part with $R > R_c$ grows. This process would lead to an unstable situation: vortices with small R or $\cos \vartheta < 0$ would annihilate and the other vortices would grow without limitation.

This unstability is resolved by reconnection. If a vortex grows $(R > R_c)$, it will eventually encounter another vortex or a wall. Then a reconnection occurs, creating a part in the vortex with small radius of curvature and $\cos \vartheta < 0$. This causes that part of the vortex to shrink. In this way both problems mentioned above are solved and the evolution of the tangle can be calculated until a dynamically stable situation is reached.

6.2a *The interpretation of the Vinen equation*

It is interesting to note that this analysis gives a contribution to the discussion about the interpretation of the Vinen equation. This equation, proposed by Vinen in 1957 [11], gives the time evolution of the line length density L. Vinen used phenomenological and dimensional arguments to make it plausible. It consists of two terms. The first produces line length and is caused by the friction with the normal fluid. The other term describes the destruction of line length and is caused by the reconnection processes.

In 1978 Schwarz derived the Vinen equation in a completely different way [6]. He introduced a probability density $\lambda(R,\vartheta,t)$ defined in such a way, that at time t, $\lambda(R,\vartheta,t)$ $R^2\cos \vartheta$ dRdϑ is the vortex line length with radius of curvature between R and R + dR and angle between ϑ and ϑ + dϑ. Next, he constructed a partial differential equation describing the time evolution of λ, which consists of "driving terms", caused by the friction and "randomizing terms", caused by the reconnection events. He showed that the solutions of this equation tend to a stationary distribution and that the total

line-length density obeys the Vinen equation. It turned out, that in this approach the randomizing terms do not give a contribution to the Vinen equation, so that both the production and destruction term are caused by the friction. From this argument Schwarz concludes that Vinen's interpretation of the destruction term is wrong. The analysis given above shows that the two interpretations of the destruction term are not contradicting: destruction is caused by the friction, when after a reconnection the radius of curvature decreases and $\cos \vartheta$ becomes negative. In this way the two interpretations are combined.

6.2b *Dimensional considerations*

Even without calculating the evolution of a vortex tangle, some properties of the dynamical equilibrium can be derived, if the relative velocity $\mathbf{v}_{ns}$ is homogeneous. In the localized induction approximation the equation of motion of the vortex can be written as

$$\frac{\partial \mathbf{s}}{\partial t} = \mathbf{v}_{s0} + \beta \mathbf{s}' \times \mathbf{s}'' + [\alpha - \alpha' \mathbf{s}' \times][\mathbf{s}' \times (\mathbf{v}_{ns} - \beta \mathbf{s}' \times \mathbf{s}'')] \quad . \tag{20}$$

The first term yields a uniform translation of the vortex and can be removed by a Galilei transformation. The parameters β and $\mathbf{v}_{ns}$ have dimensions [length^2/time] and [length/time] respectively. It is possible to define a dimensionless lengthscale and timescale by

$$\mathbf{s}_0 = \mathbf{s} \, v_{ns}/\beta \tag{21}$$

and

$$t_0 = t \, v_{ns}^2/\beta \quad . \tag{22}$$

Substitution in equation (20) yields

$$\frac{\partial \mathbf{s}_0}{\partial t_0} = \mathbf{s}_0' \times \mathbf{s}_0'' + [\alpha - \alpha' \mathbf{s}_0' \times][\mathbf{s}_0' \times (\mathbf{e}_z - \mathbf{s}_0' \times \mathbf{s}_0'')] \quad , \tag{23}$$

where the z-axis has been chosen in the direction of $\mathbf{v}_{ns}$. This

equation only depends on α and α'. Hence, if no walls are present, the solution does not depend on the applied velocity v_{ns}, and the vortex tangle is homogeneous.

The density of vortex-line-length L is given by

$$L = \frac{1}{\Omega} \int_{\mathcal{L}} d\xi \quad . \tag{24}$$

where the integration is performed over the tangle inside a volume Ω. In dimensionless units L equals

$$L = \left[\frac{v_{ns}}{\beta}\right]^2 L_0(\alpha,\alpha') \quad . \tag{25}$$

The dimensionless vortex-length density

$$L_0(\alpha,\alpha') = \int_{\mathcal{L}} d\xi_0/\Omega_0 \quad . \tag{26}$$

is only a function of α and α'. This derivation proves the statement in section 3.3, that L is proportional to v_{ns}^2.

In a similar way the average mutual-frictional-force density F can be calculated. The force exerted by the normal fluid on a unit length of vortex line equals [6]

$$f = -\rho_s k s' \times \{[\alpha - \alpha' s' \times][s' \times (v_{ns} - \beta s' \times s'')]\} \quad . \tag{27}$$

The density of the frictional force on the superfluid component equals

$$F = -\frac{\rho_s k}{\Omega} \int_{\mathcal{L}} s' \times \{[\alpha - \alpha' s' \times][s' \times (v_{ns} - \beta s' \times s'')]\} \, d\xi \quad . \tag{28}$$

and in dimensionless units

$$F = F_0(\alpha,\alpha') \rho_s k v_{ns}^3/\beta^2 \quad , \tag{29}$$

121

where the dimensionless force density equals

$$F_0(\alpha, \alpha') = -\frac{1}{\Omega_0} \int_{\mathscr{L}} s_0' \times \{[\alpha - \alpha' s_0' \times][s_0' \times (e_z - s_0' \times s_0'')]\} \, d\xi_0 \quad . \quad (30)$$

This quantity does not depend on v_{ns} or β.

With the same arguments the dependence of the critical velocity v_c on v_{ns} for flow through a rigid cylindrical tube with diameter D can be determined. The situation of dynamical equilibrium found from equation (23) is not only a function of α and α', but also of the dimensionless diameter of the tube $v_{ns}D/\beta$. Hence,

$$L = \left[\frac{v_{ns}}{\beta}\right]^2 L_0(\alpha, \alpha', v_{ns}D/\beta) \quad , \quad (31)$$

for a certain function L_0. It is known, that below the critical velocity L equals zero in the equilibrium state, while above the critical velocity a turbulent state is present. Thus $L_0 = 0$ for $v_{ns} < v_c$ and $L_0 \neq 0$ for $v_{ns} > v_c$. The function L_0 depends on v_{ns} only through $v_{ns}D/\beta$. Hence,

$$v_c \sim \beta/D \quad . \quad (32)$$

Equations (25), (29) and (32) have to first order been confirmed by experiment [12]. However, in the derivations it has been neglected that β weakly depends on the local structure of the vortex, as it involves the logarithm of the local radius of curvature. The analysis of Swanson and Donnelly [13] takes this dependence into account and gives a better agreement with experimental results. Recently, relation (32) has also been verified to first order in the flow of [3]He through superfluid [4]He [14].

6.3 *The reconnection of a vortex ring with a rigid smooth surface*

As explained in the previous section, the evolution of a vortex tangle towards a dynamically stable situation of homogeneous turbulence can be simulated numerically by solving equation (20) using

the reconnection assumption and periodic boundary conditions. In the first place, a resolution criterion for the discrete points has to be chosen. In order to get a good representation of a vortex, the distance ℓ between two neighbouring discrete points should not exceed $R/5$. On the other hand, ℓ should not be too small in order to limit the total number of discrete points, and thus the computation time. The choice of ℓ is directly related to the time step Δt of the numerical integration, for Δt should be chosen in such a way that the displacements of the discrete points in one time step are small compared to ℓ. The most important contribution to the displacements is $\beta s' \times s'' \Delta t$, which equals $10\Delta t/R$ (see page 117). Hence, the requirement for Δt is: $10\Delta t/R \ll R/5$. If Δt is proportional to R^2 this requirement can be satisfied.

At the moment of a reconnection the value of R in the region of reconnection suddenly decreases strongly (see Fig. 1c) and hence Δt decreases correspondingly. Furthermore, the number of discrete points in the reconnection region increases. As a result of the increase in the number of discrete points and decrease of Δt, the numerical solution tends to block at a reconnection. Therefore, it is important to model a reconnection in such a way, that the parts of the tangle with high curvature become smooth again after a short time.

In a first attempt to calculate the evolution of a random tangle, it appeared that the numerical procedure for the reconnection cannot be chosen arbitrarily. Therefore, a detailed investigation on the reconnection of two vortices was started. In this section the evolution of a vortex ring near a rigid wall is studied. Due to the symmetries of the problem (reflection symmetry in the plane of the wall, and in a plane perpendicular to the wall and the ring), the calculation time is limited even in the fully nonlocal calculation. The evolution can be calculated in this way until the shortest distance of the vortex to the wall is of the order of the core diameter. In this region equations (1) and (14), describing the time evolution of the vortex, are not valid. At that point the connection to the wall is established in a prescribed way. After this reconnection has taken place, the behaviour can be followed with the same numerical procedure as before the reconnection. After some time the small scale structure introduced by the reconnection vanishes.

In the calculation the relative velocity v_{ns} and the superfluid velocity at infinity have been chosen equal to zero. This does not have a great influence on the results, since in the interesting part of the calculation the radii of curvature are small, so that v_{ns} is small compared to v_0. Furthermore, the friction parameters are chosen as $\alpha = 0.1$ and $\alpha' = 0$, corresponding in good approximation to pure ^{4}He at 1.6 K, and the core diameter equals 1 Å. The wall is situated at $x = 0$. At $t = 0$ the vortex is a ring of radius R_0 in the plane $z = 0$ with positive orientation (this means moving in the positive z–direction) and centre $x = R_0 + D$ and $y = 0$. Hence, D which is positive, is the shortest distance from the vortex to the wall. The planes of symmetry are $x = 0$ and $y = 0$. From the structure of the equation of motion follows that these symmetries are conserved during the evolution. So the motion of only half of the loop has to be calculated. In the absence of a wall the ring would move parallel to the z-axis with ever increasing velocity and decreasing radius due to the friction, until it annihilates. Therefore, if the value of D is large, the friction dominates over the image force and the vortex will not approach the wall close enough for a reconnection to occur. This can be seen from Fig. 2, where the time of reconnection (where the shortest distance to the wall is $3a_0$) is plotted as a function of D in the case that $R_0 = 10$ μm.
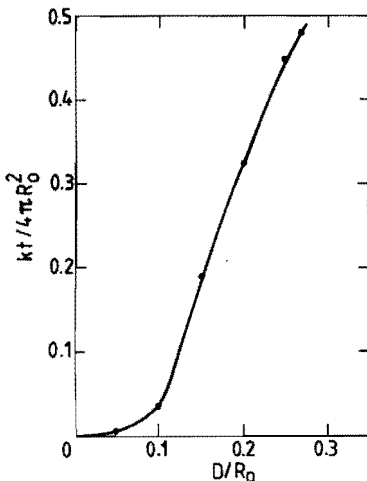

Fig. 2

The time before a reconnection with the wall occurs as a function of the initial distance between the vortex ring and the wall. In this figure the radius of the vortex ring equals $R_0 = 1$ μm and the core diameter equals $a_0 = 1$ Å. At the time of the reconnection the shortest distance from the vortex to the wall is $3a_0$. At $D \geq 0.275\,R_0$ no reconnection occurs.
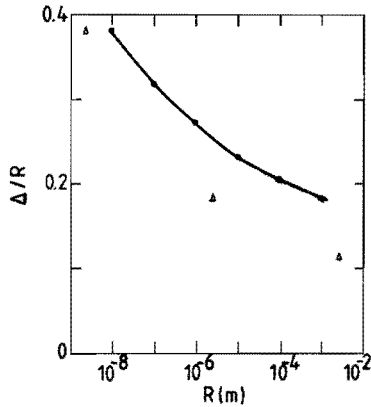
Fig. 3 *The critical initial distance from the vortex ring to the wall
as a function of the radius of the vortex ring. The triangles
are results of Schwarz [4] for the situation that the ring is
distorted to a four-lobed loop.*

There is a critical value of D, Δ, above which the vortex annihi-
lates before a reconnection takes place. In Fig. 3 the calculated
dependence of Δ/R_0 is plotted as a function of R_0. For a more general
treatment, which includes the orientation of the vortex ring and the
influence of other vortices, Schwarz [4] estimated that Δ should obey
the relationship

$$\Delta = \frac{bR_0}{c+\ln(R_0/a_0)} \quad .$$ (33)

with b and c constants of order unity. A fit to the calculated values
yields

$$b = 4.04 \pm 0.08$$ (34)

and

$$c = 5.8 \pm 0.3 \quad .$$ (35)

As a result $\Lambda < R_0$. The agreement between the calculations and equation (33) is good although the values of b and c differ from those in Ref. 2, where b = 2 and c $\simeq$ 0. The reason for this difference may be that in the calculations described here the appearance of a reconnection is determined only by the action of the friction against the image force, whereas the effects of the orientation of the vortex ring and the influence of other vortices are not included.

The important result, that Λ is smaller than the typical radius of curvature, remains. This justifies the localized induction approximation with the reconnection assumption in the simulation of superfluid turbulence, as described in the previous section. At the same time it provides a useful condition for reconnection to a wall: if the distance between a vortex line and a wall becomes smaller than Λ, a reconnection should be made. Since Λ is in first order proportional to R, and thus to ℓ, this condition can be examined by comparing the distances of a discrete point to the wall and to its neighbours.

For one situation, with $R_0 = 10~\mu m$, the reconnection process has been calculated in detail. In the first stage of the process the motion of the part of the vortex ring near the wall is slowed down by
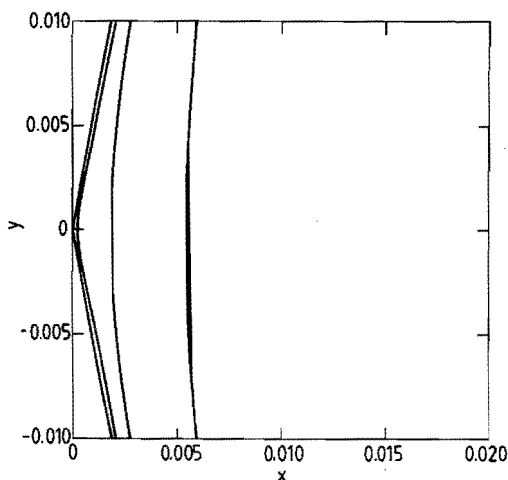

Fig. 4   Four stages of the reconnection process on a reduced scale. These drawings show a projection on the xy-plane. The left vertical axis is the wall. The numbers along the axes of Figs. 4-7 are in units of R_0.
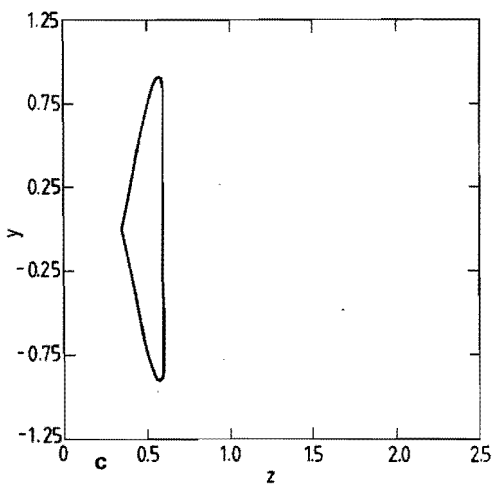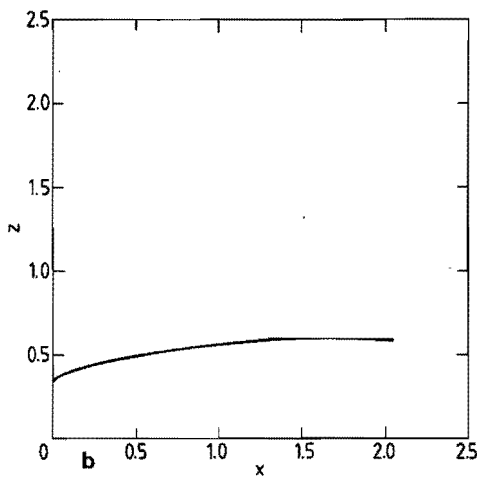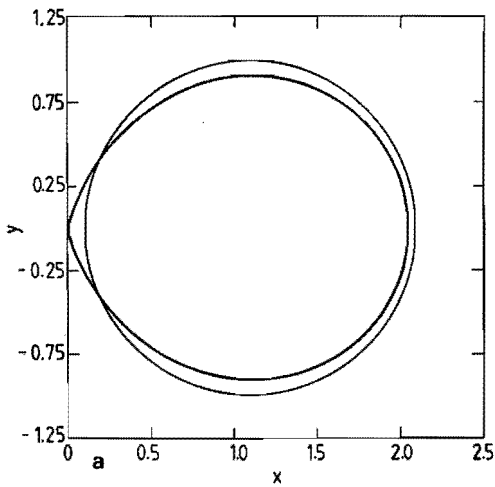
Fig. 5
Three projections of the
situation at the moment of
reconnection, where the
distance to the wall equals
$3a_0$.
a. Projection on the
xy-plane, where also the
initial situation is shown.
In this projection the left
vertical axis corresponds
with the wall.
b. Projection on the
xz-plane, where also the left
vertical axis is the wall.
c. Projection on the plane of
the wall.

127

its image. As a result, the vortex bends towards the plane of the wall, and moves towards the wall due to the self-induced velocity. A tip on the vortex develops which moves towards the wall with increasing velocity. This can be seen in Fig. 4, where the projections on the xy-plane of four stages in this process are given on a reduced scale. In Fig. 5a-c the projections of the final situation, where the distance to the wall equals $3a_0$, on three perpendicular planes are drawn. In the xy-projection the initial situation is also given. It can be seen in these figures that a part of the vortex, large compared to the core diameter, is situated almost parallel to the wall at short distance from the wall. At a large distance the velocity fields from this part of the vortex and its image tend to cancel, since they have opposite direction. Thus, this part and its image do not give a contribution to the velocity field. This justifies the reconnection assumption.

The connection to the wall is made by cutting the vortex at the point of closest approach $(y = 0)$. The two "loose ends" are connected to the wall, by requiring that the first and last of the discrete points have x-co-ordinates equal to zero. The distortions created in this way will propagate along the vortex, initially with high velocity. However, the scale of the distortions gradually increases and hence the velocity of their propagation decreases. In Fig. 6a-c the three projections of several stages of this process are plotted on a reduced scale. As can be seen by comparing the different projections, the sharp kinks in the xz-projection are only apparent, due to the projection of an almost straight line on a plane perpendicular to the line. Note that the values of the z-co-ordinate are shifted with respect to the values before the reconnection. The projections of the final shape of the vortex, where the calculation was stopped, are drawn in Fig. 7a-c. In the xy-projection the initial shape is also plotted. It can be seen that the effect of the wall on the shape of the vortex is small in the main part of the vortex.

The computation time for this fully nonlocal calculation amounted to approximately 450 seconds Cyber 205 CPU (central processing unit) time. Even in this case of a relatively small number (20-60) of discrete points, the amount of time needed to calculate the nonlocal contribution to the superfluid velocity is enormous. This can be seen
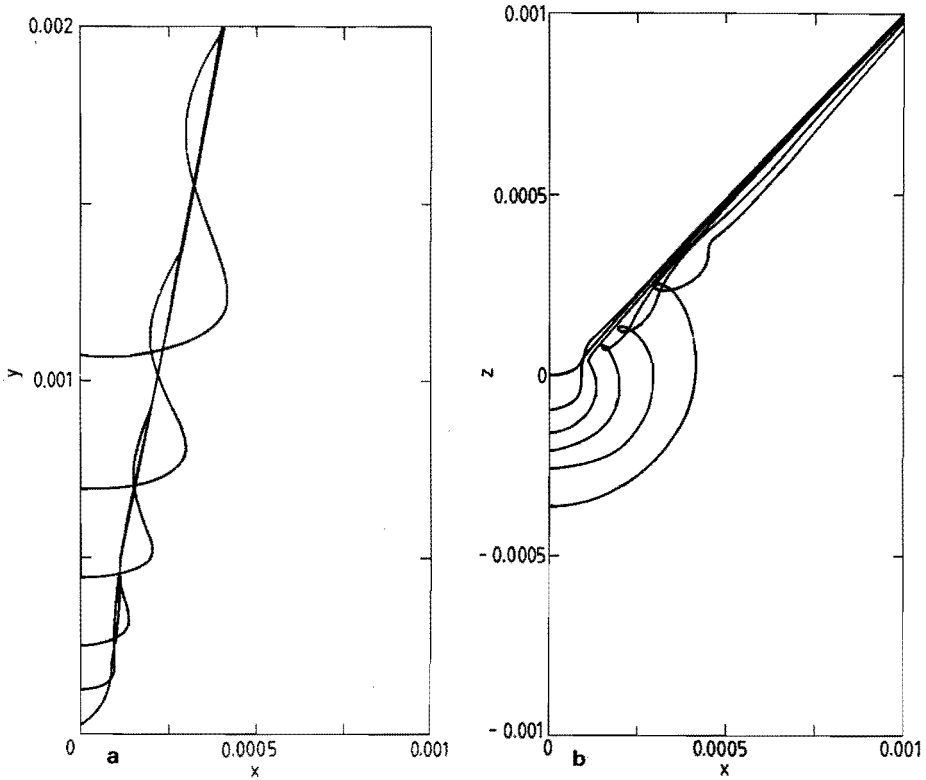
Fig. 6 Three projections on a reduced scale of several stages in the
process after the reconnection of a vortex line to a wall.

a. Projection on the xy-plane, where the wall corresponds with
the left vertical axis. Only a part of the vortex with y > 0
is shown. The part with negative y-values can be found by a
reflection in the x-axis.

b. Projection on the xz-plane. The wall is the left vertical
axis.

c. Projection on the plane of the wall (Next page).

Note that the z-values are translated with respect to Fig. 5.

129
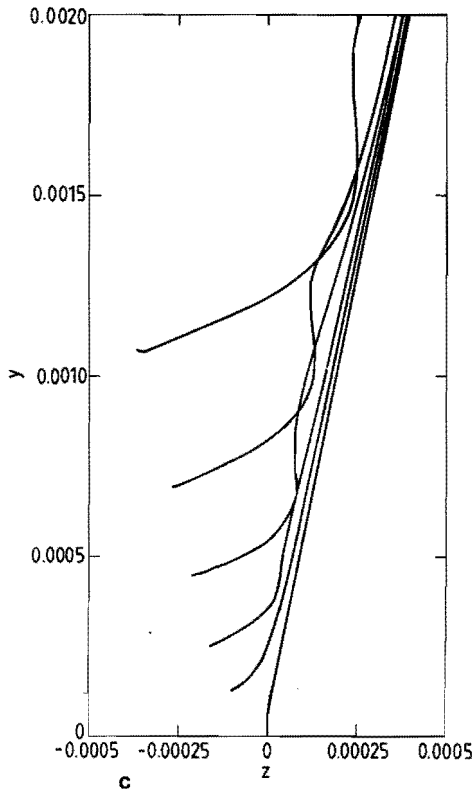
by calculating the same process in the localized induction approxima-
tion and making the connection to the wall at the beginning. The
computation time for this calculation amounted to approximately 15
seconds Cyber 205 CPU time, smaller by a factor 30 than the fully
nonlocal calculation. The results of the two calculations are qualita-
tively the same. The results can be compared quantitatively by
calculating the total line length of the vortex as a function of time.
The difference between the two calculations increases with time to
approximately 12 % at the end of the calculation. This shows the
validity of the localized induction approximation for the purpose of
this investigation and provides a useful model for a reconnection
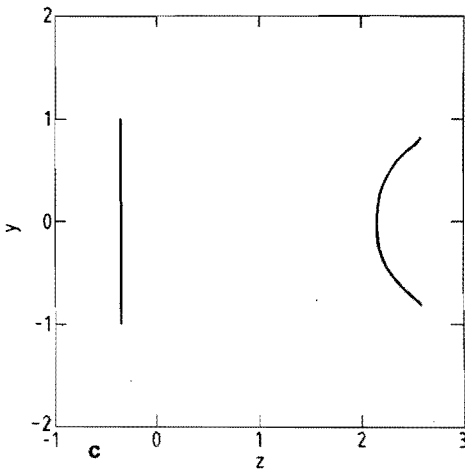event.

130
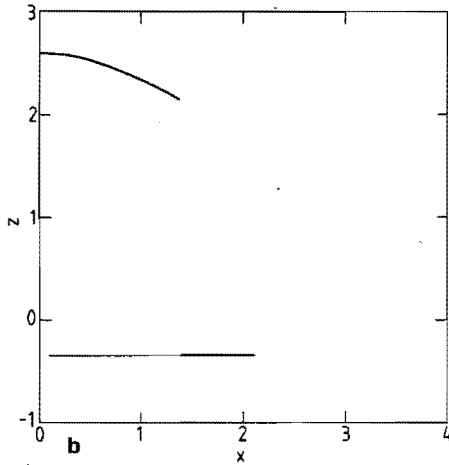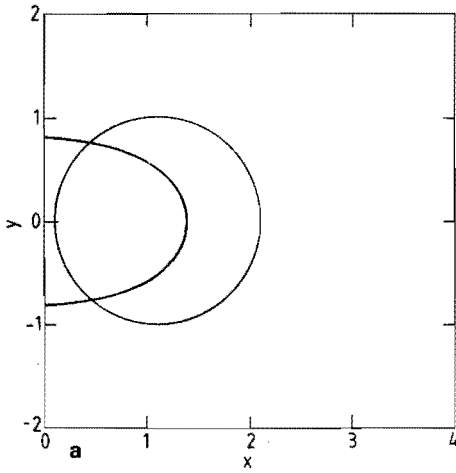
Fig. 7
Three projections of the
situation, where the
calculation was stopped, and
the initial situation.
a. Projection on the
xy- plane.
b. Projection on the
xz- plane.
c. Projection on the
yz- plane.
In this figure the same
translation of the z-values
is made as in Fig. 6.

References

[1]   A.J. Hillel, J. Phys. **C14**, 4027 (1981).

[2]   A.J. Hillel, and W.F. Vinen, J. Phys. **C16**, 3267 (1983).

[3]   K.W. Schwarz, Phys. Rev. Lett. **49**, 283 (1982).

[4]   K.W. Schwarz, Phys. Rev. **B31**, 5782 (1985).

[5]   C.F. Barenghi, R.J. Donnelly, and W.F. Vinen,
       J. Low Temp. Phys. **52**, 189 (1983).

[6]   K.W. Schwarz, Phys. Rev. **B18**, 245 (1978).

[7]   S.J. Putterman, Superfluid Hydrodynamics (North-Holland,
       Amsterdam, 1974).

[8]   See for example: J.D. Jackson, Classical Electrodynamics
       (Wiley, New York, 1975), Ch. 5.

[9]   R.J. Arms, and F.R. Hama, Phys. Fluids **8**, 553 (1965).

[10]   See for example: H. Lamb, Hydrodynamics (Dover, New York,
       1945), Ch. VII.

[11]   W.F. Vinen, Proc. Roy. Soc. **A242**, 493 (1957).

[12]   J.T. Tough, in Progress of Low Temperature Physics, Vol. VIII,
       D.F. Brewer, ed. (North-Holland, Amsterdam 1982), Ch. 3.

[13]   C.E. Swanson, and R.J. Donnelly, J. Low Temp. Phys. **61**, 363
       1985.

[14]   J. Zeegers, J.G.M. Kuerten, A.T.A.M. de Waele, and H.M.
       Gijsman, to be published.

LIST OF FREQUENTLY USED SYMBOLS

Subscripts:

c	concentrated phase
d	dilute phase
e	end of impedance
ex	external
F	Fermi gas
i	incoming ^{3}He
m	molar
	mixing chamber
n	normal fluid
s	superfluid
	saturated solution
0	zero temperature (Ch. II)
	characteristic quantity (Ch. IV)
	dimensionless quantity (Ch. VI)
3	^{3}He
4	^{4}He

Superscript:

0	pure substance
˙	derivative with respect to the arc length of a vortex line

Symbols:

a_0	core diameter
A	area of impedance
B	friction parameter (III.55)
c	mass concentration of ^{3}He
C	specific heat
D	diameter of cylindrical impedance (Ch. IV-V)
	distance between vortex ring and wall (Ch. VI)
E	energy density
f	ratio of enthalpy flows (IV.33)
f	mutual frictional force per unit mass
F	Helmholtz free energy
F	mutual-frictional-force density
g	divergence of the superfluid velocity (Ch. VI)
G	Gibbs free energy
H	enthalpy
$H_3^{\circ s}$	osmotic enthalpy per mole ^{3}He
H^E	molar excess enthalpy
j	momentum density
k	quantum of circulation
k	Boltzmann's constant
ℓ	co-ordinate in the direction of the ^{3}He flow (Ch. IV)
	distance between two neighbouring discrete points on a vortex line (Ch. VI)
L	vortex line length density
$\mathscr{L}$	the curves representing a vortex tangle
m	atomic mass
m^x	effective mass

M	molar mass
$\dot{n}$	molar flow
N	number of moles
p	pressure
$\dot{q}$	dimensionless heat load
Q	energy flux
$\dot{Q}$	cooling power, external heat load
r_0	radius of the vortex core
R	molar gas constant (Ch. II)
	dissipative function (Ch. III)
	local radius of curvature of a vortex (Ch. VI)
s, s_1	position of a point on a vortex line
S	entropy
t	reduced temperature
T	temperature
U	internal energy
$\mathbf{v}$	velocity
$\mathbf{v}_0$	superfluid velocity at the point on the vortex line
$\mathbf{v}_{s0}$	superfluid velocity due to the boundaries
V	volume
V_3	volume of one mole of ^{3}He
$\mathscr{V}_3$	partial volume of ^{3}He
x	molar ^{3}He concentration
Z	chemical potential
α	BBP parameter (Ch. II)
	friction parameter (Ch. VI)
α'	friction parameter
Δ	critical distance between vortex ring and wall
ζ	impedance factor per unit length
η	coefficient of viscosity
κ	coefficient of heat conduction
λ	reduced length
Λ	reduced length of impedance
μ	chemical potential
μ'	molar potential energy of ^{3}He
μ_{ik}	part of viscous stress tensor
ξ	dimensionless parameter (IV.31)
ξ'	dimensionless parameter (IV.65)
ξ	arc length on a vortex line (Ch. VI)
π	osmotic pressure
π_{ik}	non-dissipative stress tensor
ρ	density
σ	entropy density
τ	reduced temperature
τ_{ik}	viscous stress tensor
χ	mutual friction parameter (IV.15)
Ω	volume

The numbers in parentheses correspond to the chapter where the symbol is used, or to the formula where the symbol is defined.

134

SAMENVATTING

Dit proefschrift beschrijft een theoretische studie van de thermodynamische en hydrodynamische eigenschappen van ^{3}He-^{4}He II mengsels bij temperaturen beneden 250 mK. Deze studie was nodig, omdat gebleken was dat de bestaande theoretische beschrijvingen niet in overeenstemming waren met experimentele resultaten.

In 1967 waren de thermodynamische grootheden van ^{3}He-^{4}He mengsels bij lage temperaturen berekend en getabelleerd. Deze tabellen werden veelvuldig gebruikt met name door ontwerpers van ^{3}He circulerende mengkoelers. Het bleek echter dat de berekende waarden van bijvoorbeeld de osmotische druk en de enthalpie niet overeenstemden met latere metingen. In het gangbare hydrodynamische model van ^{3}He-^{4}He mengsels, dat eveneens aan het eind van de jaren zestig was opgesteld en geverifiëerd was bij lage ^{3}He snelheden, wordt ervan uitgegaan dat ^{3}He bij snelheden beneden 60 m/s wrijvingsloos door superfluïde ^{4}He kan stromen (Mechanisch Vacuüm Model). De basis voor deze veronderstelling is het excitatiespectrum van superfluïde ^{4}He, waaruit volgt dat bij deze snelheden geen fononen en rotonen opgewekt kunnen worden. Latere experimenten in ^{3}He circulerende mengkoelers hebben echter aangetoond, dat al bij veel lagere snelheden wrijving tussen ^{3}He en ^{4}He optreedt. Aan de andere kant was in deze experimenten het effect van een viskeuze kracht ten gevolge van de viskositeit van het ^{3}He onmeetbaar. Dit leidde tot het Wederkerige Wrijvings Model, dat uitgaat van een empirische relatie tussen de wederkerige wrijvingskracht en de relatieve snelheid tussen ^{3}He en ^{4}He. Het doel van het hier beschreven onderzoek was een nieuwe berekening van de thermodynamische grootheden van ^{3}He-^{4}He mengsels, uitgaande van nauwkeurige meetresultaten, en het opstellen van een nieuw hydrodynamisch model, waarin wel het effect van de wederkerige wrijvingskracht is verwerkt, en dat zowel bij hoge als bij lage ^{3}He snelheid in overeenstemming is met de experimenten.

Na een inleidend hoofdstuk I, waarin kort wordt ingegaan op het belang van ^{3}He-^{4}He mengsels, zowel voor hun gebruik in mengkoelers als vanuit fundamenteel oogpunt, wordt in hoofdstuk II de thermodynamica van deze mengsels behandeld. Uitgaande van metingen van de soortelijke warmte, het molaire volume en de osmotische druk, geëxtrapoleerd naar temperatuur nul, zijn alle overige grootheden, zoals de chemische potentialen, de osmotische druk en de osmotische enthalpie berekend.

135

Deze laatste grootheid is van belang, omdat ze behouden is bij de stroming van ^{3}He door ^{4}He. De afwijking van de berekende resultaten met metingen is kleiner dan 1%.

In hoofdstuk III wordt na een bespreking van superfluïditeit en van de interactie tussen ^{3}He en ^{4}He, een hydrodynamisch model opgesteld voor ^{3}He-^{4}He mengsels met wederkerige wrijving. Tevens wordt met een eenvoudige dimensionele beschouwing de vorm van deze wrijvingskracht als functie van de ^{3}He snelheid afgeleid. Deze is in overeenstemming met de empirische relatie.

In hoofdstuk IV worden de hydrodynamische vergelijkingen toegepast op ^{3}He circulerende mengkoelers, met als doel de invloed van de wederkerige wrijving op de werking van deze koelmachines te berekenen. Het blijkt dat, vooral bij het ontwerp van mengkoelers met een hoge ^{3}He circulatie, rekening gehouden moet worden met wederkerige wrijving. Dit komt tot uiting in restricties op de afmetingen van de buis waardoor het ^{3}He van de mengkamer naar de verdamper stroomt, en in een hogere minimumtemperatuur van de mengkamer in een single cycle. In systemen met een hoge ^{3}He snelheid is de wederkerige wrijving dominant, terwijl bij lagere ^{3}He snelheden de viskositeit van het ^{3}He de dissipatie bepaalt. In hoofdstuk V worden experimenten beschreven in het tussenliggende gebied, waarin zowel viskositeit als wederkerige wrijving belangrijk zijn. Zo wordt aangetoond, dat er een continue overgang van het Mechanisch Vacuüm Model naar het Wederkerige Wrijvings Model bestaat.

In hoofdstuk VI tenslotte, worden de eerste resultaten van een studie van de kwantitatieve berekening van de wederkerige wrijvingskracht besproken. In analogie met wederkerige wrijving tussen de normale en superfluïde component in zuiver ^{4}He, wordt aangenomen dat wederkerige wrijving een gevolg is van de interactie tussen ^{3}He en gequantiseerde wervels in de superfluïde component, die worden opgewekt als het ^{3}He een bepaalde snelheid overschrijdt. Door de evolutie van gequantiseerde wervels onder invloed van de interactie met ^{3}He numeriek te simuleren kan een uitdrukking voor de macroscopische wrijvingskracht gevonden worden. Bij de evolutie van wervels spelen de verschijnselen die optreden als twee wervels elkaar naderen, of als een wevel een wand nadert, een belangrijke rol. In dit hoofdstuk worden deze verschijnselen geanalyseerd voor het geval dat een wervel een vlakke wand nadert.

SUMMARY

In this thesis a theoretical study is described of the thermo-dynamic and hydrodynamic properties of ^{3}He-^{4}He II mixtures at temperatures below 250 mK. This study was necessary, as it appeared that there were substantial discrepancies between the existing theoretical models and experimental results.

In 1967 the thermodynamic properties of ^{3}He-^{4}He mixtures at low temperatures have been calculated and tabulated. The tables were frequently used by designers of dilution refrigerators. However, it appeared that the calculated values of for example the osmotic pressure and enthalpy were not consistent with later experiments. In the current hydrodynamical model of ^{3}He-^{4}He mixtures, also proposed at the end of the sixties and verified for low ^{3}He velocities, it is assumed that the ^{3}He does not experience friction, if it flows through superfluid ^{4}He with a velocity below 60 m/s (Mechanical Vacuum Model). The ground for this assumption is the excitation spectrum of superfluid ^{4}He, from which follows that it is not possible to excite phonons and rotons at these velocities. However, later experiments in ^{3}He circulating dilution refrigerators demonstrated that there is friction between ^{3}He and ^{4}He at much lower velocities. On the other hand, in these experiments the effect of a viscous force due to the viscosity of the ^{3}He was negligible. This led to the proposal of the Mutual Friction Model, based on an empirical relation between the mutual frictional force and the relative velocity between ^{3}He and ^{4}He. The purpose of the investigation described here, was a new calculation of the thermodynamic properties of ^{3}He-^{4}He mixtures, starting from accurate measurements, and a new hydrodynamical model, which incorporates the effect of the mutual friction, and that at both high and low ^{3}He velocities is consistent with experiments.

The introductory chapter I goes shortly into the importance of ^{3}He-^{4}He mixtures, both for their use in dilution refrigerators and from the fundamental point of view. In chapter II the thermodynamics of these mixtures is treated. Starting from measurements of the osmotic pressure, extrapolated to zero temperature, the specific heat and the molar volume, the other quantities such as the chemical

potentials, the osmotic pressure and the osmotic enthalpy are calculated. This latter quantity is important, since it is conserved in the flow of ^{3}He through ^{4}He. The discrepancies between the calculated results and measurements are smaller than 1%.

In chapter III first a short review of superfluidity and of the interaction between ^{3}He and ^{4}He is given. Next, a hydrodynamical model is set up which incorporates mutual friction between the two components. From a simple dimensional argument the dependence of this mutual frictional force on the relative velocity is derived, in agreement with the empirical relation.

In chapter IV the hydrodynamical equations are applied to ^{3}He circulating dilution refrigerators in order to calculate the influence of mutual friction on the operation of these cooling machines. It appears that, especially for the design of dilution refrigerators with a high ^{3}He circulation, mutual friction is important. This results in restrictions on the dimensions of the dilute exit tube and in a higher minimum temperature of the mixing chamber in single-cycle operation. In systems with a high ^{3}He velocity the mutual friction is dominant, whereas at lower ^{3}He velocities the ^{3}He viscosity determines the dissipation. In chapter V experiments in the intermediate region, where both viscosity and mutual friction are important, are described. In this way it is shown that there is a continuous transition from the Mechanical Vacuum Model to the Mutual Friction Model.

In chapter VI the first results of an investigation to the quantitative calculation of the mutual friction are reported. In analogy with mutual friction between the normal and superfluid components in pure ^{4}He, it is supposed that mutual friction is caused by the interaction between ^{3}He and quantized vortices, which are created if the ^{3}He velocity exceeds a certain critical value. An expression for the macroscopic frictional force can be found by a numerical simulation of the evolution of quantized vortices under the influence of the interaction with ^{3}He. The phenomena that occur if two vortices approach, or if a vortex approaches a wall, are important for the evolution of vortices. In this chapter these phenomena are analysed for the case that a vortex approaches a smooth solid surface.

NAWOORD

Het onderzoek dat in dit proefschrift beschreven is, is uitgevoerd in de groep Lage Temperaturen, onder leiding van Prof.dr. H.M. Gijsman, van de faculteit Technische Natuurkunde van de Technische Universiteit Eindhoven. Van de vele personen die aan de totstandkoming van dit proefschrift hebben bijgedragen, wil ik op deze plaats graag enkele met name noemen.

- Dr. Fons de Waele, de vele discussies met jou hebben altijd een stimulerende invloed op mij gehad. Bovendien wil ik je bedanken voor de gelegenheid die je me gegeven hebt college te geven.
- Kees Castelijns, de tijd die we in één kamer hebben doorgebracht zal ik niet snel vergeten. Mede door de gezellige sfeer zijn hieruit goede resultaten voortgekomen. Verder wil ik Marian en jou bedanken voor de vele malen dat ik van jullie gastvrijheid heb mogen genieten.
- Jos Zeegers, jouw ontembare werklust heeft ook mij inspiratie gegeven. Jouw vakmanschap blijkt goed uit de nauwkeurigheid van de metingen in figuur II.11.
- Jos van Geffen en Jan Rouvroye, zonder jullie bijdragen aan de computersimulaties van hoofdstuk VI zou dat werk nooit zo voorspoedig verlopen zijn.
- Rob van der Heijden, Richard van de Sanden en Richard Smokers wil ik bedanken voor alle discussies die we gevoerd hebben over uiteenlopende onderwerpen uit de fysica.
- Ook Chen Gang, Leo van Hout, Loek Penders, Jos van Amelsvoort en Wil Delissen hebben bijgedragen tot de prettige sfeer binnen de groep.
- Prof.dr. J.T.L. Devreese, Johan Witters en Gert Poppe wil ik bedanken voor hun stimulerende belangstelling voor het onderzoek in de groep.
- I like to thank Professor J.T. Tough, Donald Griswold and Claude Lorenson for their hospitality during my stay at the Ohio State University.
- Ruth Gruyters heeft op vakkundige wijze de tekeningen verzorgd.
- Tenslotte wil ik mijn ouders bedanken voor de steun die ze mij altijd hebben gegeven.

CURRICULUM VITAE

26 januari 1961   : Geboren te Bergen op Zoom.

1972-1978   : Gymnasium β,

           R.K. Gymnasium Juvenaat H. Hart te Bergen op Zoom.

sept. 1978-   : Studie natuurkunde aan de Rijksuniversiteit te

 juni 1983   Utrecht;

           Afstudeerrichting: Theoretische Natuurkunde;

           Afstudeerbegeleider: Prof.dr. N.G. van Kampen.

           Studentassistentschappen bij nakandidaatswerk-

           colleges quantummechanica en statistische

           mechanica.

sept. 1983-   : Promotie-onderzoek onder leiding van Prof.dr.

 aug. 1987   H.M. Gijsman in de groep Lage Temperaturen van de

           Technische Universiteit Eindhoven.

april 1985-   : Verblijf aan de Ohio State University te Columbus

 juni 1985   Ohio, USA, mogelijk gemaakt door een beurs van de

           Nederlandse organisatie voor zuiver wetenschappe-

           lijk onderzoek (Z.W.O.).

sept. 1986-   : docent van een gedeelte van het keuzecollege

 okt. 1986   Thermodynamica van Irreversibele Processen.

STELLINGEN

behorende bij het proefschrift van

J.C.M. Kuerten

Eindhoven, 18 september 1987

1. Er is geen wezenlijk verschil tussen de interpretaties van Vinen
    en Schwarz voor de fysische achtergrond van de produktie- en
    annihilatieterm in de Vinen vergelijking.

    *W.F. Vinen, Proc. Roy. Soc., Ser. **A242**, 493 (1957);*
    *K.W. Schwarz, Phys. Rev. **B18**, 245 (1978);*
    dit proefschrift, hoofdstuk 6.

2. In tegenstelling tot wat Hansen en Nelkin beweren, leidt de
    interactie tussen gekwantiseerde wervels in helium wel degelijk
    tot strukturen met een lengteschaal tussen de gemiddelde
    wervelafstand en de diameter van een wervelkern.

    *A. Hansen, en M. Nelkin, Phys. Rev. **B34**, 4894 (1986).*

3. De afleiding die Bowley geeft voor de snelheid van het tweede
    geluid in ^{3}He-^{4}He mengsels is onjuist. Een juiste afleiding heeft
    als resultaat

    $$u_2^2 = \frac{M_m \rho_s X}{(1+d)m_4^2 \rho_n} V_4^o \left[\frac{\partial \Pi}{\partial x}\right]_{p,s} ,$$

    waarbij dezelfde notatie gebruikt is als in de referentie, en V_4^o
    het molaire volume van zuiver ^{4}He is.

    *R.M. Bowley, J. Low Temp. Phys. **61**, 291 (1985).*

4. Door de verzwakking van tweede geluid te meten, is het, in de
    door Zeegers *et al.* beschreven experimentele opstelling, mogelijk
    de kritische snelheid van ^{3}He door superfluïde ^{4}He te bepalen in
    cilindrische buizen met een diameter tussen 5 en 20 mm.

    J. Zeegers, J.G.M. Kuerten, A.T.A.M. de Waele, en H.M. Gijsman,
    wordt gepubliceerd.

5. De toepassing van een gegeneraliseerde vorm van de master vergelijking levert een nauwkeurigere bepaling van de werkzame doorsneden voor door botsingen geïnduceerde overgangen in aangeslagen atomen dan de methode, die gebruikt is door Ciurilo en Krause.

J. Ciurilo, en L. Krause, J. Quant. Spectrosc. Radiat. Transfer **28**, 457 (1982).

6. Uit de matrix die botsingsgeïnduceerde koppelingen in een stelsel van N nabijliggende aangeslagen atomaire of moleculaire niveaus beschrijft, kan analytisch de fluorescentiematrix berekend worden. Een consequentie hiervan is dat, als aan het principe van gedetaileerd evenwicht voldaan is, een element van de fluorescentiematrix berekend kan worden, als het element op dezelfde plaats van de getransponeerde matrix bekend is.

C.W.J.M. Klaassen, stageverslag V-mf-84-75, Rijksuniversiteit Utrecht, (1984).

7. Als a een positief getal is en x_n de verzameling positieve oplossingen van de vergelijking $ax_n + tg\ x_n = 0$, dan geldt dat

$$\sum_{n=1}^{\infty} \frac{1+a^2x_n^2}{x_n^2(1+a+a^2x_n^2)} = \frac{1+3a+3a^2}{6(1+a)^2} \quad .$$

8. Het recente onderzoek aan supergeleiders met een hoge kritische temperatuur maakt duidelijk, dat er een sterke behoefte bestaat aan een ondubbelzinnig criterium voor supergeleiding.

C.W. Chu, P.H. Hor, R.L. Meng, L. Gao, Z.J. Huang, en Y.Q. Wang, Phys. Rev. Lett. **58**, 405 (1987);
M.K. Wu, J.R. Ashburn, C.J. Torng, P.H. Hor, R.L. Meng, L. Gao, Z.J. Huang, Y.Q. Wang, en C.W. Chu, Phys. Rev. Lett. **58**, 908 (1987).

9. In de analyse van Vedeneev *et al.* wordt ten onrechte geen rekening gehouden met het photon assisted tunneling effect.

   S.I. Vedeneev, V.A. Stepanov, en R.G. Gamilov, Sov. Phys. Solid State **28**, 697 (1986);
   S.N. Artemenko, A.F. Volkov, en A.V. Zaitsev, Solid State Commun. **30**, 771 (1979).

10. De beweringen van de Kam, dat de unificatie van de zwaartekracht met de andere fundamentele krachten het eindpunt van de fundamentele fysica betekent, en dat de zo verkregen theorie de potentie heeft de hele bekende natuur te verklaren, zijn uiterst discutabel.

    J. de Kam, Intermediair, **23**, nr. 19, p. 11 (8 mei 1987).